# Fast, Robust, efficient and Well-balanced Path-Conservative-based Methods on unstructured meshes for nonconservative problems

Arno Roland Ngatcha Ndengna, Abdou Njifenjou, Raphael Onguene

# Fast, Robust, efficient, Well-balanced and Positive Path-Conservative based Method on Unstructured Meshes for Nonconservative Problems: Theory, Methods and Numerical validations

Arno Roland Ngatcha Ndengna[a,*], Abdou Njifenjou[a,b], Onguene Raphael[c]

[a] *Laboratory E3M, National Higher Polytechnic school of Douala, University of Douala , P.O.BOX 2107, Douala, Cameroon*
[b] *Department of Mathematical Engineering, National Advanced School of Engineering, University of Yaounde I, P.O.BOX 8390, Yaounde, Cameroon*
[c] *Laboratory of Technology and Applied Science, University of Douala, Cameroon*

**Abstract**

In this work, we introduce a high-order unstructured path-conservative-based method to solve a novel sediment transport model in generalized shallow water equations. The high-order of accuracy of the proposed fully discrete scheme is achieved by several new strategies developed for the sediment transport context. Some important properties of the scheme such as stability, well-balanced and preserving-positivity have been proved. The performance of the method is assessed on a number of test cases. The results obtained are compared with other schemes, reference/exact solutions and experimental data. The proposed unstructured path-conservative-based method is suitable for parallel computations and allows for consideration of a wide variety of nonconservative problems available in the literature. This work extends and generalizes recently proposed unstructured positive finite volume schemes.

*Keywords:* Sediment transport(ST), Nonhomogeneous Shallow Water Equations, Path-conservative based methods, Well-balanced preserving-positivity(WBPP), Unstructured mesh, Experimental data

## 1 Introduction

We propose in this work to solve by using a new unstructured finite volume method, a novel two-dimensional(2D) sediment transport model(STM) that is able to adapt to some coastal or estuary environments and has the potential to integrate multiple physics. The developed model is a nonlinear hyperbolic nonconservative system that admits the steady states, particularly the "steady at rest" and which any analytical expressions for the eigenstructure exists. The dynamic of sediments in layer of suspended particles and the morphodynamics in bedload layer in rapidly-varying-hydraulic conditions require a coupled modeling. Decoupled approach can lead to numerical instabilities and can fail a rigorous estimation of the morphodynamics. It is more difficult to find an analytical solution due to its nonlinear nature and the presence of complex coupled terms. For a multidimensional(multiD) problem, it is important to develop multiD numerical strategies to find numerical solutions. The literature does not enough offers simple and robust unstructured path-conservative based methods able to simulate multiD sediment transport equations. We develop a new numerical method that does not require any complex resolution technique. This case can appear when we design an unstructured path-conservative method combined with a Riemann-based solver with multiple intermediate waves.

We develop here a multidimensional stable, fast and robust path-conservative based method using a simple *1D Riemann solver without any intermediate waves* to solve our proposed 2D model. The proposed method does not require any Ad-hoc assumption or simplification as in [41] or any complex method of resolution such as the fix-point method used in [1]. It is well-known that robust numerical schemes should

*Corresponding author(Arno Ngatcha): arnongatcha@gmail.com

be well-balanced and positive even in presence of wet-dry fronts [2], [12],[27], [13], [38], [50],[51]. There is the need to be a balance between flux and source terms because the solution of such a model can be a small perturbation of the steady states.

Some numerical schemes are not proved positive and fail in approximating equilibria or near equilibria 2D solutions. Here, a new unstructured well-balanced positivity-preserving scheme is developed to solve a new sediment transport model. A novel hydrostatic reconstruction is also proposed to achieve the positivity of water depth. The set of balance laws of the model has the main disadvantage of containing nonconservative products due to non-equilibrium hydrostatic pressure. The non-equilibrium pressure creates the variable bed topography and the variable sediment concentration in the $x, y-$momentum equations that lead to solutions containing shock waves. Therefore, a unique definition of possible discontinuous solutions of the model is used in path sense. The choice of a path allows to prove several shock waves definitions according to [4]. In this case many shock wave theories can be used to define a shock wave solutions of the model. The finding of shock waves connecting two states with different propagation speeds is not the objective of this paper. With the presence of nonconservative products, the explicit calculation of the eigenstructure of the proposed model is one of the complex one. To overcome this drawback, we propose to use the Gerschgorin theorem to find the one-sided local speeds needed to evaluate numerical fluctuations. Gerschgorin theorem is more refined than the Lagrange theorem used in [50]. For a nonconservative problem, the presence of nonconservative product can produce instabilities during simulations. It is well observed in some solutions generated by several Godunov-type schemes available in the literature. The difficulty related to the discretization of nonconservative products can be overcome by using smooth paths.

Some numerical path-conservative methods were developed to solve 1D and 2D nonconservative problems[9]. Path-conservative strategies are often combined with Roe solver , HLL (Harten-Lax-Leer) solver and its variants such as HLLC (Harten-Lax-Leer with Contact), HLLEM (Harten Lax Leer entropy) Riemann solvers, DOT (Dumbser-Osher-Toro) solver and other numerical techniques. All these solvers give rigorous methodologies to compute the discrete flux or numerical fluctuations at the cell interfaces. Several path-conservative methods based on these solvers have been designed and successfully applied to solve sediment transport models [8], [7], [27], [34], [32], [36], [35], [40] and the references therein. We can also combine CU scheme with path-conservative framework to derive Path-conservative central-upwind scheme. This strategy has been introduced to overcome the drawbacks of CU schemes and applied only to a large number of 1D nonconservative problems (related to SWE) by Castro et al.,[6].

Designing a well-balanced scheme is more complicated for sediment transport than for shallow water equations. For example, the well-balanced discretization developed in Castro et al.,[6] is only valid for 1D shallow water-based equations. Indeed, their strategy uses a non-singular matrix obtained by projection of the Jacobian matrix in the steady state spaces. Some well-balanced strategy developed for SWE fail for sediment transport equations. For some sediment transport models, the projected Jacobian matrix into the steady states space is singular, therefore, it is not invertible (see Ngatcha and Njifenjou [35]). In order to guarantee the exactly well-balanced property even in presence of wet-dry fronts, sophisticated numerical methods must be designed.

Several well-balanced numerical methods have been developed to solve sediment transport problems [**?** ], [38], [2], [24]. These above schemes are valid only for 1D cases. For multiD problems it is necessary to design multiD numerical methods. Here, we design a well-balanced numerical method valid for both 1D and 2D cases. With our proposed strategy we have proved that the scheme verifies the C-property. It is well-known that the HLL solver is an incomplete Riemann solver and is dissipative [5]. It is also well-known that some schemes require empirical considerations and choice of specific functions. The proposed 2D numerical methodology on structured mesh does not require the knowledge of the full eigenstructure of the flux matrix per time step as HLL Riemann solver [23] and its variants(HLLC, HLLEM), Roe scheme [37], DOT(Dumbser-Osher-Toro) Riemann solver [16].

1D solver can be extended to design 2D schemes on both structured and unstructured mesh. 2D structured finite volume schemes based on 1D solver have been developed in the literature to solve sediment transport problems. In this work a methodology to design 2D PCCU scheme on structured cartesian mesh is briefly presented. This scheme is seen as an extension of one-dimensional PCCU and does not use any empirical consideration or specify functions as in the designing of some Multidimensional approximate Riemann solvers

available in [41] and [1]. One drawback of 2D schemes on the rectangular structured mesh is that the fluxes are computed only at the interfaces of the cells. Structured numerical methods do not take into account the flux at the level of the vertices of each cell. With such a methodology the solutions obtained will be isotropic. The finding of isotropic solutions is not always desirable when solving a sediment transport problem. To take into account the conservative and nonconservative fluxes in all the directions of the cell, it is important to design a numerical method on unstructured mesh. We introduce in this work a unstructured PCCU method based on the efficient, robust and highly accurate WBPP multiD numerical methodology. With that, the proposed multiD scheme can be applied to all conservative and nonconservative problems without major modifications. WBPP shock-capturing PCCU methods combined with a high order reconstruction technique for solving multiD sediment transport models with wet-dry fronts on general triangular meshes are not reported in the literature.

In the current study, a central-upwind scheme in the path-conservative framework is developed on triangular meshes to approximate a multiD nonconservative hyperbolic system.

Few multiD path-conservative methods for nonconservative problems designed satisfy all the following major properties: (i) well-balanced that is exactly capable of preserving steady-state solutions (lake at rest states) even in the presence of wet-dry interfaces; it stably simulates the wet-dry zones without numerical oscillations; (ii) it stably handles the discontinuities since the nonconservative products are well-defined; (iii) positivity-preserving that is capable of maintaining the water depth non-negative during the simulation without reducing the global time step. The developed method satisfies all these major properties. Some schemes found in literature, although verifying some of the above properties, are not suitable complex geometries.

Our main goal is to derive a fast, robust and efficient second order unstructured path-conservative central-upwind method combined with a special spatio-temporal reconstruction that captures the steady states, shock fronts and rarefaction waves. Another important goal is to use the method for solving a new developed fully coupled STM.

The model includes in the momentum equations friction source terms. The influence of the friction term does not disappear in some practical applications (for example when the water depth is small or zero). The presence of this term increases the level of complexity in numerical computations. To overcome this difficulty, we propose to implement third-order Semi-implicit Runge-Kutta time integration method that sustains the well-balanced and positivity-preserving properties of the proposed scheme. A high-order well-balanced positivity-preserving PCCU scheme can be obtained by increasing the order of the gradient derivatives in the reconstruction procedure. Here, qualitative and quantitative comparisons between experimental, numerical, reference and analytical solutions for several benchmark problems are presented.

The rest of the paper is organized as follows. In section 2, we propose a new sediment transport model in nonconservative form. In section 3, we develop some new extensions of path-conservative based schemes for the proposed model. We present a CU scheme in a path-conservative framework in subsection 3.1 and we develop a PCCU scheme for the 1D model in subsection 3.2. In section 4, we design new well balanced positivity-preserving PCCU schemes and we prove some properties of the scheme. We introduce a multidimensional PCCU (M-PCCU) method on general triangular mesh for the proposed model in section 5. In section 6, we propose a time discretization procedure and we prove that the PCCU scheme is positive. In Section 7, we expose several numerical examples demonstrating the performances of the proposed method.

## 2 Mathematical modelings and derivation

We propose a new fully coupled nonlinear hyperbolic system consisting of five equations based on multi-physics and multi-components flow models described below (see Fig. (1)). Three layers are considered to derive these equations and these layers allows us to develop three sub-models: a hydrodynamic sub-model, a morphodynamical sub-model and a sediment concentration sub-model. Firstly, we consider three-dimensional (3D) two phases (solid and fluid) equations and we use the nonhomogeneous Navier-Stokes equations for both phases. Secondly, by summing on both phases the two-phase equations and assuming that the mixture velocity

and the fluid are equal, we find a nonhomogeneous 3D fluid flow father model:

$$\frac{\partial \rho}{\partial t} + div(\rho U) = 0, \tag{1}$$

$$\frac{\partial \rho U}{\partial t} + div(\rho U \otimes U) + grad(\mathbf{P}) = \mathcal{F}, \tag{2}$$

$$div(U) = 0, \tag{3}$$

where $t$ is the time, $U = (u, v, w)$ are component of fluid velocity. $\mathcal{F}$ is the source term and $\mathbf{P}$ is the pressure term. $\rho$ is the mixture density. $div$ and $grad$ are the 3D divergence and gradient operators respectively.

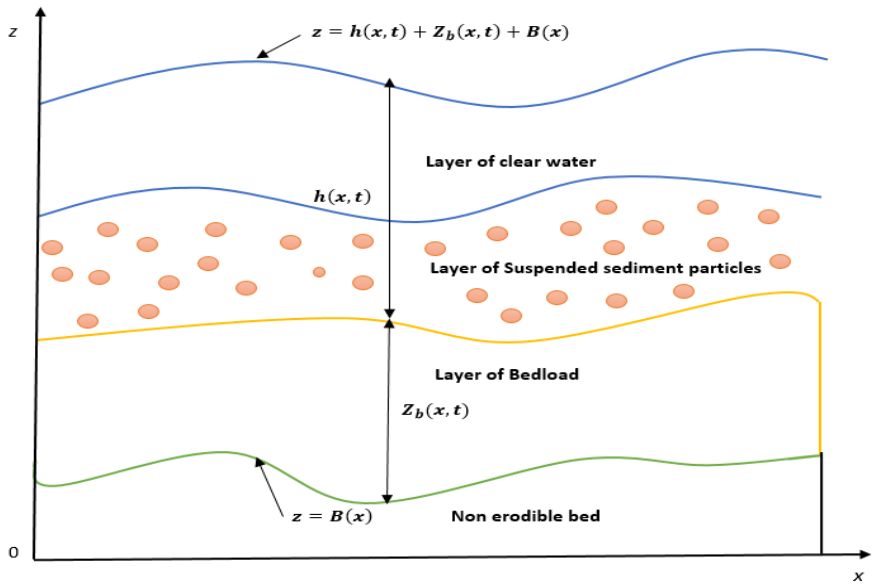


Figure 1: Multi-physics and multi-components flow models: water, water/sediment mixture and topography

We use the hydrostatic assumption consisting to neglect the vertical acceleration of the fluid. Therefore, the $z$-direction of 3D momentum equation reduces to:

$$\frac{\partial \mathbf{P}}{\partial z} = \rho g. \tag{4}$$

This implies that the pressure distribution over the vertical direction is hydrostatic.
The situation where the density is influenced by the sediment concentration $c$ is considered:

$$\rho = \rho_w(1 - c) + \rho_s c, \tag{5}$$

where the pure fluid density $\rho_w$ and the sediment density $\rho_s$ are assumed to be constant in space and time and where $c$ is the flux volumetric sediment concentration. There is a counterpart in the evolution of the fluid volume fraction that will compensate to achieve the following evolution of the mixture density:

$$\frac{\partial \rho}{\partial t} + \frac{\partial \rho u}{\partial x} + \frac{\partial \rho v}{\partial y} + \frac{\partial \rho w}{\partial z} = 0. \tag{6}$$

At the free surface, the total sediment flux is assumed to be zero:

$$\mathbf{W}_s c + \sigma_z \frac{\partial c}{\partial z} = 0, \tag{7}$$

where $\mathbf{W}_s$ is the effective settling velocity obtained by averaged Lagrange equation of the motion over the set of particles and depending of local concentration and given by:

$$\frac{\mathbf{W}_s}{W_s} = (1-c)^{\mathbf{m}}, \tag{8}$$

where $\mathbf{m}$ is a positive exponent.

A material point on a free surface $M(x,y,z,t) = -z + \eta(t,x,y)$. Thus $\dfrac{dM}{dt} = 0$ leads to:

$$\frac{\partial \eta}{\partial t} + \mathbf{u}(t,x,y,\eta)\nabla\eta - w(t,x,y,\eta) = 0. \tag{9}$$

The relation given by Eq. (9) is obtained under the assumption that, any fluid particle which is on the free surface of the fluid at the initial time will remain on the free surface for any further time. The sediment flux near the bed is function of sediment erosion ($E$) and deposition ($D$) exchange:

$$W_s c + \sigma_z \frac{\partial c}{\partial z} = D - E. \tag{10}$$

We can define a quantity $\dfrac{dF_b}{dt}$ (where $F_b(t) = z(t) - Z_b^*(t,\mathbf{x}(t))$) that describes the erosion/deposition exchange. Using this quantity we can define the bedload interface equation as:

$$\frac{\partial Z_b^*(\mathbf{x},t)}{\partial t} + \mathbf{u}(t,\mathbf{x},Z_b^*)\nabla Z_b^*(\mathbf{x},t) = \frac{dF_b}{dt} + w(t,\mathbf{x},Z_b^*) \tag{11}$$

The following assumptions are used:

1. Long waves propagating assumption $\varepsilon = \dfrac{\mathbf{H}}{\mathbf{L}} \ll 1$, where $\mathbf{H}$ and $\mathbf{L}$ are two scale length characteristics. Therefore $h = (\varepsilon)$ and $\dfrac{\partial \mathbf{P}}{\partial z} = \mathcal{O}(\varepsilon)$.
2. We assume that $|\mathbf{u} - \overline{\mathbf{u}}| \leq \mathcal{O}(\varepsilon)$ where instantaneous velocity and averaged velocity.
3. The fluid is viscous and incompressible, no heart transfer (the horizontal gradient temperature is zero).
4. The suspension is assumed to be sufficiently dilute to justify the use of the Boussinesq approximation.
5. The sediment diameters $d_{50}$ are uniform.
6. The vertical averaging technique of Saint-Venant at the first approximation is used.

We introduce here the averaged of a function $\psi$ by

$$\overline{\psi} = \frac{1}{h}\int_{Z_b}^{\eta} \psi(\mathbf{x},t)dz \;\text{ where }\; h(\mathbf{x},t) = \eta(\mathbf{x},t) - Z_b(\mathbf{x},t) \tag{12}$$

$\psi'$ is the fluctuation with respect to the average. It value is $\psi' = \psi - \overline{\psi}$ and clearly the average of fluctuation $\psi'$ is zero. $h$ and $Z_b$ and $\eta$ are the water depth, bed level and the free surface respectively (see below).

The Leibniz's relations are also used to derive the model:

$$\frac{\partial h\overline{\psi}}{\partial x} = \frac{\partial}{\partial x}\int_{Z_b}^{\eta}\psi dz = \int_{Z_b}^{\eta}\frac{\partial \psi}{\partial x}dz - \psi(\eta)\frac{\partial \eta}{\partial x} + \psi(Z_b)\frac{\partial Z_b}{\partial x}, \tag{13}$$

and

$$\frac{\partial h\overline{\psi}}{\partial t} = \frac{\partial}{\partial x}\int_{Z_b}^{\eta}\psi dz = \int_{Z_b}^{\eta}\frac{\partial \psi}{\partial t}dz - \psi(\eta)\frac{\partial \eta}{\partial x} + \psi(Z_b)\frac{\partial Z_b}{\partial t}. \tag{14}$$

The hydrostatic approximation used in the modeling leads to:

$$\frac{\partial \mathbf{P}}{\partial z} = -\rho g \Rightarrow \mathbf{P} - \mathbf{P}_a = -\rho g(z-\eta) \tag{15}$$

$$\Rightarrow \mathbf{P} = \mathbf{P}_a - \rho g(z-\eta) \tag{16}$$

$$\tag{17}$$

The pressure term in horizontal momentum equations obtained reads:

$$\begin{aligned} \nabla \mathbf{P} &= \nabla \rho g(\eta - z) = \rho g \nabla \eta - g(\eta - z)\nabla \rho, \\ \frac{1}{\rho}\nabla \mathbf{P} &= g\nabla \eta - g(\eta - z)\nabla \rho. \end{aligned} \tag{18}$$

Now the horizontal momentum equation takes the form

$$\frac{\partial \mathbf{u}}{\partial t} + \nabla.(\mathbf{u} \otimes \mathbf{u}) + \frac{\partial (uw)}{\partial z} + \frac{1}{\rho}\nabla \mathbf{P} = \mathcal{F} \tag{19}$$

Integrating the divergence-free equation over the depth of water and using the Leibniz relations we obtain the mass and momentum conservation equations. The derived system constitutes the hydrodynamic sub-model. The final model is obtained by adding sediment transport equations (bedload equation and sediment concentration equation) to the hydrodynamic sub-model.

### *2.1 Hydrodynamic sub-model*

The hydrodynamic sub-model reads:

$$\frac{\partial h}{\partial t} + \nabla.(h\mathbf{u}) = \frac{(E-D)}{(1-p)}, \tag{20a}$$

$$\frac{\partial h\mathbf{u}}{\partial t} + \nabla.\left(\mathbf{q} \otimes \mathbf{u} + \frac{1}{2}gh^2\mathbf{I}\right) = -gh\nabla Z_b^* - -\frac{1}{2\rho}gh^2(\rho_s - \rho_w)\nabla C - \frac{(E-D)}{(1-p)}\mathbf{u} - ghS_f. \tag{20b}$$

Here, $\mathbf{u} = (u, v)$ is the horizontal velocity vector with the depth-averaged components $u$ and $v$ along the coordinates axis and $\mathbf{q} = (q_1, q_2) = (hu, hv) = h\mathbf{u}$ is the mass flux. $\mathbf{I}$ is the identity square matrix in $\mathbb{R}^2$. $Z_b^* = Z_b + B$ is the total bed level, $B$ is the non erodible bed and $Z_b$ is the mobile bed level (see Fig. (1)). The mixture density $\rho = C\rho_s + (1-C)\rho_w$ where $C$ is averaged sediment volume concentration (see below). The momentum flux is $\mathbf{q}\otimes\mathbf{u} + \frac{1}{2}gh^2\mathbf{I}$ and the pressure is assumed hydrostatic. The gradient operator $\nabla$ is defined by $\nabla = (\frac{\partial}{\partial x}, \frac{\partial}{\partial y})$ and the divergence is noted by $\nabla.(.)$. The erosion/deposition exchange is represented by $\frac{(E-D)}{(1-p)}$, $p$ being the bed porosity, $E$ and $D$ are respectively the erosion and deposition rates. In the system (20b), $(S_{Fx}, S_{Fy})^T = -gh(S_{fx}, S_{fy})^T$ are the friction term components, which depend on the flow regime. When the flow is turbulent, Darcy-Weisbach law can be used:

$$(S_{fx}, S_{fy}) = \frac{n\|\mathbf{u}\|(u, v)}{8gh}, \tag{21}$$

where $n$ is the Darcy-Weisbach friction factor.

Eq. (20a) for $\frac{(E-D)}{(1-p)} = 0$ is the Lagrangian form of mass conservation equation:

$$\frac{\partial h}{\partial t} + \nabla.(h\mathbf{u}) = 0. \tag{22}$$

Note that $h\mathbf{u}$ in (22) and $\mathbf{q}$ in (20b) are different in their role. The system (20) is named generalized Shallow Water/Sediment model. Yet, for steady state or unsteady solutions, the continuity equation (22) degenerates to a constraint $\nabla.(h\mathbf{u})$ i.e. the depth-integrated velocity is a solenoidal filed. We have:

$$\nabla.(\mathbf{u} \otimes \mathbf{q}) = (\mathbf{u}.\nabla)\mathbf{q} + \mathbf{q}(\nabla.\mathbf{u}). \tag{23}$$

The first term of RHS in Eq. (23) is associated to the background flow and the second term is closely linked to the change in the water depth along flow path. Illustrating how the change in the depth $h$ are insert wined. We observe that the divergence $\nabla.(\mathbf{u} \otimes \mathbf{q})$ contains $(\mathbf{q}.\nabla)\mathbf{u}$ and $(\nabla.\mathbf{q})\mathbf{u}$. Moreover, the term $(\nabla.\mathbf{q})\mathbf{u}$ characterizes the wave propagation and $(\nabla.\mathbf{q})\mathbf{u} + gh\nabla\eta$ is the wave-like propagation on top of the background flow. This means that the depth-averaged velocity $\mathbf{u} = \mathbf{q}/h$ is transported by the mass flux $\mathbf{q}$.

*2.2 Sediment transport equations.*

Here, we expose the sediment concentration equation described in the layer of suspended sediment particles and the bedload equation in the bottom layer. We choice an Eulerian approach for both equations.

**Sediment concentration equation**

The averaged equation governing the sediment concentration reads:

$$\frac{\partial hC}{\partial t} + \nabla.\,(h\mathbf{u}_{adv}C) = \nabla.\,(\nu_s f h \nabla C) + E - D \tag{24}$$

The diffusion term is obtained by using Darcy's law into the averaged density evolution equation. Really, the advection velocity is given by $\mathbf{u}_{adv} = F_{corr}\mathbf{u}$, where $F_{corr}$ convert the averaged velocity into advection velocity [26]:

$$F_{corr} = \frac{I_2 - \log(B/30)I_1}{I_1 \log(eB/30)}, \tag{25}$$

where $I_1$, $I_2$ are given by [14]:

$$I_1 = \begin{cases} \dfrac{1}{1-Ro}(1 - B^{1-Ro}), & Ro \neq 1 \\ -\log(B), & Ro = 1 \end{cases}, \quad \text{and} \quad I_2 = \begin{cases} \dfrac{I_1 + \log(B)B^{1-Ro})}{Ro-1}, & Ro \neq 1 \\ -0.5(\log(B))^2, & Ro = 1, \end{cases}$$

where $B = \dfrac{h}{k_s}$ with $k_s$ is bed roughness taken as in [32]. For sake simplicity, we take $F_{corr} = 1$ in all the tests. The function $f$ is the sediment mode parameter introduced to represent the percentage of sediments transported by the suspended load. We adopt the following relation[21]

$$f = \min\{1,\ 2.5e^{-Ro}\}, \tag{26}$$

where $Ro = \dfrac{W_s}{\kappa \mathbf{u}_*}$ is the Rouse number used to define the mode of sediment transport (bed-load or suspension), $\kappa = 0.4$ is Von Karman number, $\mathbf{u}_*$ is the bottom velocity and $W_s$ being the settling velocity given by [42]:

$$W_s = \sqrt{(\frac{13.95\nu}{d_{50}})^2 + 1.09sgd_{50}} - 13.95\frac{\nu}{d_{50}},$$

where $d_{50}$ is the sediment diameter and where $\nu$ is the clear water viscosity. The parameter $\mathbf{s} = \dfrac{\rho_s}{\rho_w} - 1$ is the submerged specific gravity of sediment.

**Bed evolution equation**

By assuming that $\mathbf{u}(t, \mathbf{x}, Z_b^*)\nabla Z_b^*(\mathbf{x}, t) - w(t, \mathbf{x}, Z_b^*) \to \dfrac{1}{1-p}\nabla q_b$, the bed-load equation given by (11) is replaced by the Exner's equation. Here, $q_b$ is the horizontal sediment transport rate. Following Eq.(11), the bedload equation can be rewritten as:

$$\frac{\partial Z_b^*}{\partial t} + \frac{1}{1-p}\frac{\partial q_{b1}}{\partial x} + \frac{1}{1-p}\frac{\partial q_{b2}}{\partial y} = -\frac{(E-D)}{1-p}, \tag{27}$$

where $q_{b1}$, $q_{b2}$ denote volumetric sediment transport rates per unit width along the cartesian coordinates. Therefore, the morphodynamic sub-model using a Grass approximation reads:

$$\frac{\partial Z_b^*}{\partial t} + \frac{Ag}{1-p}\frac{\partial}{\partial x}\left(\frac{(hu)\left[(hu)^2 + (hv)^2\right]}{h^3}\right) + \frac{Ag}{1-p}\frac{\partial}{\partial y}\left(\frac{(hv)\left[(hu)^2 + (hv)^2\right]}{h^3}\right) = -\frac{(E-D)}{1-p}, \tag{28}$$

where $A_g[s^2/m]$ represents the intensity of fluid/sediment interaction and where we have denoted $q_b = (q_{b1},\ q_{b2}) = (hu, hv)\left(\frac{[(hu)^2+(hv)^2]}{h^3}\right)$.

Exner based equation for the conservation of mass of sediment given by (28) states that the rate of change of bed elevation within a control volume is driven by the sediment fluxes crossing the boundaries of that volume and the erosion/deposition exchange.

**Closure model**

In above equations, $D$ is the deposition rate [10]:

$$D = W_s(1-C_a)^{\mathbf{m}}C_a, \tag{29}$$

where $\mathbf{m}$ is a parameter indicating the hindered influence of high sediment concentrations on settling velocity. The function $C_a$ is the local near-bed uniform sediment concentration in volume, which can be determined for uniform grain size as:

$$C_a = \alpha_c C, \tag{30}$$

where $\alpha_c$ is given as in [10]:

$$\alpha_c = \min\{2, \frac{1-p}{c}\}.$$

The erosion rate $E$ is calculated in as [2]:

$$E := \begin{cases} \dfrac{\varphi(\theta-\theta_{cr})\sqrt{u^2+v^2}}{hd^{0.2}}, & \theta > \theta_{cr} \\ 0, \quad \text{otherwise} \end{cases} \tag{31}$$

For sediment entrainment $E$, $\varphi[m^{1.2}]$ is the coefficient that controls the erosion force. The function $\theta_{cr}$ is the critical value of Shields parameter $\theta$ defined by

$$\theta = \frac{\mathbf{u}_*}{gsd_{50}}, \tag{32}$$

where, $\mathbf{u}_*$ is the function velocity defined using the manning coefficient $\mathbf{u}_* = \sqrt{C_f\mathbf{u}^2}$. Another formulation account the sediment supply condition can be given (for dunes):

$$\mathbf{u}_* = \frac{\mathbf{u}}{6+2.5\ln(\frac{h}{k_s})}, \tag{33}$$

where $k_s$ is a roughness coefficient depending on sediment supply condition [32].

### *2.3 Nonconservative form of the model*

The final two-dimensional sediment transport model in generalized shallow water equations reads:

$$\frac{\partial h}{\partial t} + \nabla.(h\mathbf{u}) = \frac{(E-D)}{1-p}, \tag{34a}$$

$$\frac{\partial h\mathbf{u}}{\partial t} + \nabla.\left(h\mathbf{u}\otimes\mathbf{u} + \frac{1}{2}gh^2\mathbf{I}\right) + gh\nabla Z_b^* + -\frac{1}{2\rho}gh^2(\rho_s-\rho_w)\nabla C = -\frac{(E-D)}{(1-p)}\mathbf{u} - ghS_f, \tag{34b}$$

$$\frac{\partial hC}{\partial t} + \frac{\partial F_{corr}huC}{\partial x} + \frac{\partial F_{corr}hvC}{\partial y} = \nabla.(h\nu_s f\nabla C) + (E-D), \tag{34c}$$

$$\frac{\partial Z_b}{\partial t} + \frac{Ag}{1-p}\frac{\partial}{\partial x}\left(\frac{(hu)\left[(hu)^2+(hv)^2\right]}{h^3}\right) + \frac{Ag}{1-p}\frac{\partial}{\partial y}\left(\frac{(hv)\left[(hu)^2+(hv)^2\right]}{h^3}\right) = -\frac{(E-D)}{1-p}, \tag{34d}$$

$$\frac{\partial B}{\partial t} = 0. \tag{34e}$$

The proposed model can be seen as an extension of those proposed by Clare et al.,[14], Greimann et al.,[21], Huybrechts et al.,[26], Huabin et al.,[27], Holly et al.,[25]. It very similar to the one recently developed by Ngatcha et al.,[32]. Moreover, it extends the model developed b y Cao et al.,[10] and its extensions used in some papers such as [2], [30] and [49]. The proposed model can reformulate in nonconservative form as:

$$\begin{cases} \dfrac{\partial \mathbf{W}}{\partial t} + \dfrac{\partial F_1(\mathbf{W})}{\partial x} + \dfrac{\partial F_2(\mathbf{W})}{\partial y} = T_1(\mathbf{W})\dfrac{\partial \mathbf{W}}{\partial x} + T_2(\mathbf{W})\dfrac{\partial \mathbf{W}}{\partial y} + Q_1(\mathbf{W})\dfrac{\partial \mathbf{W}}{\partial x} + Q_2(\mathbf{W})\dfrac{\partial \mathbf{W}}{\partial y} \\ +S_1(W)\dfrac{\partial \mathbf{W}}{\partial x} + S_2(W)\dfrac{\partial \mathbf{W}}{\partial y} + S_e(\mathbf{W}) + S_D(\mathbf{W}) + S_F(\mathbf{W}) \quad x, y \in \Omega \subset \mathbb{R},\ t \in ]0, T]. \end{cases} \tag{35}$$

Here, $x, y \in \Omega \subset \mathbb{R}^2, t \in (0, T)$, $W = \begin{pmatrix} h \\ hu \\ hv \\ hC \\ Z_b \end{pmatrix}$ is the vector containing the conserved variables and $\mathbf{W} = (W, B)$.

The functions $F_{1,2}(W, B)$ are the physical fluxes on both x,y-directions given by:

$$F_1(W,B) = \begin{pmatrix} hu \\ hu^2 + 1/2gh^2 \\ huv \\ F_{corr} huC \\ \widetilde{q}_{b1} \\ 0 \end{pmatrix}, \quad F_2(W,B) = \begin{pmatrix} hv \\ huv \\ hv^2 + 1/2gh^2 \\ F_{corr} hvC \\ \widetilde{q}_{b2} \\ 0 \end{pmatrix}, \tag{36}$$

where $(\widetilde{q}_{b1}, \widetilde{q}_{b1}) = \dfrac{A_g}{1-p}(q_{b1}, q_{b1})$ and where $\dfrac{\partial F_k(W,B)}{\partial B} = 0,\ k = 1, 2$. The nonconservative vectors read:

$$T_1(W,B) = \begin{pmatrix} 0 \\ -gh \\ 0 \\ 0 \\ 0 \\ 0 \end{pmatrix}, \quad T_2(W,B) = \begin{pmatrix} 0 \\ 0 \\ -gh \\ 0 \\ 0 \\ 0 \end{pmatrix}$$

$$Q_1(W,B) = \begin{pmatrix} 0 \\ -gh^2 \dfrac{\rho_w - \rho_s}{2\rho} \\ 0 \\ 0 \\ 0 \\ 0 \end{pmatrix}, \quad Q_2(W,B) = \begin{pmatrix} 0 \\ 0 \\ -gh^2 \dfrac{\rho_w - \rho_s}{2\rho} \\ 0 \\ 0 \\ 0 \end{pmatrix}, \quad S_1(W) = \begin{pmatrix} 0 \\ -gh \\ 0 \\ 0 \\ 0 \\ 0 \end{pmatrix}, \quad S_2(W) = \begin{pmatrix} 0 \\ 0 \\ -gh \\ 0 \\ 0 \\ 0 \end{pmatrix}.$$

The bottom friction, the erosion/deposition exchange and diffusion source terms are defined respectively by:

$$S_F = \begin{pmatrix} 0 \\ -ghS_{fx} \\ -ghS_{fy} \\ 0 \\ 0 \\ 0 \end{pmatrix}, \quad S_e = \begin{pmatrix} \dfrac{(E-D)}{(1-p)} \\ -\dfrac{(E-D)}{(1-p)}u \\ -\dfrac{(E-D)}{(1-p)}v \\ E - D \\ -\dfrac{E-D}{1-p} \\ 0 \end{pmatrix} \quad \text{and} \quad S_D = \begin{pmatrix} 0 \\ 0 \\ 0 \\ \dfrac{\partial}{\partial x}\left(h\nu_s f \dfrac{\partial C}{\partial x}\right) + \dfrac{\partial}{\partial y}\left(h\nu_s f \dfrac{\partial C}{\partial y}\right) \\ 0 \\ 0 \end{pmatrix}.$$

The smooth solution must satisfy some positivity constraints which lead to the following solution space for physically admissible solutions

$$\mathcal{W} = \left\{ \mathbf{W} \in \mathbf{R}^6, \quad h > 0, C > 0 \right\},$$

The Jacobian matrix of the system reads:

$$\mathcal{A}_k(\mathbf{W}) = A_k(\mathbf{W}) - T_k(\mathbf{W}) - Q_k(\mathbf{W}) - S_k(W), \quad k = 1, 2. \tag{37}$$

where $A_k(\mathbf{W}) = \dfrac{\partial F_k(\mathbf{W})}{\partial \mathbf{W}}$. We note that

$$\mathcal{A}_\mathbf{n} = \mathcal{A}.\mathbf{n} = \mathcal{A}_1.\mathbf{n}_1 + \mathcal{A}_2.\mathbf{n}_2, \tag{38}$$

where $\mathbf{n} = (\mathbf{n}_1, \mathbf{n}_2)$ is unit normal vector.

*2.4 Steady state solution*

We develop steady-state solutions for the one-dimensional sediment transport in a nonhomogeneous shallow water system obtained from our proposed model. We start by computing the steady-state solution in the 1D case. In situations when the erosion/deposition effects are zero($E - D = 0$), the stationary solutions satisfying $\dfrac{dW}{dt} = 0$ can be obtained:

$$h \equiv \text{constant}, \quad hu \equiv \text{constant in time}, \quad Z_b^* \equiv \text{constant in time}, \quad C \equiv \text{constant in time}, \quad \rho \equiv \text{constant in time}. \tag{39}$$

If we assume that:

$$hu \equiv q_0, \quad \partial_x Z_b^* \equiv -K_0, \quad \partial_x C \equiv -H_0, \quad \rho \equiv \rho_0. \tag{40}$$

The last equation of (40), corresponds to saturated sediment medium. According to Eq(40), we obtain the constant water depth $h_0$ defined by:

$$F(h_0) = 0, \quad \text{with} \quad F(h_0) = \frac{g\delta\rho H_0}{\rho_0} h_0^4 + gK_0 h_0^3 - \frac{nq_0^2}{8}. \tag{41}$$

The structure of 2D steady-state is not easy, but it is possible to find a quasi 1D steady-state solutions:

$$\begin{aligned} h &\equiv \textit{constant}, \quad hu \equiv \textit{constant}, hv \equiv 0, \quad \partial_x Z_b^* \equiv \text{constant in time}, \quad \partial_y Z_b^* \equiv 0, \\ \partial_x C &\equiv \text{constant in time}, \partial_y C \equiv 0, \quad \rho \equiv \text{constant in time}, \end{aligned} \tag{42}$$

or

$$\begin{aligned} h &\equiv \textit{constant}, \quad hv \equiv \textit{constant}, hu \equiv 0, \quad \partial_y Z_b^* \equiv \text{constant in time}, \quad \partial_x Z_b^* \equiv 0, \\ \partial_y C &\equiv \text{constant in time}, \partial_x C \equiv 0, \quad \rho \equiv \text{constant in time}. \end{aligned} \tag{43}$$

When the bed $Z_b^*$ and the sediment concentration $C$ are constant in time, we set $Z_b^*(x, y, t) = Z_b^*(x, y)$ and $C(x, y, t) = C(x, y)$.

## 3 Finite volume methods

In this section, we develop a WBPP path-conservative central-upwind scheme. We start with considering an open bounded interval of $\mathbb{R}$, denoted by $\Omega$ and representing the flow domain. A uniform grid $\{x_i = i\,\Delta x\}_{i\in I}$ is defined on $\overline{\Omega}$ (recall that $\overline{\Omega}$ is the closure of $\Omega$ in the topological sense), where $\Delta x$ is the grid size. The associated finite-volume cells $K_i$ (named also control-volumes) are defined as: $K_i = [x_{i-1/2}, x_{i+1/2}]$. These control-volumes should meet the following condition $\overline{\Omega} = \bigcup_{i=1}^{N} K_i$, where $N = Card(I)$ is a given nonnegative integer assigned to tend to $+\infty$. The family of control-volumes $K_i$ is denoted by $\mathcal{T}$. Sometimes $\Delta x$ is called the size of $\mathcal{T}$. We assume that at any time $t \geq 0$ the average (in space) $\overline{W}_i(t)$ of the solution over any control-volume $K_i$ is available. Recall that $\overline{W}_i(t) = \dfrac{1}{\Delta x} \int_{K_i} W(x, t)dx$. $\overline{W}_i$ interpreted as the average of $\widetilde{W}$ (a piecewise constant approximation for all $x \in K$ of $W(x, t)$ at time $t + \Delta t$). The design of CU scheme in path-conservative framework requires the choice of sufficiently smooth paths in the normed space $\mathbb{R}^6$

*3.1 A well-balanced CU scheme*

In this subsection, we begin by develop a CU scheme in path-conservative version for the one-dimensional version of the proposed model:

$$\frac{\partial \mathbf{W}}{\partial t} + A_1(\mathbf{W}) = \mathcal{S}(\mathbf{W}(x,t)); \quad x \in \Omega \subset \mathbb{R}, t \in ]0,T] \tag{44}$$

Here, $\mathbf{W} = (W, B)$ is the unknown vector, $F(\mathbf{W}) = F_1(\mathbf{W})$ is the physical flux and $A_1(\mathbf{W}) = \dfrac{\partial F_1(\mathbf{W})}{\partial x}$. The source term expresses as:

$$\mathcal{S} = S_0(\mathbf{W}) + S(W) + S_c(\mathbf{W}) + S_e(\mathbf{W}) + S_D(\mathbf{W}) + S_F(\mathbf{W}),$$

where $S_0,\ S_c,\ S$ are respectively given by:

$$S_0 = \begin{pmatrix} 0 \\ -gh\dfrac{\partial Z_b}{\partial x} \\ 0 \\ 0 \\ 0 \\ 0 \end{pmatrix}, \quad S_c = \begin{pmatrix} 0 \\ -\dfrac{gh^2(\rho_s - \rho_w)}{2\rho}\dfrac{\partial C}{\partial x} \\ 0 \\ 0 \\ 0 \\ 0 \end{pmatrix}, \quad S = \begin{pmatrix} 0 \\ -gh\dfrac{\partial B}{\partial x} \\ 0 \\ 0 \\ 0 \\ 0 \end{pmatrix} \tag{45}$$

The first-order semi-discrete CU scheme for quasi 1-D model reads:

$$\frac{1}{\Delta x}\frac{d}{dt}\left(\int_{K_i} W(x,t)dx\right) = -\left(\frac{\mathcal{F}_{i+1/2}(t) - \mathcal{F}_{i-1/2}(t)}{\Delta x} - \mathcal{S}(\overline{W}_i(t))\right), K_i \in \mathcal{T}, i \in \mathbb{Z}. \tag{46}$$

Here, the CU flux $\mathcal{F}_{i+1/2}$ reads:

$$\mathcal{F}_{i+1/2} = \frac{1-\alpha_1^{i+1/2}}{2}F(\mathbf{W}^+_{i+1/2}) + \frac{1+\alpha_1^{i+1/2}}{2}F(\mathbf{W}^-_{i+1/2}) - \frac{\alpha_0^{i+1/2}}{2}\left(W^+_{i+1/2} - W^-_{i+1/2}\right), \quad i \in \mathbb{Z}. \tag{47}$$

where

$$F(\mathbf{W}) = \begin{pmatrix} hu \\ hu^2 + \dfrac{1}{2}gh^2 \\ huv \\ F_{corr}huC \\ \dfrac{1}{1-p}\left(\dfrac{(hu)\left[(hu)^2 + (hv)^2\right]}{h^3}\right) \\ 0 \end{pmatrix}. \tag{48}$$

**Remark 3.1.** *and where*

$$\alpha_0^{i+1/2} = \frac{-2a^+_{i+1/2}a^-_{i+1/2}}{a^+_{i+1/2} - a^-_{i+1/2}}, \quad \alpha_1^{i+1/2} = \frac{a^+_{i+1/2} + a^-_{i+1/2}}{a^+_{i+1/2} - a^-_{i+1/2}}, \tag{49}$$

*The one-sided local speeds of propagation $a^{\pm}_{i+1/2}$ are upper/lower bounds on the largest/smallest eigenvalues of Jacobian matrix of the system $\mathcal{A}_1$ determined by the polynomial characteristic given at first order approximation by:*

$$\begin{aligned} a^+_{i+1/2} &= \min\left\{\lambda_1(\mathcal{A}_1(\boldsymbol{W}^+_{i+1/2})), \lambda_1(\mathcal{A}_1(\boldsymbol{W}^-_{i+1/2})), 0\right\}, \\ a^-_{i+1/2} &= \max\left\{\lambda_6(\mathcal{A}_1(\boldsymbol{W}^+_{i+1/2})), \lambda_6(\mathcal{A}_1(\boldsymbol{W}^-_{i+1/2})), 0\right\}. \end{aligned} \tag{50}$$

In absence of sediment flux $q_b$, the eigenvalues of the quasi-1D system are given by:

$$\lambda_{1,6} = u \pm \sqrt{gh},\ \lambda_{2,3} = 0,\ \lambda_4 = u,\ \lambda_5 = F_{corr}u. \tag{51}$$

Thus the semi-discrete CU scheme can be rewritten in term of fluctuations as:

$$\begin{aligned} \frac{d}{dt}\overline{\mathbf{W}}_i(t) &= -\left(\frac{\mathcal{F}_{i+1/2}(t) - (F(\mathbf{W}^+_{i-1/2}) - F(\mathbf{W}^-_{i+1/2})) - \mathcal{F}_{i-1/2}(t) + (F(\mathbf{W}^+_{i-1/2}) - F(\mathbf{W}^-_{i+1/2}))}{\Delta x}\right) + \mathcal{S}(\overline{\mathbf{W}}_i(t)) \\ &= \left(\frac{\mathcal{D}^-_{i+1/2} + \mathcal{D}^+_{i-1/2} - (F(\mathbf{W}^+_{i-1/2}) - F(\mathbf{W}^-_{i+1/2}))}{\Delta x}\right) + \mathcal{S}(\overline{\mathbf{W}}_i(t)), \end{aligned} \tag{52}$$

where $\mathcal{D}^{\pm}_{i+1/2}$ are the fluctuations given by:

$$\mathcal{D}^-_{i+1/2} = \mathcal{F}_{i+1/2} - F(\mathbf{W}^-_{i+1/2}), \quad \text{and} \quad \mathcal{D}^+_{i+1/2} = -\mathcal{F}_{i+1/2} + F(\mathbf{W}^+_{i+1/2}). \tag{53}$$

Particularly, the condensed form of the definition of fluctuations for CU scheme is written as follows:

$$\mathcal{D}^{\pm}_{i+1/2} = \frac{1+\alpha_1^{i+1/2}}{2}\int_0^1 A_1(\mathbf{\Psi}_{i+1/2}(s))\frac{d\mathbf{\Psi}_{i+1/2}}{ds}ds \pm \frac{\alpha_0^{i+1/2}}{2}\left(W^+_{i+1/2} - W^-_{i+1/2}\right). \tag{54}$$

We expose this formulation to show how the CU technique does not account the nonconservative terms in the definition of fluctuations given by (53) or (68). In this semi-discrete CU scheme, we denoted $\mathbf{W}^+_{i+1/2}$ and $\mathbf{W}^-_{i+1/2}$ the left and right intermediate values of polynomial reconstruction

$$\widetilde{\mathbf{W}}(x,t) = \sum_i \mathbf{P}_i\mathcal{X}_{K_i}(x), \mathbf{P}_i = \left(P_i^{(1)}, P_i^{(2)}, ...., P_i^{(N)}\right)^T, \tag{55}$$

where $\mathcal{X}$-the characteristic function, $P_i^{(j)}$-polynomials of a certain degree satisfying the conservation and accuracy requirements defined for all $i$ by:

$$\frac{1}{\Delta x}\int_{K_i}\mathbf{P}_i(x)dx = \overline{W}_i, \ \text{ and } \ P_i^{(j)}(x) = W^{(j)}(x) + O((\Delta x)^{s_1}), \quad x \in K_i$$

with $s_1$ a (formal) order of accuracy and $\mathbf{W}(x) = (\mathbf{W}^{(1)}, ...., \mathbf{W}^{(N)})^t$-is the exact smooth solution. We are interested at boundary extrapolated values. One has:

$$\mathbf{W}^-_{i+1/2} = \widetilde{\mathbf{W}}(x_{i+1/2}, 0) = \mathbf{P}_i(x_{i+1/2}), \quad \mathbf{W}^+_{i+1/2} = \widetilde{\mathbf{W}}(x_{i+1/2}, 0) = \mathbf{P}_{i+1}(x_{i+1/2}). \tag{56}$$

Here, $\mathbf{W}^-_{i+1/2}$ and $\mathbf{W}^+_{i+1/2}$ are connected via Riemann fan by $\gamma(\mathbf{W}^+_{i+1/2}, \mathbf{W}^-_{i+1/2})$ (a curve in phase space). For some smooth $\mathbf{W}$, we have:

$$\mathbf{W}^{\pm}_{i+1/2} = \mathbf{W}(x_{i+1/2}) + \mathcal{O}(|K_i|^s), \quad \forall i \in \mathbb{Z}. \tag{57}$$

At the first order we have:

$$\mathbf{W}^-_{i+1/2} = \mathbf{W}_i \ \text{ and } \ \mathbf{W}^+_{i+1/2} = \mathbf{W}_{i+1}. \tag{58}$$

Note that the quantities $\mathbf{W}_i$, $\mathbf{W}^{\pm}_{i+1/2}$, $a^{\pm}_{i+1/2}$ are the quantities depending on time, but we simplify the notation by suppressing this dependence. The source terms are discretized in well-balanced sense as follows:

$$\begin{aligned} (S_c)_i^{(2)} &= -\frac{(\rho_s - \rho_w)\,g}{2\overline{\rho}_i}\left[\left(h^-_{i+1/2} + h^+_{i+1/2}\right)\left((hC)^-_{i+1/2} - (hC)^+_{i-1/2}\right)\right. \\ &- \left.\left((hC)^-_{i+1/2} + (hC)^+_{i+1/2}\right)\left(h^-_{i+1/2} - h^+_{i-1/2}\right)\right] \end{aligned} \tag{59}$$

$$(S_0)_i^{(2)} = \frac{g}{2}\left(h^-_{i+1/2} + h^+_{i+1/2}\right)\left(Z^-_{b,i+1/2} - Z^+_{b,i-1/2}\right), \tag{60}$$

**Remark 3.2.** *The semi-discrete well-balanced CU scheme for the 1D proposed model is given by (48), (53), (55), (56),(58), (50) and (59). This scheme does not account the nonconservative products present in the model that modify the wave speed propagation. It important to design a numerical scheme that take in consideration these terms.*

### *3.2 A one-dimensional PCCU scheme.*

In this section, we develop a new PCCU scheme for 1D version of the proposed model. The designed scheme is an extension of the one developed in Ngatcha and Njifenjou [35] (see also [32]). A quasi-1D nonconservative problem derived from our model reads:

$$\frac{\partial \mathbf{W}}{\partial t} + \mathcal{A}(\mathbf{W})\frac{\partial \mathbf{W}}{\partial x} = S_e(\mathbf{W}) + S_D(\mathbf{W}) + S_F(\mathbf{W}), \quad x \in \Omega \subset \mathbb{R}, t \in ]0T], T > 0, \tag{61}$$

where $\mathcal{A}(\mathbf{W}) = \mathcal{A}_1(\mathbf{W}) = \dfrac{\partial F_1(\mathbf{W})}{\partial W} - T_1(\mathbf{W}) - Q_1(\mathbf{W}) - S_1(W)$, $T_1 = T$, $Q_1 = Q$, $S_1 = S$.

We start by choosing the linear path $\mathbf{\Psi}$:

$$\mathbf{\Psi}_{i+1/2}(s) = \left(\Psi^{(1)}_{i+1/2}, \Psi^{(2)}_{i+1/2}, ...., \Psi^{(N)}_{i+1/2}, \Psi^{(N+1)}_{i+1/2}\right) := \mathbf{\Psi}(s, \mathbf{W}^+_{i+1/2}, \mathbf{W}^-_{i+1/2}).$$

Next, we defined the discretization of nonconservative terms using these paths. The nonconservative vectors $T_1 = T$ and $Q_1 = Q$ are associated to multiple paths $(\Psi^{(1)}_{i+1/2}, \Psi^{(2)}_{i+1/2}, ...., \Psi^{(N)}_{i+1/2})$ and the fixe topography vector $S_1 = S$ is associated only to $(\Psi^{(N+1)}_{i+1/2})$.

These linear paths connect both states $\mathbf{W}^+_{i+1/2}$ and $\mathbf{W}^-_{i+1/2}$ across the jump discontinuity at $\mathbf{x} = \mathbf{x}_0$, such that a local-Lipschitz application $\mathbf{\Psi} : [0,\ 1] \times \Omega \times \Omega \to \Omega$ satisfies the following property:

$$\mathbf{\Psi}(0, \mathbf{W}^-_{i+1/2}, \mathbf{W}^+_{i+1/2}) = \mathbf{W}^-_{i+1/2} \text{and} \quad \mathbf{\Psi}(1, \mathbf{W}^-_{i+1/2}, \mathbf{W}^+_{i+1/2}) = \mathbf{W}^+_{i+1/2}, \ \text{ for all } \ \mathbf{W}^-_{i+1/2}, \mathbf{W}^+_{i+1/2} \in \Omega. \tag{62}$$

We can define a nonconservative product $[X\partial_x Y]$, with $X \in \mathbb{R}^N, N > 0$ and $Y \in \mathbb{R}$ as:

$$[X.\partial_x Y]_\Phi = \left[\int_0^1 X(\mathbf{\Psi}(s, W^-_{i+1/2}, W^+_{i+1/2}))\frac{d\mathbf{\Psi}}{ds}(s, Y^-_{i+1/2}, Y^+_{i+1/2})ds\right] = X_{\mathbf{\Psi}_{i+1/2}}. \tag{63}$$

Now, we will noted by $M_{\mathbf{\Psi}_{i+1/2}}, M = T, Q, S$ to represent the nonconservative contribution terms at discrete level. This definition is similar to the one proposed by Volpert [47] for the nonconservative product. We take a particular example of the simplest linear segment paths:

$$\mathbf{\Psi}_{i+1/2}(s) = \mathbf{W}^-_{i+1/2} + s(\mathbf{W}^+_{i+1/2} - \mathbf{W}^-_{i+1/2}), \quad s \in [0, 1]. \tag{64}$$

The jump condition using the definition of paths reads:

$$\begin{aligned}
&\int_0^1 \mathcal{A}(\mathbf{\Psi}(s, \mathbf{W}^-_{i+1/2}, \mathbf{W}^+_{i+1/2}))\frac{d\mathbf{\Psi}}{ds}(s, \mathbf{W}^-_{i+1/2}, \mathbf{W}^+_{i+1/2})ds \\
&= [A(\mathbf{W})\partial_x \mathbf{W}]_{\mathbf{\Psi}} - [T(\mathbf{W})\partial_x Z_b]_{\mathbf{\Psi}} - [Q(\mathbf{W})\partial_x C]_{\mathbf{\Psi}} - [S(\mathbf{W})\partial_x B]_{\mathbf{\Psi}} \\
&= F(\mathbf{W}^+_{i+1/2}) - F(\mathbf{W}^-_{i+1/2}) + T(\mathbf{W}^+_{i+1/2}, \mathbf{W}^-_{i+1/2})(Z^+_{b,i+1/2} - Z^-_{b,i+1/2}) \\
&+ Q(\mathbf{W}^+_{i+1/2}, \mathbf{W}^-_{i+1/2})(C^+_{i+1/2} - C^-_{i+1/2}) + S(\mathbf{W}^+_{i+1/2}, \mathbf{W}^-_{i+1/2})(B_{i+1/2} - B_{i-1/2}) \\
&= \sigma(\mathbf{W}^+_{i+1/2} - \mathbf{W}^-_{i+1/2}),
\end{aligned} \tag{65}$$

where $\sigma$ is speed of discontinuity. The LHS term of (65) is the fluctuation which is split right moving waves arising in the Riemann solution the fluctuation is defined by:

$$\mathcal{D}(\mathbf{W}^+_{i+1/2}, \mathbf{W}^-_{i+1/2}) = \int_0^1 \mathcal{A}(\mathbf{\Psi})\frac{d\mathbf{\Psi}}{ds}ds = \mathcal{D}^-(\mathbf{W}^+_{i+1/2}, \mathbf{W}^-_{i+1/2}) + \mathcal{D}^+(\mathbf{W}^+_{i+1/2}, \mathbf{W}^-_{i+1/2}), \tag{66}$$

where $\mathcal{D}^-(\mathbf{W}^+_{i+1/2},\mathbf{W}^-_{i+1/2})$, $\mathcal{D}^+(\mathbf{W}^+_{i+1/2},\mathbf{W}^-_{i+1/2})$ represents the difference between the numerical flux and the physical flux at both sides of the cell interface and are computed using Central-Upwind technique. In Eq.(65), we have used a quadrature method to compute the integral for all the nonlinear functions associated to nonconservative terms:

$$\begin{aligned} T(\mathbf{W}^+_{i+1/2},\mathbf{W}^-_{i+1/2}) &= \int_0^1 T(\mathbf{\Psi}_{i+1/2}(s))ds = \overline{T}(\frac{\mathbf{W}^+_{i+1/2}+\mathbf{W}^-_{i+1/2}}{2}), \\ Q(\mathbf{W}^+_{i+1/2},\mathbf{W}^-_{i+1/2})(C^+_{i+1/2}-C^-_{i+1/2}) &= \int_0^1 Q(\mathbf{\Psi}_{i+1/2}(s))\frac{d\mathbf{\Psi}_{i+1/2}(s)}{ds}ds, \text{and} \\ S(W^+_{i+1/2},W^-_{i+1/2}) &= \int_0^1 S(\mathbf{\Psi}_{i+1/2}(s))ds = \overline{S}\left(\frac{W^+_{i+1/2}+W_{i-1/2}}{2}\right) \end{aligned} \tag{67}$$

Particularly, the nonconservative contribution for sediment concentration reads:

$$\begin{aligned} &\int_0^1 Q(\mathbf{\Psi}_{i+1/2}(s))\frac{d\mathbf{\Psi}_{i+1/2}(s)}{ds}ds \\ = &\left(\frac{\delta\rho}{\rho^+_{i+1/2}+\rho^-_{i+1/2}}((hC)^+_{i+1/2}-(hC)^-_{i+1/2}) - \frac{(\delta\rho)(C^+_{i+1/2}+C^-_{i+1/2})}{2(\rho^+_{i+1/2}+\rho^-_{i+1/2})}(h^+_{i+1/2}-h^-_{i+1/2})\right) T\left(\frac{\mathbf{W}^+_{i+1/2}+\mathbf{W}^-_{i+1/2}}{2}\right). \end{aligned}$$

The components of $\mathbf{\Psi}_{i+1/2}$ are: $\mathbf{\Psi}_{i+1/2} = \left(\Psi_{h,i+1/2},\Psi_{hu,i+1/2},\Psi_{hv,i+1/2}\Psi_{hC,i+1/2},\Psi_{Z_b,i+1/2},\Psi_{B,i+1/2}\right)^T$.
We have for example:

$$g[h\partial_x Z_b]_{\mathbf{\Psi}} = g\int_0^1 \Psi_h(s)\frac{\partial\Psi_{Z_b}(s)}{\partial s} = \frac{h^+_{i+1/2}+h^-_{i+1/2}}{2}((Z_b)^+_{i+1/2}-(Z_b)^-_{i+1/2}).$$

Therefore, we rewrite the fluctuations $\mathcal{D}^\pm_{i+1/2}$ for the nonconservative system as follows:

$$\mathcal{D}^\pm_{i+1/2} = \frac{1+\alpha_1^{i+1/2}}{2}\int_0^1 \mathcal{A}(\mathbf{\Psi}_{i+1/2}(s))\frac{d\mathbf{\Psi}_{i+1/2}}{ds}ds \pm \frac{\alpha_0^{i+1/2}}{2}\left(\mathbf{W}^+_{i+1/2}-\mathbf{W}^-_{i+1/2}\right). \tag{68}$$

We retrieve the fluctuation formulation for conservative systems developed in CU scheme when $\mathcal{A}=A$.

With this new formulation of fluctuation, the second order semi-discrete PCCU scheme reads:

$$\frac{d\overline{\mathbf{W}}_i(t)}{dt} = -\frac{1}{\Delta x}\left(\mathcal{D}^-_{i+1/2}+\mathcal{D}^+_{i-1/2}+F(\mathbf{W}^-_{i+1/2})-F(\mathbf{W}^+_{i-1/2})-T_i-Q_i-S_i\right)+(S_e)_i+(S_D)_i+(S_F)_i. \tag{69}$$

Here, we have used the definition of the polynomial reconstruction to compute $T_i, Q_i, S_i$:

$$\begin{aligned} T_i &= \left(\int_{K_i} T\left(\mathbf{P}_i(x)\right)dx\right)\left(Z^-_{b,i+1/2}-Z^+_{b,i-1/2}\right), \\ Q_i &= \left(\int_{K_i} Q\left(\mathbf{P}_i(x)\right)dx\right)\left(C^-_{i+1/2}-C^+_{i-1/2}\right), \\ S_i &= \left(\int_{K_i} S\left(\mathbf{P}_i(x)\right)dx\right)\left(B_{i+1/2}-B_{i-1/2}\right) \end{aligned} \tag{70}$$

where

$$M_i = \left(\int_{K_i} M\left(\mathbf{P}_i(x)\right)dx\right) = M\left(\frac{\mathbf{W}^-_{i+1/2}+\mathbf{W}^+_{i-1/2}}{2}\right), M = T, Q, S.$$

The one-dimensional semi-discrete PCCU scheme for the 1D proposed model can be rewritten as:

$$\frac{d}{dt}\overline{\mathbf{W}}_i(t) = -\frac{1}{\Delta x}\left(\mathcal{F}_{i+1/2}-\mathcal{F}_{i-1/2}\right)-\frac{1}{\Delta x}\left(-T_i-Q_i-S_i\right)-\frac{1}{\Delta x}\mathcal{H}_{\mathbf{\Psi},i+1/2}+S_D(\overline{\mathbf{W}}_i(t))+S_F(\overline{\mathbf{W}}_i(t))+S_e(\overline{\mathbf{W}}_i(t)), \tag{71}$$

where we denoted the jump contribution $\mathcal{H}_{\Psi,i+1/2}$ reads:

$$\mathcal{H}_{\mathbf{\Psi},i+1/2} = \frac{a^+_{i-1/2}}{a^+_{i-1/2} - a^-_{i-1/2}} \left[T_{\mathbf{\Psi},i-1/2} + Q_{\mathbf{\Psi},i-1/2} + S_{\mathbf{\Psi},i-1/2}\right] - \frac{a^-_{i+1/2}}{a^+_{i+1/2} - a^-_{i+1/2}} \left[T_{\mathbf{\Psi},i+1/2} + Q_{\mathbf{\Psi},i+1/2} + S_{\mathbf{\Psi},i+1/2}\right]. \quad (72)$$

The source terms $S_{D,i} = S_D(\overline{\mathbf{W}}_i(t))$ $S_{F,i} = S_F(\overline{\mathbf{W}}_i(t))$ and $S_{e,i} = S_e(\overline{\mathbf{W}}_i(t))$ are discretized as follows:

$$S_{e,i} = \begin{pmatrix} \dfrac{E-D}{1-p} \\ -\dfrac{(E-D)\overline{u}_i}{(1-p)} \\ -\dfrac{(E-D)\overline{v}_i}{(1-p)} \\ E-D \\ -\dfrac{E-D}{1-p} \\ 0 \end{pmatrix}, \quad S_{F,i} = \begin{pmatrix} 0 \\ -g\dfrac{\left(h^-_{i+1/2} + h^+_{i+1/2}\right)}{2} S_{1f,i} \\ -g\dfrac{\left(h^-_{i+1/2} + h^+_{i+1/2}\right)}{2} S_{2f,i} \\ 0 \\ 0 \\ 0 \end{pmatrix}, \quad S_{D,i} = \begin{pmatrix} 0 \\ 0 \\ 0 \\ \delta^x_i(h\nu fC) \\ 0 \\ 0 \end{pmatrix}.$$

where the operator $\delta^x_i$ expressed as $\delta^x_i(.) = \dfrac{(.)_{i+1} - (.)_i}{\Delta x}$.

**Remark 3.3.** *The Path-conservative central-upwind method is formally consistent with the particular definition of weak solutions while the original CU is only consistent with smooth solutions. The use of PCCU scheme is a great interest than the original CU-scheme. The semi-discrete PCCU scheme coincides with a semi-discrete version of path-conservative HLL Riemann solver with intermediate wave.*

**Remark 3.4** (**2D PCCU scheme on cartesian mesh**). *A simple 2D PCCU scheme on structured meshes can be derived directly without any difficulty following the methodology described in Fig. (2) and by using to the previous results.*

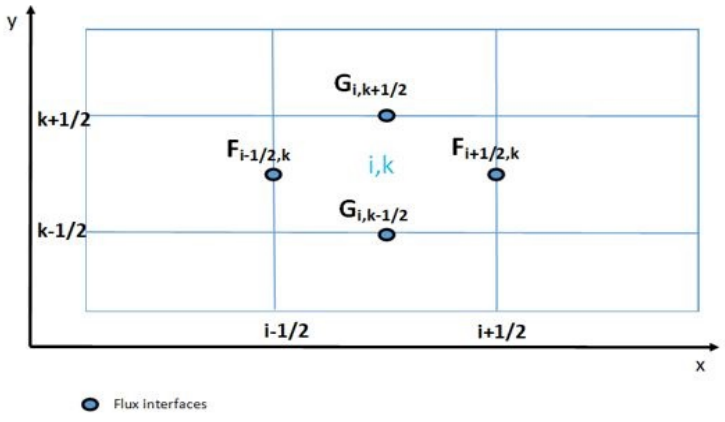


Figure 2: 2D structured meshes, methodology to evaluate the fluctuations. In this methodology, the fluctuations $\mathcal{D}^{\pm}_{i,k+1/2}$ and $\mathcal{D}^{\pm}_{i+1/2,k}$ are computed at each cell faces of the meshes and the half indices $(i+1/2,k)$ and $(i,k+1/2)$ to denote cell faces

## 4 AENO nonlinear reconstructions and main properties

### *4.1 Generalized AENO nonlinear reconstruction for 1D schemes*

We present a computational economical second order limiter. This limiter is inspired from the ENO methodology of [39]. We start by writing the piecewise polynomial as follows:

$$\mathbf{P}_i(x) = \overline{\mathbf{W}}_i + (x - x_i)\boldsymbol{\Delta}_i; \quad x \in K_i, \quad \text{with } x_i = \frac{x_{i+1/2} - x_{i-1/2}}{2}, \tag{73}$$

where $\boldsymbol{\Delta}_i = (\nabla \mathbf{W})_i, i \in \mathbb{Z}$ are the slopes that approximate $(\nabla \mathbf{W}(x_i, t^n)$ in a non-oscillatory manner using a nonlinear slope obtained by convex combination of $\boldsymbol{\Delta}_{i+1/2}(\overline{\mathbf{W}}_i, \overline{\mathbf{W}}_{i+1})$ and $\boldsymbol{\Delta}_{i-1/2}(\overline{\mathbf{W}}_i, \overline{\mathbf{W}}_{i-1})$ as follows:

$$(\nabla \overline{\mathbf{W}})_i = \boldsymbol{\Delta}_i = \begin{cases} \boldsymbol{\Delta}_{i+1/2} + \beta^+(\boldsymbol{\Delta}_{i-1/2} - \boldsymbol{\Delta}_{i+1/2})\phi, & \text{if } |\boldsymbol{\Delta}_{i+1/2}| > |\boldsymbol{\Delta}_{i-1/2}|, \\ \boldsymbol{\Delta}_{i-1/2} + \beta^-(\boldsymbol{\Delta}_{i+1/2} - \boldsymbol{\Delta}_{i-1/2})\phi, & \text{if } |\boldsymbol{\Delta}_{i-1/2}| > |\boldsymbol{\Delta}_{i+1/2}|. \end{cases} \tag{74}$$

In Eq. (74), $\phi = abs\left(\dfrac{sign(\boldsymbol{\Delta}_{i+1/2}) + sign(\boldsymbol{\Delta}_{i-1/2})}{2}\right)$. The parameters $\beta^{\pm}$ are defined as:

$$\beta^{\pm}(r) = \frac{r^{\pm}}{\sqrt{\gamma^2 + r^{\pm 2}}}, \quad r^{\pm} > 0 \tag{75}$$

where

$$\begin{aligned} r^+ &= abs\left(\frac{\boldsymbol{\Delta}_{i+1/2}}{\boldsymbol{\Delta}_{i-1/2} + \epsilon}\right) \quad \text{if } |\boldsymbol{\Delta}_{i+1/2}| > |\boldsymbol{\Delta}_{i-1/2}|, \\ r^- &= abs\left(\frac{\boldsymbol{\Delta}_{i-1/2}}{\boldsymbol{\Delta}_{i+1/2} + \epsilon}\right) \quad \text{if } |\boldsymbol{\Delta}_{i-1/2}| > |\boldsymbol{\Delta}_{i+1/2}|. \end{aligned} \tag{76}$$

In Eqs (74)-(76), the slopes $\boldsymbol{\Delta}_{i\pm 1/2}$ are defined as follows:

$$\boldsymbol{\Delta}_{i+1/2} = \frac{\overline{\mathbf{W}}_{i+1} - \overline{\mathbf{W}}_i}{\Delta x}, \quad \boldsymbol{\Delta}_{i-1/2} = \frac{\overline{\mathbf{W}}_i - \overline{\mathbf{W}}_{i-1}}{\Delta x}. \tag{77}$$

In the above equation (75), $\gamma$ is a positive parameter, and $\epsilon$ is a small positive tolerance to avoid division by zero.

Some minmod based reconstructions choose the absolute minimum of the slopes between right and left slopes. This can produce diffusion for a second order scheme and even for a high order scheme. The choice of highest slope can produce small oscillations during the simulation. To overcome this drawback we can use an AENO methodology. The above AENO-based procedure given by (73)-(77) uses also the ADER methodology and ENO strategy. This reconstruction technique is proven to have a formal second accuracy and is computationally economic than the classical AENO reconstruction developed in [44]. This methodology reconstruction can be naturally extended in 2D schemes.

### *4.2 AENO nonlinear reconstructions for 2D schemes*

Here, we extend the above modified AENO reconstruction following two step process.

$$\mathbf{P}(x,y) = \overline{\mathbf{W}}_{i,k} + \boldsymbol{\Delta}_i(x - x_i) + \boldsymbol{\Delta}_k(y - y_k); \quad x, y \in K_i, \quad \text{with } x_i = \frac{x_{i+1/2,k} - x_{i-1/2,k}}{2}, \quad y_k = \frac{y_{i,k+1/2} - y_{i,k-1/2}}{2} \tag{78}$$

where the above slopes $\boldsymbol{\Delta}_i(\boldsymbol{\Delta}_{i+1/2,k}, \boldsymbol{\Delta}_{i-1/2,k})$ and $\boldsymbol{\Delta}_k(\boldsymbol{\Delta}_{i,k+1/2}, \boldsymbol{\Delta}_{i,k-1/2})$ are defined in 2D manner using (74) with

$$\begin{aligned} \boldsymbol{\Delta}_{i+1/2,k} &= \frac{\overline{\mathbf{W}}_{i+1,k} - \overline{\mathbf{W}}_{i,k}}{\Delta x}, \quad \boldsymbol{\Delta}_{i-1/2,k} = \frac{\overline{\mathbf{W}}_{i,k} - \overline{\mathbf{W}}_{i-1,k}}{\Delta x} \\ \boldsymbol{\Delta}_{i,k+1/2} &= \frac{\overline{\mathbf{W}}_{i,k+1} - \overline{\mathbf{W}}_{i,k}}{\Delta y}, \quad \boldsymbol{\Delta}_{i,k-1/2} = \frac{\overline{\mathbf{W}}_{i,k} - \overline{\mathbf{W}}_{i,k-1}}{\Delta y}. \end{aligned} \tag{79}$$

Now we can estimate the solution at the face centers by linear reconstruction:

$$\mathbf{W}^{+}_{i-1/2,k} = \overline{\mathbf{W}}_{i,k} - \frac{1}{2}\mathbf{\Delta}_i, \quad \mathbf{W}^{-}_{i+1/2,k} = \overline{\mathbf{W}}_{i,k} + \frac{1}{2}\mathbf{\Delta}_i, \tag{80}$$

and

$$\mathbf{W}^{+}_{i,k-1/2} = \overline{\mathbf{W}}_{i,k} - \frac{1}{2}\mathbf{\Delta}_k, \quad \mathbf{W}^{-}_{i,k+1/2} = \overline{\mathbf{W}}_{i,k} + \frac{1}{2}\mathbf{\Delta}_k. \tag{81}$$

Using this 2D reconstruction, we can obtain easily a second order 2D PCCU (or 2D PCCU-AENO for short) scheme in space. However we can increase the order of derivatives of $\mathbf{W}_i$ to obtain a high order scheme but a high order scheme do not still ensure a high order accuracy.

**Remark 4.1.** ***(High order PCCU schemes)*** *The order of the proposed scheme depends on the choice of the functions* $\boldsymbol{P}|_{K_i} = \left(P^{(1)}, P^{(2)}, ....., P^{(N+1)}\right)$. *For any smooth functions* $\boldsymbol{W}$, *and according to Eq. (57) we have:*

$$\begin{aligned} \boldsymbol{P}(x) &= \boldsymbol{W}(x) + \mathcal{O}(|K_i|^{s_1}), \forall x \in K_i \\ \frac{d\boldsymbol{P}_i}{dx} &= \boldsymbol{W}'(x) + \mathcal{O}(|K_i|^{s_2}). \end{aligned} \tag{82}$$

*Then, the semi-discrete PCCU-AENO scheme (71)is an approximation of order at least* $r = \min(s, s_1+1, s_2+1)$ *of the nonconservative quasi-1D system (61) in the following sense:*

$$\left(\mathcal{D}^{+}_{i+1/2} + \mathcal{D}^{-}_{i-1/2} + \int_{K_i} \mathcal{A}(\boldsymbol{P}(x))\frac{d\boldsymbol{P}}{dx}dx\right) - \boldsymbol{S}_i = \int_{K_i} \mathcal{A}(\boldsymbol{W})\frac{\partial \boldsymbol{W}}{\partial x} + \boldsymbol{S}(\boldsymbol{W}_i) + \mathcal{O}(|K_i|^{r}), \tag{83}$$

*where* $\boldsymbol{S}(\boldsymbol{W}_i) = S_e(\boldsymbol{W}_i) + S_D(\boldsymbol{W}_i) + S_F(\boldsymbol{W}_i)$ *computed in each cell by using a barycenter formula. According to remark 4.1, the order of PCCU is at least* $r$, *we can obtain the high order methods based on first order PCCU numerical scheme by increasing the derivative of* $\boldsymbol{W}$.

### *4.3 Well-balanced discretization strategy for PCCU schemes*

In this subsection, we propose a well-balanced discretization for the proposed model in quasi-1D case. According to Eqs.(40)-(41), the proposed numerical method satisfy the C-property for the derived STM if the condition:

$$E - D = 0, \;\; u = 0, \;\; v = 0, \;\; Z^{*}_{b} = \overline{Z}^{*}_{b}(\mathbf{x}), \;\; h + Z^{*}_{b} = w_0, \;\; C = K_0, \tag{84}$$

holds for stationary flows at rest. Using (84), the source terms are treated in such a way are preserved at a discrete level.

In Eq.(84), $K_0$, $C_0$ are the positive constant. Using the reconstructed unknown values by AENO reconstruction, the discretization of source terms must preserve (84) at discrete level.

The numerical methodology proposed here is a robust and highly accurate technique and among other things very suitable for sediment transport problems. We denote by: $\mathcal{W}$ the admissible space that satisfies Eq. (84), $\mathcal{W}_0$ the admissible space guaranteeing that "lake at rest" solutions are exactly preserved at discrete level and $\mathcal{W}^{+}_{0} = \mathcal{W}^{h>0}_{0}$ the admissible space in which "lake at rest" solutions and the positivity of water depth at discrete level is exactly preserved. To obtain a stationary solution, i.e. $\dfrac{d\mathbf{W}_i(t)}{dt} = 0, \quad \forall \mathbf{W} \in \mathcal{W}_0$, the following relation must be satisfied:

$$\begin{aligned} T^{(2)}_i + S^{(2)}_i &= \left(\mathcal{F}^{(2)}_{i+1/2} - \mathcal{F}^{(2)}_{i-1/2} - \mathcal{H}^{(2)}_{\mathbf{\Psi},i+1/2}\right), \\ &= \mathcal{F}^{(2)}_{i+1/2} - \mathcal{F}^{(2)}_{i-1/2} - \frac{a^{+}_{i-1/2}}{a^{+}_{i-1/2} - a^{-}_{i-1/2}}(T^{(2)}_{\mathbf{\Psi},i-1/2} + S^{(2)}_{\mathbf{\Psi},i-1/2}) \\ &+ \frac{a^{-}_{i+1/2}}{a^{+}_{i+1/2} - a^{-}_{i+1/2}}(T^{(2)}_{\mathbf{\Psi},i+1/2} + S^{(2)}_{\mathbf{\Psi},i+1/2}), \end{aligned} \tag{85}$$

where $\mathcal{F}^{(2)}_{i+1/2} = \mathcal{F}(\mathbf{W}^{+}_{i+1/2}, \mathbf{W}^{+}_{i+1/2})$ is the second component of well-balanced numerical flux defined for reconstructed unknowns $\mathbf{W}^{+}_{i+1/2}$, $\mathbf{W}^{+}_{i+1/2} \in \mathcal{W}_0$, that is:

$$\mathcal{F}^{(2)}_{i+1/2} = \frac{1-\alpha_1^{i+1/2}}{2} F^{(2)}(\mathbf{W}^{+}_{i+1/2}) + \frac{1+\alpha_1^{i+1/2}}{2} F^{(2)}(\mathbf{W}^{-}_{i+1/2}), \quad \text{with} \quad \mathbf{W}^{+}_{i+1/2}, \mathbf{W}^{+}_{i+1/2} \in \mathcal{W}_0 \tag{86}$$

Here, $T^{(2)}_i$, $S^{(2)}_i$ are the second components of nonconservative topography term defined above. Since $\mathbf{W}^{+}_{i+1/2}, \mathbf{W}^{+}_{i+1/2} \in \mathcal{W}_0$, one has:

$$w^{+}_{i+1/2} = w^{-}_{i+1/2} \Rightarrow h^{+}_{i+1/2} + Z^{*,+}_{b,i+1/2} = h^{-}_{i+1/2} + Z^{*,-}_{b,i+1/2}, \tag{87}$$

where the above unknowns $h$ and $Z_b$ are computed in positivity-preserving sense (see below). In Eq. (87), we have noted that

$$Z^{*,\pm}_{b,i+1/2} = Z^{\pm}_{b,i+1/2} \pm B_{i\pm 1/2}. \tag{88}$$

The jump contribution for topography source term is given by:

$$T^{(2)}_{\mathbf{\Psi},i+1/2} + S^{(2)}_{\mathbf{\Psi},i+1/2} = -g(\frac{h^{+}_{i+1/2} + h^{-}_{i+1/2}}{2})(h^{-}_{i+1/2} - h^{+}_{i+1/2}). \tag{89}$$

Therefore, the well-balanced discretization strategy for the topography source term is obtained by combining (85) and (89). This strategy can be easily extended on unstructured mesh. With this well-balanced procedure, the steady solution at rest can be easily obtained.

### *4.4 AENO positivity-preserving reconstruction procedures*

In this subsection, we present some important results showing that the proposed unstructured method is able of preserving the positivity of the water depth at each time-step. The proposed technique is similar to the one exposed in a recent work of Ngatcha and Njifenjou [35] (see also Ngatcha et al.,[32]).

*Well-balanced positive hydrostatic reconstruction*

A good PCCU-AENO method for the proposed model should thus be well-balanced (in the sense that it must exactly preserve physically relevant steady states) and positivity preserving (in the sense that the computed values of $h$ must be positive). Negative values of $h$ can lead to an impossibility of calculating the eigenvalues (51). In this subsection, we present a procedure originally developed in [35], extended in [32] to preserve the positivity of water depth. We introduce the above reconstructed AENO values $h^{\pm}_{i+1/2}$, $(hu)^{\pm}_{i+1/2}$, $(hv)^{\pm}_{i+1/2}$, $Z^{*,\pm}_{b,i+1/2}$ of the unknowns to the left and right of $i+1/2$. The velocity and concentration components at the interface are calculated as:

$$u^{+}_{i+1/2} = \frac{(hu)^{+}_{i+1/2}}{h^{+}_{i+1/2}}, \quad u^{-}_{i+1/2} = \frac{(hu)^{-}_{i+1/2}}{h^{-}_{i+1/2}} \tag{90}$$

and

$$v^{+}_{i+1/2} = \frac{(hv)^{+}_{i+1/2}}{h^{+}_{i+1/2}}, \quad v^{-}_{i+1/2} = \frac{(hv)^{-}_{i+1/2}}{h^{-}_{i+1/2}}, \tag{91}$$

The right/left bed elevation at the cell interface $i+1/2$ in right is given by:

$$Z^{*,+}_{b,i+1/2} = \min(\max(Z^{*}_{b,i+1}, Z^{*}_{b,i}), \eta_{i+1}), \quad Z^{*,-}_{b,i+1/2} = \min(\max(Z^{*}_{b,i+1}, Z^{*}_{b,i}), \eta_{i}). \tag{92}$$

Therefore, $Z^{*,\pm}_{b,i+1/2} = B_{i+1/2} + Z^{*,\pm}_{b,i+1/2}$ which should satisfy that $Z^{*,\pm}_{b,i+1/2} + h^{\pm}_{i+1/2} = \eta^{\pm}_{i+1/2} = const$ if the still water $\eta_i + Z^{*}_{b,i} = const$ is given. This treatment makes the reconstructed bed elevation equal to the

water free surface level at the interface of wet/dry cells. In order to preserve the reconstructed water depth nonnegative, the values of water depth are corrected as:

$$h^-_{i+1/2} = \max(0, \min(\eta_i - Z^*_{b,i+1/2}, h_i)), \quad h^+_{i+1/2} = \max(0, \min(\eta_{i+1} - Z^*_{b,i+1/2}, h_{i+1})), \tag{93}$$

which verified at the steady states $h^+_{i+1/2} = h^-_{i+1/2}$. where $Z_{i+1/2} = \max(Z^{*,-}_{b,i+1/2}, Z^{*,+}_{b,i+1/2})$ Finally the rest of unknowns can be recalculated as:

$$u^+_{i+1/2} = \frac{(hu)^+_{i+1/2}}{h^+_{i+1/2}}, \quad u^-_{i+1/2} = \frac{(hu)^-_{i+1/2}}{h^-_{i+1/2}}, \tag{94}$$

$$v^+_{i+1/2} = \frac{(hv)^+_{i+1/2}}{h^+_{i+1/2}}, \quad v^-_{i+1/2} = \frac{(hv)^-_{i+1/2}}{h^-_{i+1/2}}, \tag{95}$$

and

$$C^+_{i+1/2} = \frac{(hC)^+_{i+1/2}}{h^+_{i+1/2}}, \quad C^-_{i+1/2} = \frac{(hC)^-_{i+1/2}}{h^-_{i+1/2}}, \tag{96}$$

$\eta^\pm_{i+1/2} = h^\pm_{i+1/2} + (Z^*)^\pm_{b,i+1/2}$.

This procedure does not affect the C-property of the scheme. Moreover, this procedure is adapted in the case where the bed elevation of the dry cell is higher than the water surface elevation of the neighbor's wet cell. With this procedure, we ensure the C-property of our scheme for the dry-bed application.

**Remark 4.2.** *Although the 2D well-balanced positivity-preserving PCCU-AENO scheme on structured mesh is interesting, it cannot produce anisotropic solutions. The finding of anisotropic solutions is recommended for a multiD STM. In next section, the multidimensional CU (M-CU for short) scheme is reformulated in path-conservative framework and using this later we derived particularly simple-yet highly accurate and robust-multidimensional PCCU scheme.*

## 5 A well-balanced unstructured path-conservative central-upwind method

In this section, we develop for the first time a genuinely path-conservative central-upwind method for nonconservative problems on general triangular grids. The designed method is applied to the nonconservative problems governing by sediment transport equations but can also be used for all nonconservative equations available in the literature. To design this method, we develop a CU scheme for 2D model on general triangular grids in path-conservative framework. The jump contributions are added simply in the fluctuation formulations for unstructured mesh. The proposed unstructured PCCU method is view as a linear combination of simple solvers. Only one path connecting two waves (without intermediate waves) is used to obtain it. With this method, it not necessary to design a unstructured method based on multidimensional solver that can become difficult to implement when the number of unknowns becomes greater.

### *5.1 Finite volume gridding*

We assume that $K_i$ is a triangular cells of size $|K_i|$. The mesh $\mathcal{T}$ is given by $\mathcal{T} := \bigcup_i K_i$. We denote by $n_{ij} := (\cos(\theta_{ij}), \sin(\theta_{ij}))$ the outer unit normal to the corresponding sides of $K_i$ of length $l_{ij}$ such that $n_{ij} = -n_{ji}$. Let $(x_i, y_i)$ be the coordinates of the center of mass for $K_i$ and $p = (x_{p_{ij}}, y_{p_{ij}})$, be the mid point of $j-th$ side of $K_i$ the set of neighboring of cells $K_i$ is denoted by $\mathcal{V}_i = \{K_j \in \mathcal{T}, K_i \bigcap K_j \neq \varnothing\}$. We have $K_i := \bigcup_{j\in\mathcal{V}_i} K_{ij}$, where $K_{ij}$ is a non-overlapping sub-cells which contain an edge of the cell $K_i$. $K_{ij}$ is associated to the interface of $\partial K_i \bigcap \partial K_j = \partial K_{ij} \bigcap \partial K_j$. The distance between $p_{ij}$ and $C_i$(the center of the cell $K_i$) is noted $d(p_{ij}, C_i)$. We note by $\Lambda_i$ the minimum of this distance, that is $\Lambda_i = \min_{j\in\mathcal{V}_i}(d(p_{ij}, C_i))$. All these notations can be found in Fig. (3).

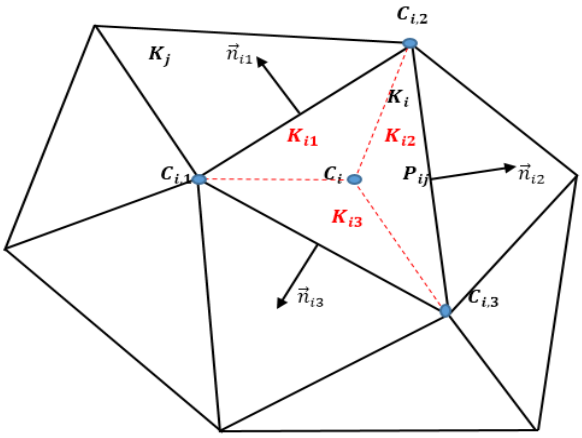


Figure 3: meshes and notations

**General path-conservative formulation**

Using the above unstructured mesh described in Fig. (3), it is possible to design a high order unstructured path-conservative based scheme of the form:

$$\frac{\overline{\mathbf{W}}_i(t)}{dt} = \int_{K_i} \mathcal{A}(\mathbf{P}(\mathbf{x}))\frac{d\mathbf{P}}{d\mathbf{x}}d\mathbf{x} + \sum_{j\in\mathcal{V}_i} D_{ij}(\mathbf{W}_i, \mathbf{W}_j, n_{ij}) = \mathbf{S}(\overline{\mathbf{W}}_i(t)). \tag{97}$$

The term $\int_{K_i} \mathcal{A}(\mathbf{P}(\mathbf{x}))\frac{d\mathbf{P}}{d\mathbf{x}}d\mathbf{x}$ is a approximation of the regular measure of Lebesgues decomposition of $[\mathcal{A}(\mathbf{W})\frac{\partial \mathbf{W}}{\partial x}]_{K_i}$ while the terms $\mathcal{D}_{ji} = \mathcal{D}(\mathbf{W}_i, \mathbf{W}_j, n_{ji})$ and $\mathcal{D}_{ij} = \mathcal{D}(\mathbf{W}_i, \mathbf{W}_j, n_{ij})$ are to its singular part. We have, $\mathcal{D}(\mathbf{W}_i, \mathbf{W}_j, n_{ij}) = \mathcal{D}(\mathbf{W}_i, \mathbf{W}_j, -n_{ji})$. At the first order accuracy, the first term in RHS disappears. For conservative hyperbolic equations, a first order semi-discrete scheme reads:

$$\frac{\overline{\mathbf{W}}_i(t)}{dt} = \sum_{j\in\mathcal{V}_i} D_{ij}(\mathbf{W}_i, \mathbf{W}_j, n_{ij}) = \mathbf{S}(\overline{\mathbf{W}}_i(t)), \tag{98}$$

where the fluctuation terms $D_{ij}$ take account only the conservative flux:

$$D_{ij}(\mathbf{W}_i, \mathbf{W}_j, n_{ij}) = \int_{\partial K_i \bigcap \partial K_j} \frac{\partial F_k}{\partial x_k}.\mathbf{n}ds, \qquad n_{ij} = \int_{\partial K_i \bigcap \partial K_j} \mathbf{n}ds \tag{99}$$

Next, we will introduce a methodology to design PCCU scheme on unstructured mesh. To simplify the presentation we will remove $S_\Psi$, the nonconservative contribution due to fixe topography. We assume that the non-erodible topography is constant and this leads to consider $W$ instead of $\mathbf{W} = (W, B)$.

*5.2 Reformulated M-CU scheme*

In this subsection, we rewrite a M-CU scheme in path-conservative form. We start by proposing a multidimensional CU (M-CU for short) scheme for the proposed model. This scheme reads:

$$\begin{aligned}\frac{\overline{W}_i(t)}{dt} &= -\frac{1}{|K_i|}\sum_{j\in\mathcal{V}_i}\frac{l_{ij}\cos(\theta_{ij})}{a_{ij}+a_{ji}}\left[a_{ji}F_1\left(W_j(p_{ij})\right)+a_{ij}F_1\left(W_i(p_{ij})\right)\right] \\ &- \frac{1}{|K_i|}\sum_{j\in\mathcal{V}_i}\frac{l_{ij}\sin(\theta_{ij})}{a_{ij}+a_{ji}}\left[a_{ji}F_2(W_j(p_{ij}))+a_{ij}F_2(W_i(p_{ij}))\right] \\ &+ \sum_{j\in\mathcal{V}_i}\frac{a_{ij}a_{ij}}{a_{ji}+a_{ji}}\left[W_i(p_{ij})-W_j(p_{ij})\right]+\mathbf{S}(\overline{W}_i(t)),\end{aligned} \tag{100}$$

where the source term is $\mathbf{S}(\overline{W}_i(t)) = S_0(\overline{W}_i(t)) + S_c(\overline{W}_i(t)) + S(\overline{W}_i(t)) + S_e(\overline{W}_i(t)) + S_F(W_i(t))$, and where $\overline{W}_i(p_{ij})$ and $\overline{W}_j(p_{ij})$ are the corresponding values to the $p_{ij}$ of the piecewise linear reconstruction. These values read:

$$W_i(p_{ij}) := \lim_{\mathbf{x}\to p_{ij},\,\mathbf{x}\in K_i}\widetilde{W}(\mathbf{x}), \quad W_j(p_{ij}) := \lim_{\mathbf{x}\to p_{ij},\,\mathbf{x}\in K_j, j\in\mathcal{V}_i}\widetilde{W}(\mathbf{x}). \tag{101}$$

We neglected in this equation the nonconservative terms present in (35) and thus the resulting method is only consistent with smooth solutions. The order of method is given in sense of remark (4.1). A reformulation of the M-CU scheme in term of fluctuations is possible and one has:

$$\begin{aligned}\frac{\overline{W}_i(t)}{dt} &= -\frac{1}{|K_i|}\sum_{j\in\mathcal{V}_i}\frac{a_{ji}l_{ij}}{a_{ij}+a_{ji}}\left[\cos(\theta_{ij})F_1\left(W_j(p_{ij})\right)+\sin(\theta_{ij})F_2(W_j(p_{ij}))\right] \\ &- \frac{1}{|K_i|}\sum_{j\in\mathcal{V}_i}\frac{l_{ij}a_{ij}}{a_{ij}+a_{ji}}\left[\cos(\theta_{ij})F_1(W_i(p_{ij}))+\sin(\theta_{ij})F_2(W_i(p_{ij}))\right] \\ &- \frac{1}{2}\sum_{j\in\mathcal{V}_i}\frac{-2a_{ij}a_{ji}}{a_{ji}+a_{ij}}\left[W_i(p_{ij})-W_j(p_{ij})\right] \\ &+ \mathbf{S}(\overline{W}_i(t)).\end{aligned} \tag{102}$$

We denote the fluctuations at interface $\partial K_{ij}\bigcap\partial K_j$ by $D_{ij}(W_i,W_j)$ and $D_{ji}(W_i,W_j)$. The M-CU scheme is rewritten in path-conservative framework as:

$$\begin{aligned}\frac{\overline{W}_i(t)}{dt} &= -\frac{1}{|K_i|}\sum_{j\in\mathcal{V}_i}\left(D_{ij}(W_i,W_j)+D_{ji}(W_i,W_j)\right) \\ &+ \frac{1}{|K_i|}\sum_{j\in\mathcal{V}_i}l_{ij}\left[\cos(\theta_{ij})\left(F_1(W_i(p_{ij}))-F_1(W_j(p_{ij}))\right)+\sin(\theta_{ij})\left(F_2(W_i(p_{ij}))-F_2(W_j(p_{ij}))\right)\right]+\mathbf{S}(\overline{W}_i(t)),\end{aligned} \tag{103}$$

where the fluctuations read:

$$\begin{aligned}D_{ij,ji} &= \frac{1}{2}\left(1\pm\alpha_1^{ij}\right)l_{ij}\cos(\theta_{ij})(F_1\left(W_j(p_{ij})\right)-F_1\left(W_i(p_{ij})\right)+l_{ij}\sin(\theta_{ij})\left(F_2\left(W_j(p_{ij})\right)-F_2\left(W_i(p_{ij})\right)\right. \\ &\pm \alpha_0^{ij}\left(W_j(p_{ij})-W_i(p_{ij})\right)\end{aligned} \tag{104}$$

where the terms $\alpha_0^{ij}$ and $\alpha_1^{ij}$ are respectively:

$$\alpha_0^{ij} = \frac{-2a_{ij}a_{ji}}{a_{ij}-a_{ji}} \quad \text{and} \quad \alpha_1^{ij} = \frac{a_{ij}+a_{ji}}{a_{ij}-a_{ji}}.$$

**Remark 5.1.** *This reformulation helps us (i) to show that the main drawback of the original multidimensional central-upwind scheme was the fact that the jump in the nonconservative product terms across cell interfaces have never been taken into account and (ii) to understand how the nonconservative products discretized on unstructured mesh can influence the numerical solution.*

*5.3 PCCU scheme on unstructured meshes: M-PCCU scheme*

Here, a new version of path-conservative methodology for nonconservative is developed. The semi-discrete M-CU scheme given by (100) can be directly reformulated into a M-PCCU scheme by adding the nonconservative products in the fluctuation terms:

$$\begin{aligned}\frac{\overline{W}_i(t)}{dt} &= \frac{1}{|K_i|}\sum_{j\in\mathcal{V}_i}(D_{ij}+D_{ji}) \\ &+ \frac{1}{|K_i|}\sum_{j\in\mathcal{V}_i} l_{ij}\left[\cos(\theta_{ij})\left(F_1(W_i(p_{ij}))-F_1(W_j(p_{ij}))\right)+\sin(\theta_{ij})\left(F_2(W_i(p_{ij}))-F_2(W_j(p_{ij}))\right)\right] \\ &+ \frac{1}{|K_i|}(-T_i-Q_i)+\mathbf{S}(\overline{W}_i(t)).\end{aligned} \tag{105}$$

where the source term decomposes as follows:

$$\mathbf{S}(\overline{W}_i(t)) = S_D(\overline{W}_i(t)) + S_e(\overline{W}_i(t)) + S_F(W_i(t)).$$

Unlike the M-CU scheme, the developed M-PCCU method incorporates all the nonconservative terms, precisely in the definition of terms linked to fluctuations. We have defined the fluctuations for M-PCCU scheme as follows:

$$\begin{aligned}D_{ij,ji} &= \frac{1}{2}\left(1\pm\alpha_1^{ij}\right)\left[l_{ij}\cos(\theta_{ij})\left(F_1\left(W_j(p_{ij})\right)-F_1\left(W_i(p_{ij})\right)\right)+l_{ij}\sin(\theta_{ij})\left(F_2\left(W_j(p_{ij})\right)-F_2\left(W_i(p_{ij})\right)\right)\right. \\ &- \frac{1}{2}\left(1\pm\alpha_1^{ij}\right)\left[-T_{\mathbf{\Psi}_{ij,ji}}-Q_{\mathbf{\Psi}_{ij,ji}}\right]\pm\alpha_0^{ij}\left(W_j(p_{ij})-W_i(p_{ij})\right).\end{aligned} \tag{106}$$

Here, $D_{ji}=D(W_i,W_j,-n_{ij})$, $D_{ij}=D(W_i,W_j,n_{ij})$ are the fluctuations that represent the difference between the numerical flux and the physical flux at both sides of the cell interface.

In this formulation, we have considered a sufficiently smooth path $\mathbf{\Psi}_{ij,ji}:[0,1]\times\mathbb{R}^5\times\mathbb{R}^5\longrightarrow\mathbb{R}^5$ such that:

$$\begin{aligned}\mathbf{\Psi}_{ij}(1,W_i(p_{ij}),W_j(p_{ij}),n_{ij}) &= W_i(p_{ij}), \quad \mathbf{\Psi}_{ji}(1,W_i(p_{ij}),W_j(p_{ij}),n_{ji}) = W_j(p_{ij}) \\ \mathbf{\Psi}_{ij}(0,W_i(p_{ij}),W_j(p_{ij}),n_{ji}) &= W_i(p_{ij}), \quad \mathbf{\Psi}_{ji}(0,W_j(p_{ij}),W_i(p_{ij}),n_{ij}) = W_i(p_{ij}).\end{aligned} \tag{107}$$

Using this definition, we can define the matrix $T_{\mathbf{\Psi}_{ij,ji}}$, $Q_{\mathbf{\Psi}_{ij,ji}}$ as:

$$\begin{aligned}T_{\mathbf{\Psi}_{ij,ji}} &= \int_0^1 T(\mathbf{\Psi}_{ij,ji}(s,W_i(p_{ij}),W_j(p_{ij}),\mathbf{n}),\mathbf{n})\frac{d\mathbf{\Psi}_{ij,ji}}{ds}ds, \\ Q_{\mathbf{\Psi}_{ij,ji}} &= \int_0^1 Q(\mathbf{\Psi}_{ij,ji}(s,W_i(p_{ij}),W_j(p_{ij}),\mathbf{n}),\mathbf{n})\frac{d\mathbf{\Psi}_{ij,ji}}{ds}ds,\end{aligned} \tag{108}$$

and $T_i$, $Q_i$ by:

$$T_i=\int_{K_i}T(\mathbf{P}_i(\mathbf{x}))\frac{d\mathbf{P}_i(\mathbf{x})}{d\mathbf{x}}d\mathbf{x}, \quad Q_i=\int_{K_i}Q(\mathbf{P}_i(\mathbf{x}))\frac{d\mathbf{P}_i(\mathbf{x})}{d\mathbf{x}}d\mathbf{x}, \tag{109}$$

The terms $\frac{1}{2}\left(1\pm\alpha_1^{ij}\right)\left[-T_{\mathbf{\Psi}_{ij,ji}}-Q_{\mathbf{\Psi}_{ij,ji}}\right]$ take account the contributions of the jumps of the nonconservative products at the cell interfaces. The terms $T_i, Q_i$ account the contribution of nonconservative product in the cell center. These terms disappear in a first order accuracy scheme.

**Remark 5.2.** *The nonconservative terms make the numerical scheme to become formally consistent with a particular definition of weak solutions. Unlike the M-CU scheme, the designed M-PCCU scheme incorporates all the nonconservative terms. precisely in the definition of terms linked to fluctuations.*

*5.4 MultiD well balanced discretization*

Following the same procedure presented for 1D case a well balanced discretization can be obtained. One has:

$$\left(T_i^{(2)} + Q_i^{(2)}\right) = \sum_{j\in\mathcal{V}_i}\left(D_{ij}^{(2)} + D_{ji}^{(2)}\right) \tag{110}$$
$$+ \sum_{j\in\mathcal{V}_i} l_{ij}\left[\cos(\theta_{ij})\left(F_1^{(2)}(W_i(p_{ij})) - F_1^{(2)}(W_j(p_{ij}))\right) + \sin(\theta_{ij})\left(F_2^{(2)}(W_i(p_{ij})) - F_2^{(2)}(W_j(p_{ij}))\right)\right].$$

where

$$\begin{aligned} D_{ij,ji}^{(2)} &= \frac{1}{2}\left(1 \pm \alpha_1^{ij}\right)\left[l_{ij}\cos(\theta_{ij})\left(F_1^{(2)}\left(W_j(p_{ij})\right) - F_1^{(2)}\left(W_i(p_{ij})\right)\right)\right] \\ &+ \left[l_{ij}\sin(\theta_{ij})\left(F_2^{(2)}\left(W_j(p_{ij})\right) - F_2^{(2)}\left(W_i(p_{ij})\right)\right)\right] - \frac{1}{2}\left(1 \pm \alpha_1^{ij}\right)\left[T_{\mathbf{\Psi}_{ij,ji}}^{(2)} - Q_{\mathbf{\Psi}_{ij,ji}}^{(2)}\right], \end{aligned} \tag{111}$$

where $F_i^{(2)},\ \ i = 1, 2$ are given in well-balanced sense (particularly according to Eq. (84)).

*5.5 New Hybrid reconstruction state procedure*

We employ an approximation of $W$ at each interface $\Gamma_{ij}$ using combination gradients of center of cells, gradients of center of subcells and a ponderation parameter $\alpha \in [0, 1]$.

$$W_i(p_{ij}) = W_i + \frac{1}{2}\left(\alpha\nabla W_i.C_ip + (1-\alpha)\nabla W_{il}.C_{il}p\right), \tag{112}$$
$$W_j(p_{ij}) = W_j + \frac{1}{2}\left(\alpha\nabla W_j.C_jp + (1-\alpha)\nabla W_{jl}.C_{jl}p\right). \tag{113}$$

Note that the spatial discretization in (56) does not necessarily monotone and non-physical oscillations may occur during the simulations. Therefore to eliminate these numerical oscillations and order to obtain a TVD M-PCCU method, we introduce an appropriate slope limiter:

$$W_i(p_{ij}) = W_i + \frac{1}{2}Limit\left(\alpha\nabla W_i.C_ip + (1-\alpha)\nabla W_{il}.C_{il}p, \nabla W_{il}\right), \tag{114}$$
$$W_j(p_{ij}) = W_j + \frac{1}{2}Limit\left(\alpha\nabla W_j.C_jp + (1-\alpha)\nabla W_{jl}.C_{jl}p, \nabla W_{jl}\right). \tag{115}$$

Another method consists to use the neighboring triangle in the discretization:

$$W_i(p_{ij}) = W_i + \frac{1}{2}Limit\left(\alpha\nabla W_i.C_ip + (1-\alpha)(W_{jl} - W_{il}), W_{jl} - W_{il}\right), \tag{116}$$
$$W_j(p_{ij}) = W_j + \frac{1}{2}Limit\left(\alpha\nabla W_j.C_jp + (1-\alpha)(W_{jl} - W_{il}), W_{jl} - W_{il}\right), \tag{117}$$

where *Limit* in (114) and (116) is a slope limiter function such as the well-known MinMod limiter function:

$$Limit(a, b) = \max(0, \min(1, \frac{a}{b})) \tag{118}$$

Other slope limiter functions can be used (see [31]).

**Gradient approximation**

Let consider $C_{i,l}$, l=1,2,3 the vertices of cell $K_i$. The vertices of subcells $K_{il}$ are $\{C_i, C_{i,l}, C_{i,ip(j)}\}$ where $ip(1) = 2,\ \ ip(2) = 3,\ \ ip(3) = 1$. We consider in $K_{il}$ a linear approximation of gradient $\nabla W_{il}$ using the values

$W_i$, $W_{i,l}$, $l = 1, 2, 3$ which are second order approximation of $W(C_i), W(C_{i,1}), W(C_{i,2}), W(C_{i,3})$ respectively. This approximation can be written as:

$$\nabla W_{jl} = W_{i,0}\nabla\lambda_j^0 + W_{i,l}\nabla\lambda_j^j + W_{i,ip(j)}\nabla\lambda_j^{ip(j)}, \tag{119}$$

where $\lambda_j^0, \lambda_j^j, \lambda_j^{ip(j)}$ are the barycentric coordinates associated to the vertices. We also denote by $b_{ij}$, $j = 1, 2, 3$ the corresponding barycenters of subcells $K_{il}$. Given a smooth function $W$ by applying the quadrature formula of the barycenter, we obtain:

$$\frac{1}{|K_{il}|}\int_{K_{il}} W(\mathbf{x})d\mathbf{x} = W(b_{il}) + O(\Delta^2), l = 1, 2, 3 \tag{120}$$

and thus the following equality holds:

$$\overline{W}_i = \frac{1}{|K_i|}\int_{K_i} W(\mathbf{x})d\mathbf{x} = \sum_{j=1}^{3}\frac{|K_{ij}|}{|K_i|}W(b_{ij}) + O(\Delta^2). \tag{121}$$

We can easily verified that:

$$\frac{|K_{i1}|}{|K_i|}W(b_{i1}) + \frac{|K_{i2}|}{|K_i|}W(b_{i2}) + \frac{|K_{i3}|}{|K_i|}W(b_{i3}) = W\left(\frac{|K_{i1}|}{|K_i|}b_{i1} + \frac{|K_{i2}|}{|K_i|}b_{i2} + \frac{|K_{i3}|}{|K_i|}b_{i3}\right) + O(\Delta^2). \tag{122}$$

Therefore, the following equality also holds:

$$W_i = W(C_i) + O(\Delta^2), \tag{123}$$

where $C_i = \sum_{j=1}^{3}\frac{|K_{ij}|}{|K_i|}b_{ij}$.

The constant gradient deduced from a $P_1$ approximation on the subcells $K_{ij}$ is given by a weighted average of the gradients on the subcells of $K_i$,

$$\nabla W_i = \nabla W|_{K_i} = \frac{\sum_{j=1}^{3}|K_{ij}|\,\nabla W|_{K_{ij}}}{\sum_{j=1}^{3}|K_{ij}|}. \tag{124}$$

The directional local speeds $a_{ij}$ and $a_{ji}$ are defined by:

$$\begin{aligned} a_{ij}(p_{ij}) &= \min\left\{\lambda_1(\mathcal{A}_{ij}(W_i(p_{ij}))), \lambda_1(\mathcal{A}_{ij}(W_j(p_{ij}))), 0\right\}, \\ a_{ji}(p_{ij}) &= \max\left\{\lambda_5(\mathcal{A}_{ij}(W_i(p_{ij})), \lambda_5(\mathcal{A}_{ij}(W_j(p_{ij})), 0\right\}, \end{aligned} \tag{125}$$

Here $\lambda_1(W_i(p_{ij}))$ and $\lambda_5(W_i(p_{ij}))$ are the upper bound on the largest eigenvalue and lower bound on the smallest eigenvalue of $\mathcal{A}_{ij}(W_i(p_{ij}))$ and $\mathcal{A}_{ij}(W_j(p_{ij}))$ respectively. The Jacobian matrices of the nonconservative system of the proposed model read

$$\begin{aligned} \mathcal{A}_{ij}(W_j(p_{ij})) &= \cos(\theta_{ij})\left[\frac{\partial F_1}{\partial W}(W_j(p_{ij})) - T_1(W_j(p_{ij})) - Q_1(W_j(p_{ij}))\right] \\ &+ \sin(\theta_{ij})\left[\frac{\partial F_2}{\partial W}(W_j(p_{ij})) - T_1(W_j(p_{ij})) - Q_1(W_j(p_{ij}))\right], \end{aligned} \tag{126}$$

and

$$\begin{aligned} \mathcal{A}_{ij}(W_i(p_{ij})) &= \cos(\theta_{ij})\left[\frac{\partial F_1}{\partial W}(W_i(p_{ij})) - T_2(W_i(p_{ij})) - Q_2(W_i(p_{ij}))\right] \\ &+ \sin(\theta_{ij})\left[\frac{\partial F_2}{\partial W}(W_i(p_{ij})) - T_2(W_i(p_{ij})) - Q_2(W_i(p_{ij}))\right]. \end{aligned} \tag{127}$$

The proposed scheme converges to steady-state solutions, preserves the positivity of the water depth, captures the shock near the moving bottom and conserves local properties of conservation.

**General remark on the Gerschgorin's disc theorem**

The Gerschgorin theorem gives a good methodology to obtain an upper bound on the largest positive root of a polynomial. This theorem is based on the following concept:

**Remark 5.3.** *Let us the Jacobian matrices for our model given by (126) and (127). The concept of the Gerschgorin's disc theorem for our model is that one can take the diagonal entries of matrices $\mathcal{A}_{ij}(W_i(p_{ij}))$ and $\mathcal{A}_{ij}(W_j(p_{ij}))$ respectively $\boldsymbol{a}_{ij}(W_i(p_{ij})) = \boldsymbol{a}_{ij}^1$ and $\boldsymbol{a}_{ij}(W_j(p_{ij})) = \boldsymbol{a}_{ij}^2$ as coordinates of complex plane. These points then, act as the centers of 5 discs. Each disc is centered at $\boldsymbol{a}_{ij}$ on the complex plane with radius $V_i(\mathcal{A}_{ij}^l)$, $l = 1, 2$ that are the sum of magnitudes of the 4 others entries from the same row noted $V_i(\mathcal{A}_{ij}^l) = \sum_{i \neq j} |\boldsymbol{a}_{ij}^l|, l = 1, 2$. For short, the Gerschgorin disc for each matrix can be noted $D(\boldsymbol{a}_{ij}^l, V_i(\mathcal{A}_{ij}^l))$. Here, for each matrix $\mathcal{A}_{ij}(W_i(p_{ij}))$ and $\mathcal{A}_{ij}(W_j(p_{ij}))$ at least one of these Gerschgorin discs has radius 0, since each matrix admits one row with non diagonal entries all equal to zero. Then, all the eigenvalues of these matrices will lie within the union of these discs. The following result generalizes this concept.*

**Proposition 5.1** (**Existence of Gerschgorin disc**). *Every eigenvalue of $\mathcal{A}_{ij}(W_i(p_{ij}))$ and $\mathcal{A}_{ij}(W_j(p_{ij}))$ given by (126) and (127) respectively lies within at least one Gerschgorin disc.*

**Remark 5.4.** *The proposed multidimensional scheme depends on the definition of the state reconstruction operator $\boldsymbol{P}_i(t)$ that depends on $W_j(p_{ij})$, $W_i(p_{ij})$. Therefore the order of multi-dimensional PCCU depends on the order of the operator $\boldsymbol{P}_i(t)$ and its derivative. A first-order method is a high-order method where the order of the operator is zeros. A second-order is a high-order where the order of the operator is one. It is possible we can easily extend the above reconstruction in space to obtain the high-order TVD scheme by using a high-order approximation of $W(C_i)$, $W(C_{i,1})$, $W(C_{i,2})$, $W(C_{i,3})$. We can also extend in the time discretization method presented above to four and even fifth order without major modifications. A nonlinear approximation of gradient $\nabla W_{il}$ using the values $W_i$, $W_{i,l}$, $l = 1, 2, 3$ is not discussed in this paper.*

## 6 A time positive discretization method for Path-conservative-based schemes

The equation (52), (71) and (105) represent second order semi-discrete schemes in space. We start by rewriting the Eq. (**??**) as follows:

$$\begin{aligned}
\frac{d\overline{h}_i}{dt} &= \mathcal{L}^{(1)}[\overline{W}]_i, \\
\frac{d\overline{\mathbf{q}}_i}{dt} &= \mathcal{L}^{(2)}[\overline{W}]_i + \mathcal{Z}[\overline{W}]_i \mathbf{q}_i, \quad q = hu, hv \\
\frac{d\overline{(hC)}_i}{dt} &= \mathcal{L}^{(4)}[\overline{W}]_i, \\
\frac{d\overline{Z}_{b,i}}{dt} &= \mathcal{L}^{(5)}[\overline{W}]_i,
\end{aligned} \tag{128}$$

where $j - th$ component of $\mathcal{L}$ reads:

$$\mathcal{L}^{(j)} = \mathcal{D}^{(j)} + S_D^{(j)} + S_e^{(j)}, \quad j = h, hu, hv, hC, Z_b \tag{129}$$

where $\mathcal{Z}[\overline{W}]_i = C_f|\mathbf{q}_i|$ with $S_F^{(2,3)} = \mathcal{Z}[\overline{W}]_i \mathbf{q}_i$.

Path-Conservative schemes can be re-written as:

$$\frac{\partial \overline{W}}{\partial t} + \mathcal{D}(\overline{W}) = \widehat{\mathbf{S}}(\overline{W})\overline{W} \tag{130}$$

where $\widehat{\mathbf{S}}(\overline{W})$ is substituted to $S(\overline{W})_F$. This system of ODEs with stiff source term $\widehat{\mathbf{S}}(\overline{W})(t)$ is solved using the third-order semi-implicit Runge-Kutta (SI-RK3) method which is a modified version of the third-order

strong stability preserving RK (SSPRK) method. The method treats the non-stiff terms using explicit RK methods while the stiff terms use implicit methods. Without stiff terms, the SI-RK method reduces to the corresponding explicit RK method. To write the fully discrete M-PCCU scheme, we starting by write the following three steps:

$$\overline{W}^{(1)} = \frac{\overline{W}^n + \Delta t\ \mathcal{D}(\overline{W}^n)}{1 - \Delta t\ \widehat{\mathbf{S}}(\overline{W}^n)} \tag{131}$$

$$\overline{W}^{(2)} = \frac{3}{4}\overline{W}^n + \frac{1}{4}\ \frac{\overline{W}^{(1)} + \Delta t\ \mathcal{D}(\overline{W}^{(1)})}{1 - \Delta t\ \widehat{\mathbf{S}}(\overline{W}^{(1)})} \tag{132}$$

$$\overline{W}^{(3)} = \frac{1}{3}\overline{W}^n + \frac{2}{3}\ \frac{\overline{W}^{(2)} + \Delta t\ \mathcal{D}(\overline{W}^{(2)})}{1 - \Delta t\ \widehat{\mathbf{S}}(\overline{W}^{(2)})} \tag{133}$$

$$\tag{134}$$

where $\overline{W}^{(k)} = (\overline{h}^{(k)}, \overline{hu}^{(k)}, \overline{hv}^{(k)}, \overline{hC}^{(k)}, (\overline{Z}_b)^{(k)}), k = 1, 2, 3.$

Thus the fully discrete M-PCCU scheme reads:

$$\overline{M}^{n+1} = \overline{M}^{(3)}, \quad \text{for} \quad M = h,\ hC,\ Z_b \tag{135}$$

$$\overline{\mathbf{q}}^{n+1} = \frac{\overline{\mathbf{q}}^{(3)} - (\Delta t)^2\ \mathcal{D}^{(k)}(\overline{W}^{(3)})\ \widehat{\mathbf{S}}(\overline{W}^{(3)})}{1 + [\Delta t\ \widehat{\mathbf{S}}(\overline{W}^{(3)})]^2}, \quad \mathbf{q} = hu, hv \tag{136}$$

$$\tag{137}$$

where $k = 2, 3$ and $\mathcal{D}^{(k)}$ is the second and third component of the vector $\mathcal{D}$. The SI-RK3 method allows us the use of a important time step compared to its explicit counterpart. It maintains the discrete balance between the fluxes and source terms capturing the steady states and preserving the positivity of water depth.

### A proof of Positivity of PCCU schemes

Here, we prove that the proposed numerical method is positivity-preserving at discrete level. We have the following result.

**Lema 6.1.** *Consider the general fully discrete PCCU scheme given above by Eq. (131)-(135). If* $\overline{h}_i^n \geq 0; \forall i$*; then* $\overline{h}_i^{n+1} \geq 0; \forall i$.

We prove this result in a one-dimensional case and the 2D version of lemma 6.1 can be proved in a similar manner.

*Proof.* For the $M = h$ we have:

$$\overline{h}^{(1)} = \overline{h}_i^n + \Delta t\ \mathcal{D}^{(h)}(\overline{W}^n), \tag{138}$$

$$\overline{h}^{(2)} = \frac{3}{4}\overline{h}_i^n + \frac{1}{4}\overline{h}^{(1)} + \Delta t\ \mathcal{D}^{(h)}(\overline{W}^{(1)}), \tag{139}$$

$$\overline{h}^{(3)} = \frac{1}{3}\overline{h}_i^n + \frac{2}{3}\overline{h}^{(2)} + \Delta t\ \mathcal{D}^{(h)}(\overline{W}^{(2)}), \tag{140}$$

$$\overline{h}^{n+1} = \overline{h}^{(3)}, \tag{141}$$

$$\tag{142}$$

where $\overline{W}^{(k)}, k = 1, 2$ are defined in (135). The rest of unknowns expressed in the form (135).

Here, considering the fact that the $h$ component of fluctuations and friction source term is zero, we have:

$$\begin{aligned}\mathcal{D}^{(h)}(\overline{W}^n) &= \frac{1}{mes(K)}\left[\left(\frac{1-\alpha_1^{i+1/2}}{2}F^h(W^+_{i+1/2})+\frac{1+\alpha_1^{i+1/2}}{2}F^h(W^-_{i+1/2})-\frac{\alpha_0^{i+1/2}}{2}\left(h^+_{i+1/2}-h^-_{i+1/2}\right)\right)\right] \\ &- \frac{1}{mes(K)}\left[\left(\frac{1-\alpha_1^{i-1/2}}{2}F^h(W^+_{i-1/2})+\frac{1+\alpha_1^{i-1/2}}{2}F^h(W^-_{i-1/2})-\frac{\alpha_0^{i-1/2}}{2}\left(h^+_{i-1/2}-h^-_{i-1/2}\right)\right)\right]\end{aligned} \tag{143}$$

We can express $\overline{h}_i^{(1)}$ as linear combination of $h^+_{i+1/2}$, $h^-_{i+1/2}$, $h^-_{i-1/2}$ since we have used the fact that $\overline{h}_i^{(n)} = \dfrac{h^+_{i+1/2}+h^-_{i+1/2}}{2}$ and assumed that $h^+_{i-1/2}=0$. Following the above considerations, one has:

$$\begin{aligned}\overline{h}_i^{(1)} &= \left[\frac{1}{2}+c\left(-\frac{1}{2}u^-_{i+1/2}-\frac{1}{2}\alpha^2_{i+1/2}u^-_{i+1/2}-\frac{\alpha_1^{i+1/2}}{2}\right)\right]h^-_{i+1/2} \\ &+ c\left(\frac{1}{2}u^-_{i-1/2}-\frac{1}{2}\alpha_1^{i-1/2}u^-_{i-1/2}+\frac{\alpha_0^{i-1/2}}{2}\right)h^-_{i-1/2} \\ &+ \left[\frac{1}{2}+c\left(-\frac{1}{2}u^+_{i+1/2}+\frac{1}{2}\alpha_1^{i+1/2}u^+_{i+1/2}+\frac{\alpha_0^{i+1/2}}{2}\right)\right]h^+_{i+1/2},\end{aligned} \tag{144}$$

where $c=\dfrac{\Delta t}{mes(K)}$.

We will show that each coefficient of $\overline{h}_i^{(1)}$ see as linear combination of three nonnegative reconstructed values $h^+_{i+1/2}, h^-_{i+1/2}, h^-_{i-1/2}$. We have according to equation (50), $\alpha_0^{i+1/2}\geq 0$ since $a^+_{i\pm1/2}\geq 0$, $a^-_{i\pm1/2}\leq 0$, $a^+_{i\pm1/2}-a^-_{i\pm1/2}\geq 0$. Moreover, because all the reconstructed water depth are nonnegative, we have $\sqrt{gh^+_{i+1/2}}\geq 0$ and thus $a^+_{i+1/2}-u^+_{i+1/2}\geq 0$ and $u^-_{i+1/2}-a^-_{i+1/2}\geq 0$. This leads to conclude that the two first coefficient are positive. Using the above same arguments and the fact that:

$$\frac{\alpha_1^{i+1/2}+\alpha_0^{i+1/2}}{2}\leq\frac{a^+_{i+1/2}-a^-_{i+1/2}}{2}\leq\frac{a^+_{i+1/2}}{2},$$

we get the following relations:

$$0\leq\left(-\frac{1}{2}u^+_{i+1/2}-\frac{1}{2}\alpha_1^{i+1/2}u^+_{i+1/2}-\frac{\alpha_0^{i+1/2}}{2}\right)\leq\frac{a^+_{i+1/2}}{2}$$

and

$$0\leq\left(\frac{1}{2}u^+_{i-1/2}-\frac{1}{2}\alpha_1^{i-1/2}u^+_{i-1/2}-\frac{\alpha_0^{i-1/2}}{2}\right)\leq\frac{a^+_{i-1/2}}{2}.$$

We conclude that the coefficient in $h^+_{i+1/2}$ will be also nonnegative, if the following restriction

$$0\leq c\leq\frac{1}{\max\{a^+_{i+1/2},-a^-_{i+1/2}\}}$$

is satisfied.

Since and all the coefficients are non-negative, which leads to $\overline{h}_i^{(1)}\geq 0$. We prove using same way that $\overline{h}_i^{(k)}$; $k=2,3$ are non-negative. We can seen that $\overline{h}_i^{(n+1)}$ can expressed as linear combination of $\overline{h}_i^{(k)}$; $k=1,2,3$. Therefore $\overline{h}_i^{(n+1)}, \forall i$ is non-negative. □

## 7 Numerical Results

In this section, several 1D and 2D tests are proposed to assess the performance of the proposed PCCU method on unstructured meshes. In this section, we run a series of test cases to verify our implementation and evaluate the M-PCCU MATLAB program. A study of the efficiency and a acceptable validation of 1D and 2D PCCU-AENO methods are exposed using reference solutions, exact solutions, CU scheme and one experimental data set. Our main objectives are to:

1. Verify that the well-balanced discretization strategy here interesting
2. Test if the method is able to recover the exact solution for a problem with exact solution
3. Study the effect of interaction between sediment and fluid on the stability of the scheme and prove the importance of high-order methods
4. Test the ability to resolve a multi-class sediment transport model
5. Verify if at least the second order accuracy is achieved
6. Study the convergence and compute the rates of convergence
7. Compare with some of the existing methods in terms of accuracy, efficiency and robustness
8. Compare with experimental data
9. Verify the adaptability of our model in several environment contexts

For one-dimensional tests, the numerical stability is imposed by the Courant-Friedrich-Lewy (CFL) condition. The integration time step is evaluated as:

$$\Delta t = CFL\frac{mes(K_i)}{a}, \tag{145}$$

where $K_i = [x_{j-1/2}, x_{j-1/2}]$ and where $a = \max(a^+_{j+1/2}, -a^-_{j+1/2})$, with $a^{\pm}_{j+1/2}$ is the local propagation speeds defined in (50).

For 2D structured grid we use the following stability condition:

$$\Delta t = CFL \min\left(\frac{\Delta x}{4a}, \frac{\Delta y}{4b}\right), \tag{146}$$

where $a = \max(a^+_{i+1/2},\ a^+_{i+1/2}), b = \max(b^+_{i+1/2},\ b^+_{i+1/2})$.

For general triangular mesh, we use the following restriction:

$$\Delta t = CFL \min_{i,j}\left(\frac{\Lambda_i}{\max(a_{ij}, a_{ji})}\right). \tag{147}$$

where $\Lambda_i = \min_i(d(p_{ij}, C_i))$.

For the test cases where the exact solution exists, the error estimate ($err$) is computed between the numerical solutions and the exact solution:

$$\|err\|_{L^p} = \left(\sum_{K_j \in \mathcal{T}} |K_j||W^{ex}_{\mathcal{T}} - W^{app}_{\mathcal{T}}|^p\right)^{\frac{1}{p}} \tag{148}$$

where $W^{ex}$ and $W^{app}$ are the exact solution and numerical solution respectively. And the convergence rate is deduced. For the test cases that do not admit reference solution, we verify the convergence of the proposed method by using the measure of the difference between the solutions computed on two consecutive grids. The $L^1 - norm$ is given by:

$$\|\Phi^N - \Psi^N\|_1 = \frac{1}{N^2}\sum_{i=1}^{N}\sum_{k=1}^{N}|\Phi^N_{i,k} - \Psi^N_{i,k}| \tag{149}$$

where $\Phi^N := \{\Phi^N_{i,k}\}$ and $\Psi^N := \{\Psi^N_{i,k}\}$ are two functions prescribed on structured mesh of $N \times N$ cells. The rates of convergence are calculated as:

$$\mathcal{O}(L^1) = Log_2\left(\frac{\|\varphi^{N/2} - \varphi^{N/4}\|_1}{\|\varphi^N - \varphi^{N/2}\|_1}\right), \tag{150}$$

where we have noted that $Log_b(x) = y \Rightarrow b^y = x$. More generally, the error estimate is evaluated in $L^p - norm, \quad p = 1, 2, \infty$ at the time $t = T$, where $T$ is the final time. The computational parameters used in some simulations are found in Table. (1).

Table 1: Computational parameters

| quantity | $\rho_w$ | $\rho_s$ | $g$ | $\varphi$ | $\nu_f$ | $\lambda$ |
|---|---|---|---|---|---|---|
| Reference value | $1000Kg/m^3$ | $2650Kg/m^3$ | $1m/s^2$ | $0.015m^{1.2}$ | $1.2 * 10^{-6}$ | 0.25 |

**General algorithm**

In the following, we briefly present the algorithmic steps necessary for implementation of the second order M-PCCU scheme:

1. *Construct the unstructured mesh.*
2. *We locate each cell with its center and its interfaces via a special pre-processing procedure.*
3. *We perform the reconstruction states in order to obtain the slope* $(\nabla W)_i$ *in equation (124).*
4. *We extrapolate values at cell boundaries* $p_{ij}$, $W_i(p_{ij})$ *and* $W_j(p_{ij})$, *by using Eq. (116).*
5. *We compute the family paths* $\Phi_{ij}(s, W_i(p_{ij}), W_j(p_{ij}), n)$ *and* $\Phi_{ji}(s, W_i(p_{ij}), W_j(p_{ij}), n)$.
6. *At each interfaces, we compute the flux* $F(W_i(p_{ij}))$ *and* $F(W_j(p_{ij}))$ *and we use these flux to compute the fluctuation* $D_{ij,ji}$ *given by Eqs.(106).*
7. *At each interfaces: use the values* $W_i(p_{ij})$ *and* $W_j(p_{ij})$ *to compute the contribution of the jumps of nonconservative products* $T_{\Psi_{ij,ji}}$, $Q_{\Psi_{ij,ji}}$ *and* $S_{\Psi_{ij,ji}}$ *by using Eqs.(108).*
8. *Via Gerschgorin disc, we compute the eigenvalues of Jacobian matrices given by (126) and (127)*
9. *We use these eigenvalues to compute the local speeds propagation* $a_{ji}(p_{ij})$ *and* $a_{ji}(p_{ij})$.
10. *We compute the vectors* $T_i$, $Q_i$, $S_i$ *via Eq. (109).*
11. *We implement a procedure of type SI-RK3 perform the update cells averaged by using the multidimensional semi-discrete scheme* (105).

### *7.1 Accuracy tests with Shallow Water Equations(SWE)*

This test is performed to assess the accuracy of our WBPP PCCU-AENO scheme. We consider a 1D SWE (20a)-(20b) with flat topography, dry/wet zones and without sediment transport ($Ag = 0, \quad E - D = 0$) and friction source term ($n = 0$). The domain of simulation $\Omega = [0, 2000]$ is discretized with N=1000 uniform cells. A similar test is performed in some works in the literature. The initial velocity and the initial water depth for both tests are respectively:

$$h(x,0) = \begin{cases} 6 \ \text{ if } \ x \leq 1000m \\ 0.01 \ \text{ if } \ x > 1000m \end{cases}, \quad h(x,0) = \begin{cases} 6 \ \text{ if } \ x \leq 1000m \\ 0.2 \ \text{ if } \ x > 1000m \end{cases}, u(x,0) = 0. \tag{151}$$

Neumann condition is used at all boundaries:

$$h.\nu = 0, \quad h\mathbf{u}.\nu = 0$$

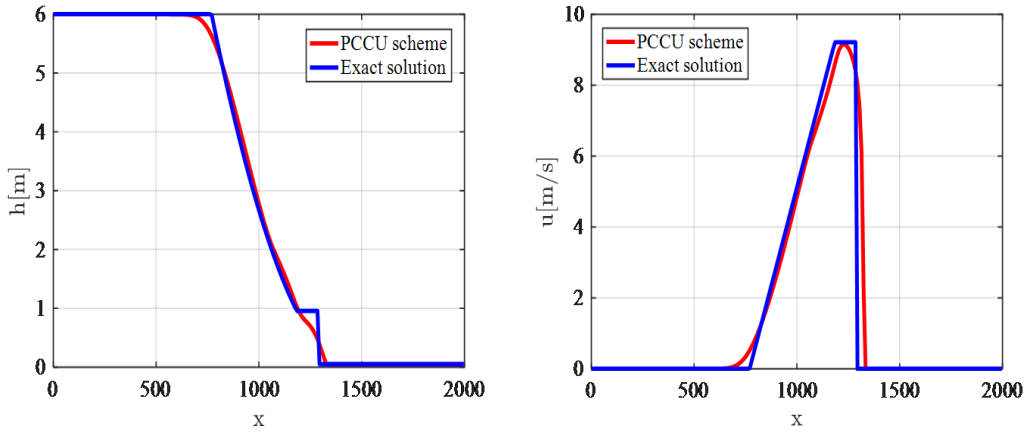


Figure 4: Accuracy test with dry zones. Comparison between exact solution and numerical solution obtained by PCCU scheme at the first order.

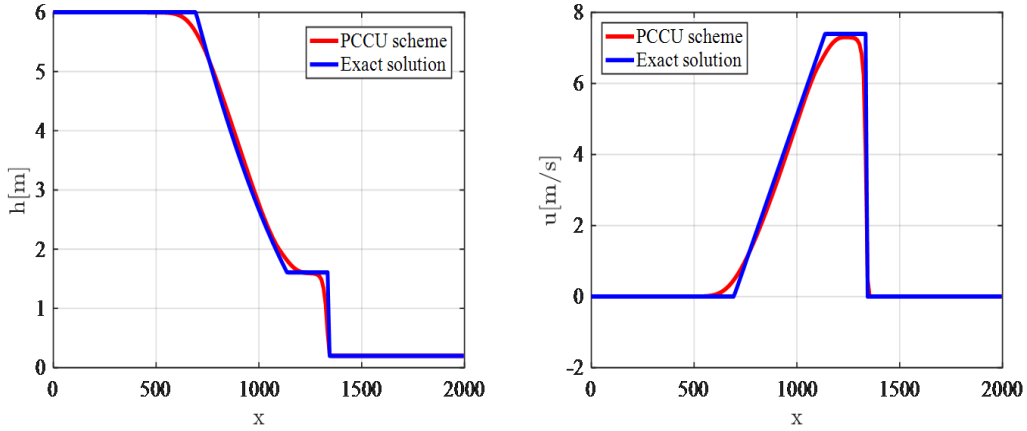


Figure 5: Accuracy test with wet zones. Comparison between exact solution and numerical solution ibtained by using PCCU scheme at the first order.

The numerical solutions for both tests are computed via the proposed WBPP method at the final time $T = 40s$. The exact solutions of SWE are compared to PCCU solutions. The results of these comparisons are displayed in Figs. (4)-(5). Our PCCU-AENO method exhibits good convergence behaviour for this well-known nonlinear hyperbolic problem.

Our scheme accurately locates the dry-wet transition and reproduces quite well the profile of the wave tip. Figs. (4)-(5) show that shock waves and rarefaction waves are well captured by the scheme. In both tests, the positivity of the water depth is well preserved. The robustness and the efficiency of the method is well observed.

A variant of this test is performed to assess the ability of the scheme to achieve a high order accuracy. A dam break with small water depth is performed to test this ability. The domain of simulation is $\Omega = [0, 1]$.

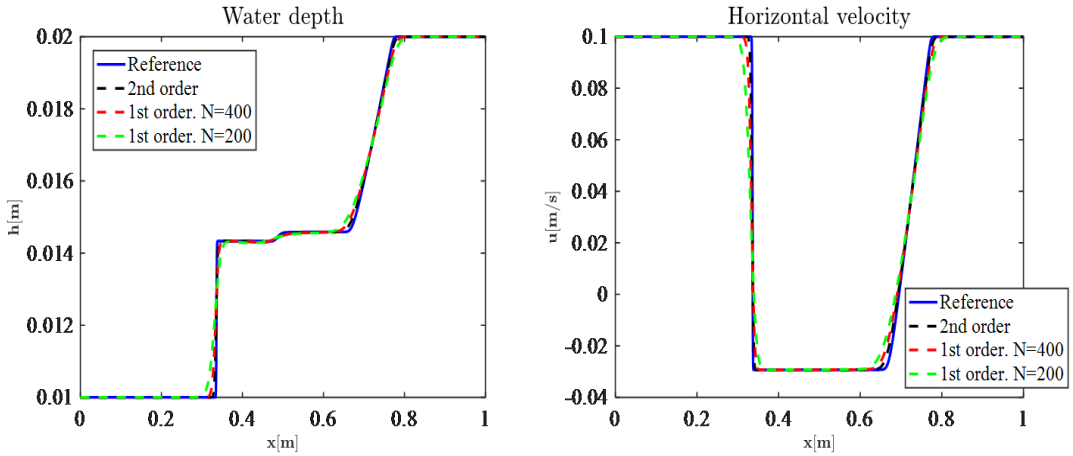


Figure 6: Accuracy test for dam break problem. Water depth and velocity computed via the proposed first and second PCCU schemes at time t =0.5.

The initial condition is:

$$h(x,0) = \begin{cases} 0.01 \ \text{ if } \ x \leq 0.5m \\ 0.02 \ \text{ if } \ x > 0.5m \end{cases}, u(x,0) = 0.1 \tag{152}$$

and the Neumann condition as in the previous test is used. In all the simulation the $CFL = 0.5$. The results of this test is displayed in Fig. (6).

One expects that for all the cases the computed solution at the first and second order (computed with $N = 100$) convergence to reference obtained via a refined mesh. We show that the proposed scheme can solve complex problems with at least a second order accuracy. This test confirm our theoretical results presented above state an order of convergence (at least 2).

### *7.2 Accuracy test with Shallow-Water-Exner equations*

We consider a simple 1D Saint-Venant-Exner test where a smooth analytical solution exists. This solution refers to a steady-state condition for a subcritical water flow coupled with a linear-in-time bed erosion, as proposed by Berthon et al.,[3]. A similar test problem has been studied in [24] and [8]. The SVE problem is a variant obtained from the proposed model when we set $E - D \equiv 0, B = 0$ and when the friction source term and sediment concentration vanished. In this application we use the first order path-conservative central-upwind scheme to approximate the 1D Saint-Exner model without source terms in domain $\Omega = [0,\ L]$, $L = 7m$. The exact solution is given by [3]:

$$\begin{cases} q_{exact} = 1, \\ u_{exact} = \left[\dfrac{\varrho x + \beta}{Ag}\right]^{1/3}, \\ h_{exact} = \dfrac{q_{exact}}{u_{exact}}, \\ Z_{b,exact} = 1 - \dfrac{u_{exact} + 2gq_{exact}(x)^2}{2gu_{exact}}, \end{cases} \tag{153}$$

where the coefficients are given by $\varrho = \beta = Ag = 0.005$. The comparison is made for both exact and numerical solutions and is plotted in Fig.(7).

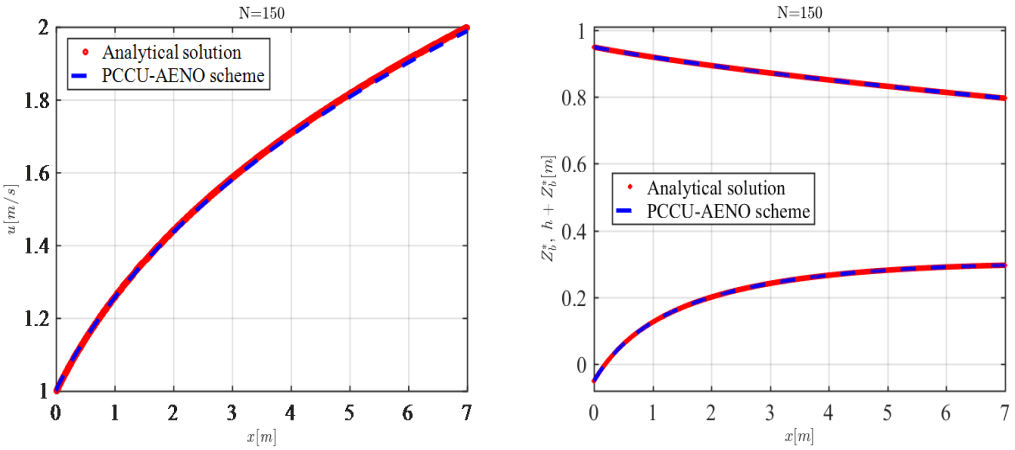


Figure 7: Comparison between analytical solution and numerical solution computed by the proposed PCCU-AENO scheme.

Table 2: The L1-errors and convergence rates for $h$, $u$ and $Z_b$ at the first order.

| | $h$ | | $hu$ | | $Z_b$ | |
|---|---|---|---|---|---|---|
| $N$ | $L^1-norm$ | $\mathcal{O}(L^1)$ | $L^1-norm$ | $\mathcal{O}(L^1)$ | $L^1-norm$ | $\mathcal{O}(L^1)$ |
| **50** | 5.78E-3 | / | 2.34E-2 | / | 4.569E-2 | / |
| **100** | 2.78E-3 | 1.053 | 1.32E-2 | 0.821 | 2.31E-3 | 0.981 |
| **200** | 1.36E-3 | 1.028 | 6.98E-3 | 0.922 | 1.03E-3 | 1.0417 |
| **400** | 7.101E-4 | 0.941 | 3.45E-3 | 1.011 | 5.46E-4 | 1.041 |

The Result displayed in Fig. (7) demonstrates that the proposed scheme can describe the bed level and water height evolution with good accuracy. We can see that our first order PCCU scheme provides a good approximation of the exact solution. Similar results were also obtained in literature in [8], [24], [3]. We run the computation on different grids varying the number of cells $N$ from 50 to 400. We show the $L^1-norm$ of the errors and the convergence rates $\mathcal{O}(L^1)$ at the first order in Table (2). We expected that the convergence rate tends to 1.

### *7.3 Steady state solutions at rest*

In this test we show that our M-PCCU scheme can capture steady-state solutions and thus satisfy the well-balanced property. This test is designed to verify that, when the erosion/deposition exchange source term is zero, all the rest of the contributions will not affect the well-balanced property in quiescent water with uniform sediment deposition. A similar test is done in [50]. We see also the behavior of the bottom in quiescent water. The computational domain is $[0,2]\times[0,2]$ and is divided into $N=400$ cells and set zero-order extrapolation boundary conditions at both ends of the domain, that is $W^0=W^1$, $W^N=W^{N+1}$. The initial conditions read:

$$h(x,y,0)=1, u(x,y,0)\equiv v(x,y,0)\equiv 0, \quad Z_b(x,y,0)\equiv C(x,y,0)=1.2\exp(-0.2(x-1.4)^2-0.2(y-0.8)^2). \tag{154}$$

Grass formula is used with $A_g=0.003$. In Fig.(8), we show the computed quiescent water surface, sediment concentration and bed evolution profiles at time $t=2s$.

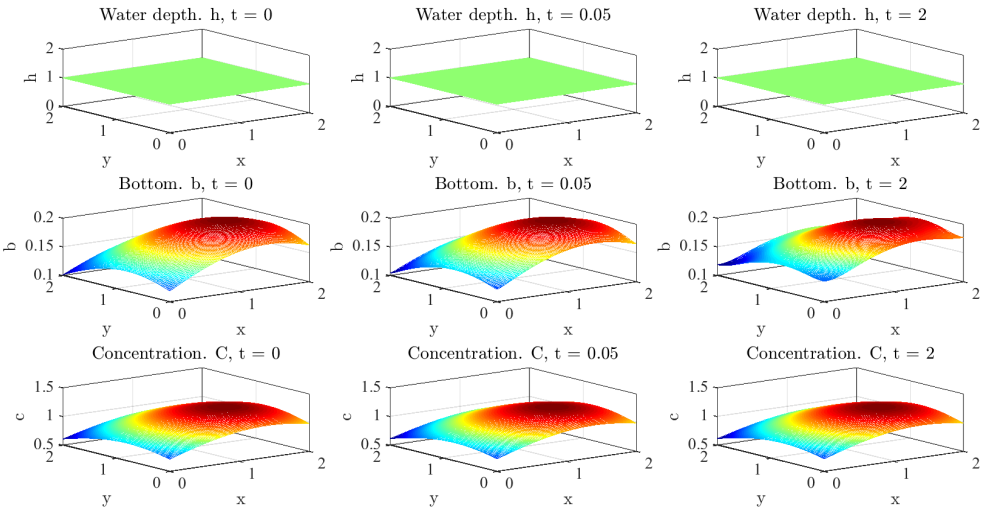


Figure 8: Free surface, bottom elevation and sediment concentration computed by the proposed well-balanced PCCU scheme. CFL =0.1

As one can see, no oscillations are developed at the quiescent water surface. When the erosion/deposition exchange source term is zero, all the rest of the contributions do not affect the *lake at rest* steady state at a discrete level. This test prove also the fact that $Z_b^*(x,y,t) \approx Z_b^*(x,y)$ and $C(x,y,t) \approx C(x,y)$. The Table (3) clearly illustrates that our 2D PCCU scheme preserves the studied steady-state solutions within the machine.

Table 3: The $L1-errors$ for $h$, $C$ and $Z_b$

| $N$ | $\|h^N - h^{N/2}\|_1$ | $\|C^N - C^{N/2}\|_1$ | $\|Z_b^N - Z_b^{N/2}\|_1$ |
|---|---|---|---|
| **100** | 1.16E-14 | 1.879E-8 | 2.548E-7 |
| **200** | 6.254E-16 | 2.547E-10 | 2.454E-9 |
| **400** | 5.2147E-17 | 4.011E-11 | 9.0124E-11 |
| **800** | 4.321E-17 | 8.471E-11 | 1.245E-13 |
| **1600** | 2.78E-18 | 7.584E-14 | 1.365E-15 |

### *7.4 Comparison with reference solution.*

We consider here to solve a reduced model obtained when $q_b = 0$ by using 1D PCCU scheme. The solved model has been originally proposed by Cao et al.,[10] and solved by a flux limiting method by Benkhaldoun et al., [2]. In this test, fourth sediment of diameters $d = 0.002, 0.001, 0.0008, 0.0001$ are tested to show the ability of the model to adapt to a wide range environments. The domain of simulation is $\Omega = [0, 50000]$ with a dam located at the middle of $\Omega$. The initial conditions are given:

$$h(x,0) = \begin{cases} 40 \text{ if } x \leq 25000m \\ 2 \text{ if } x > 25000m \end{cases}, \quad u(x,0) = 0, \;\; C(x,0) = 0.001, \;\; Z_b(x,0) = 0 \tag{155}$$

The Neumann condition is used for all the variables. The PCCU scheme is computed and plotted in Fig.(11). There is no analytical solution to this problem therefore a reference solution is computed with the PCCU scheme on a fine grid $N = 2000$. The reference solution is compared with the solutions obtained at first,

second and third order. The obtained results using our PCCU-AENO method are also in good agreement with those reported in [2].

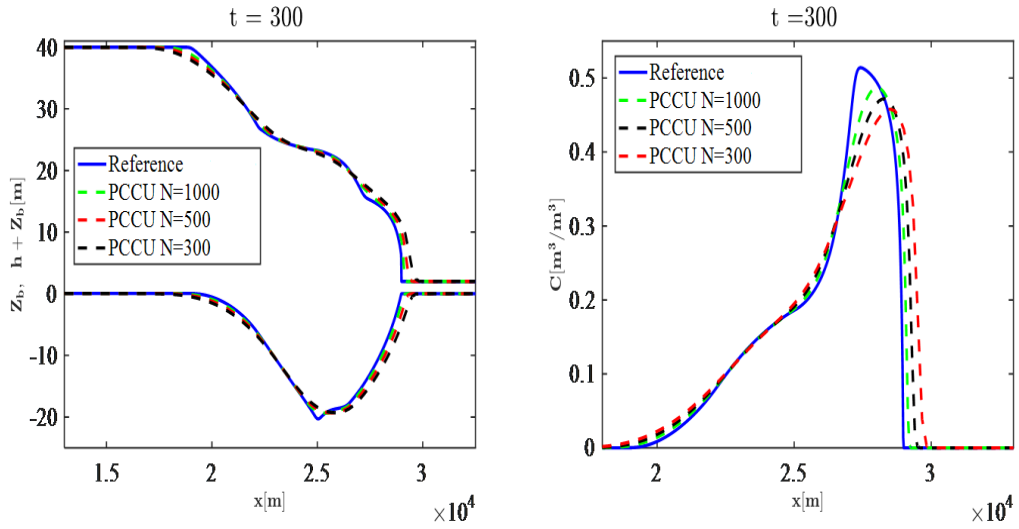


Figure 9: Comparison with reference solution. Free surfaces, bottom evolutions and sediment concentrations computed at the second order for d=0.001 and N=2000 cells, CFL = 0.55.

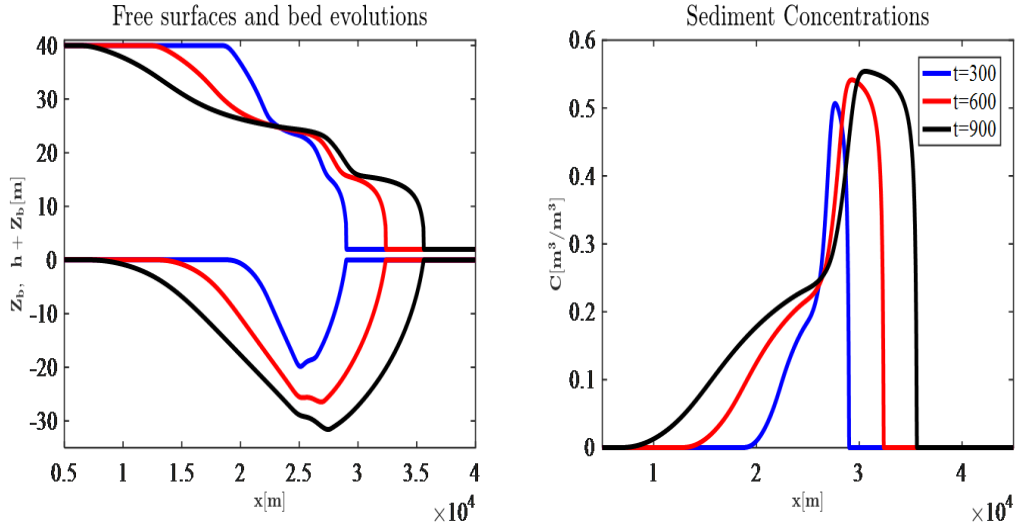


Figure 10: Comparison at different times of simulation. Free surfaces, bottom evolutions and sediment concentrations computed at the second order for d=0.001 and N=2000 cells CFL = 0.55.

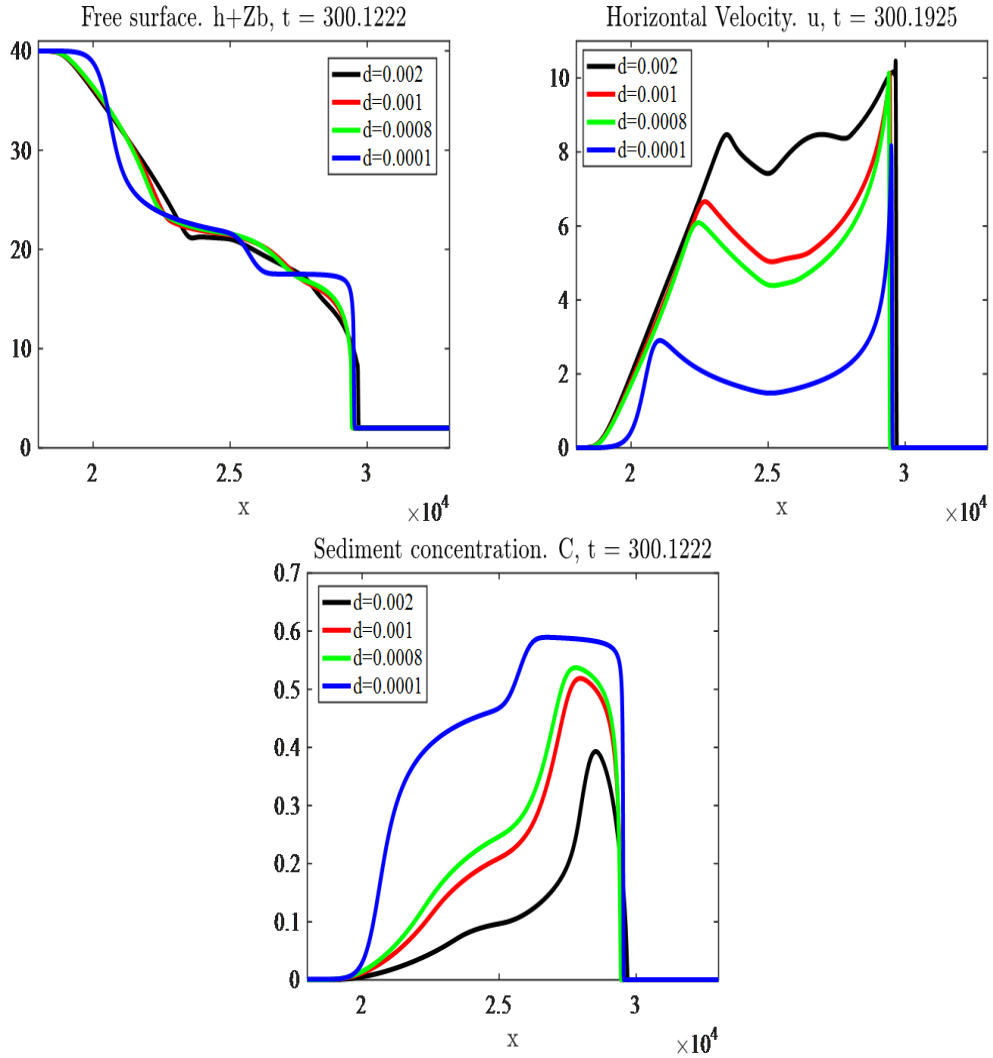


Figure 11: Free surface, horizontal velocity and sediment concentration profiles computed at first order for fourth different grain sizes. N=2000 cells CFL = 0.55

It is expected that the solution for each sediment size $d$ does not present any numerical diffusion. These results show that the dam break over the mobile bed can participate in the creation of a highly concentrated wavefront, which is limited by the forefront and a sediment transport contact discontinuity and decreases with time. It is observed that the sediment concentration is more intense for fine grains and this situation is associated with low velocity due to dilute flow (Boussinesq assumption). The presence of fine sediments in the water reduces the flow velocity and is well suitable to use Boussinesq assumption. However when the size of the sediment becomes greater, the concentration becomes low and fluid/sediment velocity has the same behavior as clear fluid velocity. In this situation the Boussisnesq assumption becomes questionable and the longitudinal diffusion coefficient can be revised. Moreover, the proposed method captures well the sediment concentration near the regions of large gradients without any oscillation.

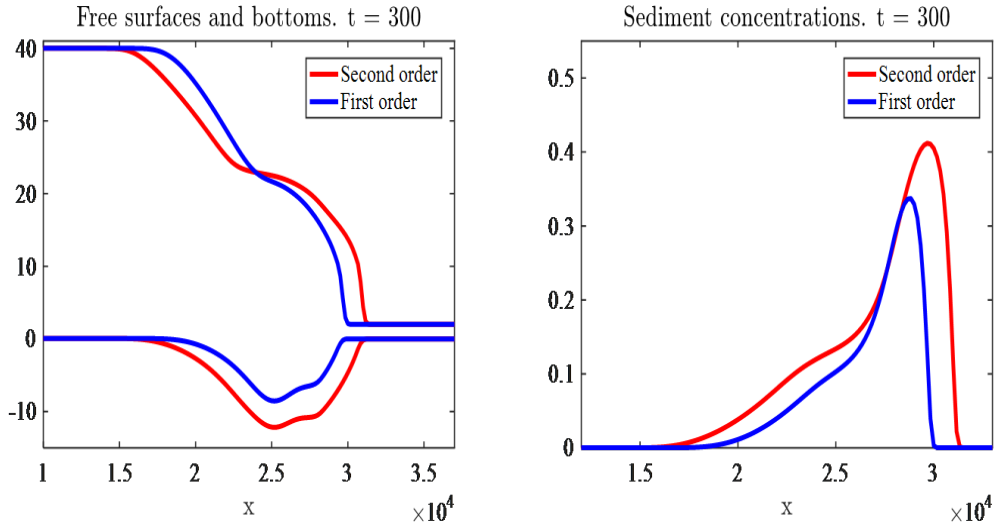


Figure 12: Comparison both first and second order schemes. Free surface, bottom evolution and sediment concentration computed at the first and second order accuracy for d=0.0018, CFL = 0.5. N=100

**First and second order schemes**

We compare now the results obtained by both first and second order scheme different sediment diameters $d = 0.18mm$, $d = 3mm$ with the same computational parameters as previously. The first order scheme is computed at different grid numbers $N = 100, 200, 400$. The obtained results are displayed in Figs.(12)-(13).

**Comparison with existing methods**

Next we compare the performance of the proposed PCCU scheme to the well-known CU scheme developed in Eq. (52). We consider the same parameters of simulation as previously and the computational solutions at different grid-points are plotted in Fig.(14).

The result Fig. (14) shows how the lack of well balanced discretization of nonconservative terms can fail the numerical convergence. It observed that the CU scheme does not detect the jump and does not accurately capture the shock waves possible solution of the model. The WBPP PCCU-AENO method proposed here eliminates the excess diffusion due to the presence of nonconservative terms. This confirm the drawbacks of CU scheme stated and proved in [35]. The computational time is very important aspect when long-term bed evolution of a river, estuaries and coastal environment must be investigated in engineering management application. With a various computational grids resolution, the PCCU-AENO method presents a better performance than the CU-AENO scheme.

*7.5 Experimental validation with a dry-wet transition test*

In this test, a reduced model named SVE (Saint-Venant-Exner) model is solved by our numerical method and compared with explicit staggered finite volume of Gunawan et al.,[24] and experimental data of [11]. The

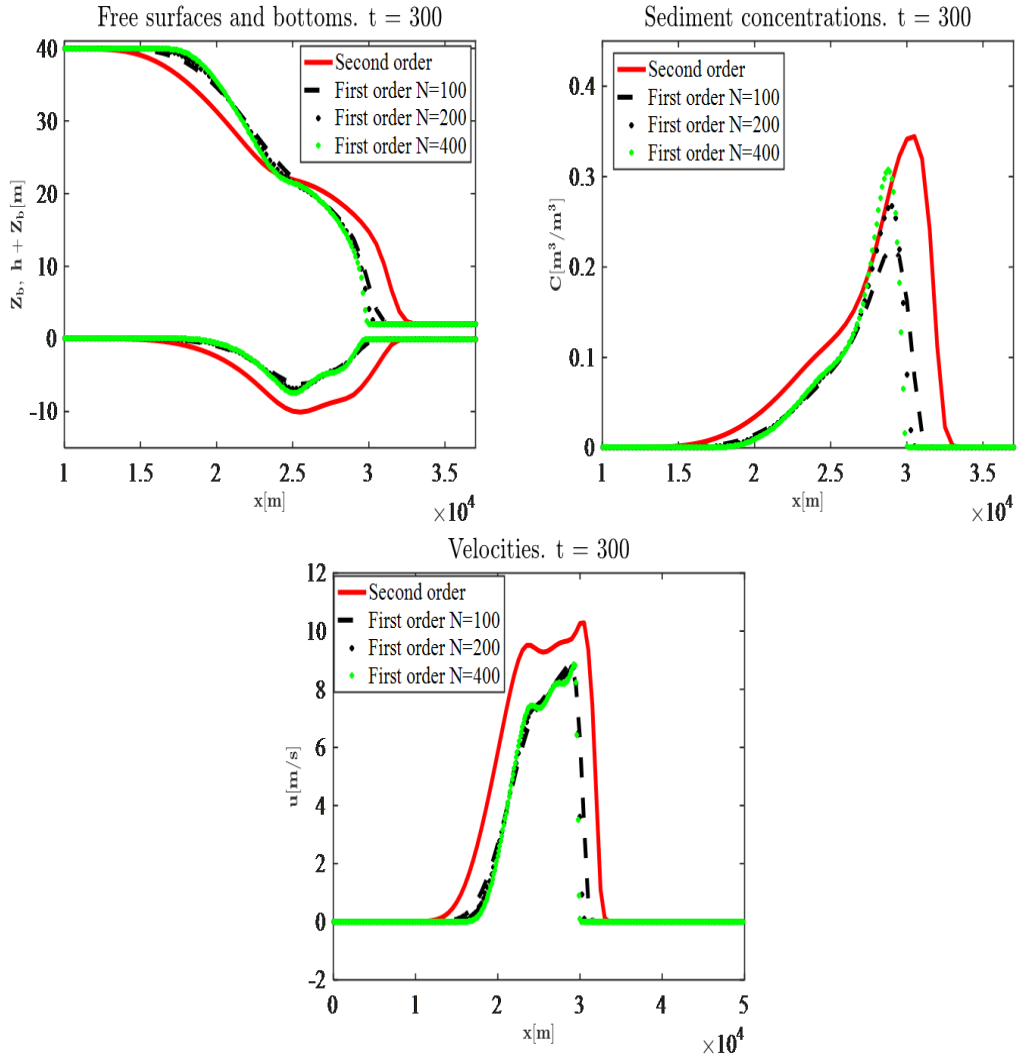


Figure 13: Comparison both first and second order schemes. Free surface, bottom evolution, horizontal velocity and sediment concentration computed at the first and second order accuracy for d=0.003, CFL = 0.5. We computed the second order scheme with $N = 100$ gridpoints

SVE is obtained from our model by removing the sediment exchange and bottom friction source terms in Eq. (20). The initial conditions are given:

$$h(x,0) = \begin{cases} 0.1 \ \text{ if } \ x \leq 0 \\ 0. \ \text{ if } \ x > 0 \end{cases}, \quad u(x,0) = 0, \quad Z_b(x,0) = 0. \tag{156}$$

The Neumann boundary conditions are used:

$$h.n_1 = 0, \quad u.n_1 = 0, Z_b.n_1 = 0. \tag{157}$$

The sediment diameter is $d_{50} = 0.0032$, the sediment density is $\rho_s = 1.540$, the domain of simulation is $\Omega = [-1.25; 1.25]$, Grass formula is used with $A_g = 0.003$. The free surface and bed level profiles at different times are shown in Figure (15) they show a good agreement between the numerical solution and the experiment data of [11].

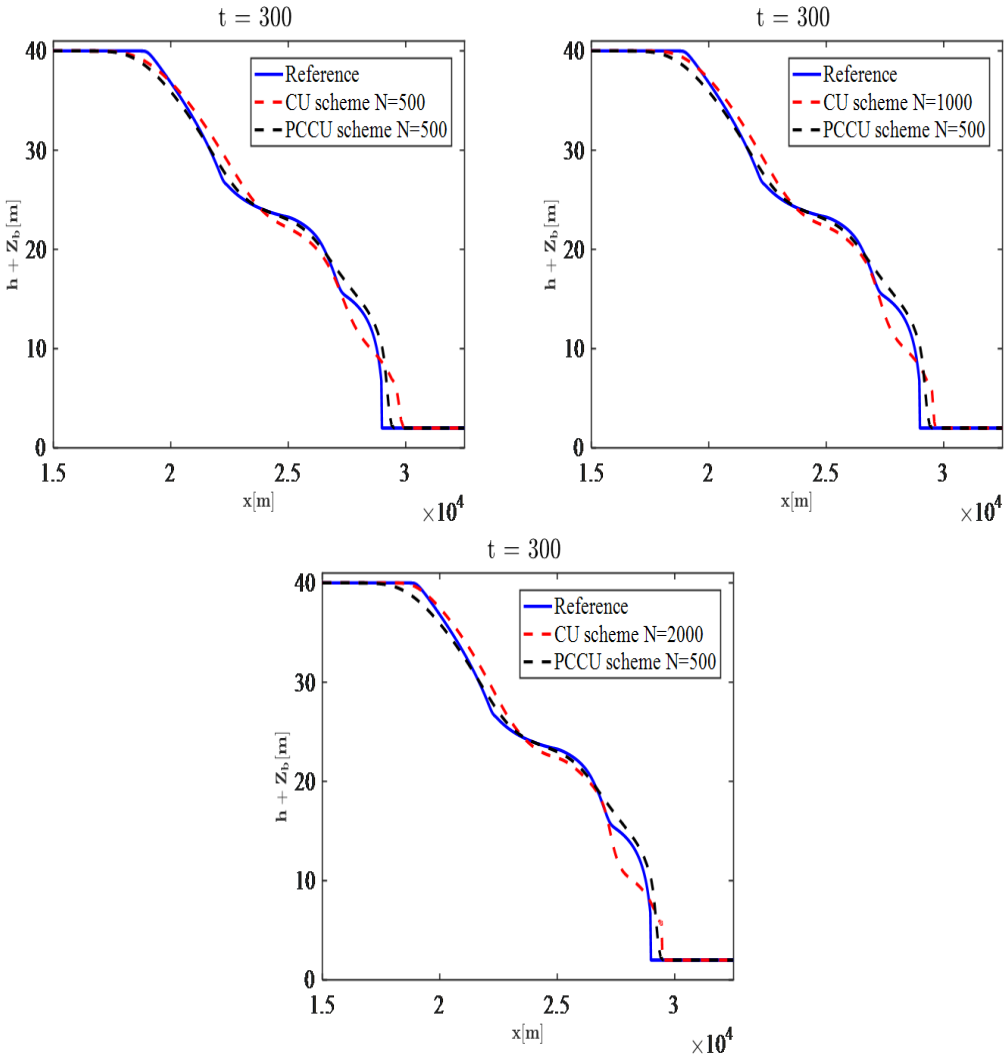


Figure 14: Free surfaces computed at second order for both CU and PCCU schemes. The sediment diameter is $d = 0.0005$, CFL $= 0.55$

The results obtained in Fig. (15) are practically similar to those obtained by [24] using an explicit finite volume scheme on a staggered grid. The test shows that the developed WBPP AENO scheme can treat the wet/dry zones without difficulty. We recall that the bedload equation is given by (11). The mass conservation of moving particles can be applied to formulate the transport at the bedload interface in term of a transport discharge flux $q_b$:

$$\mathbf{u}(t, \mathbf{x}, Z_b^*)\nabla Z_b^*(\mathbf{x}, t) - u_3(\mathbf{x}, t, Z_b) = \nabla . q_b. \tag{158}$$

In Exner equation obtained by (11) and (158), we assume that the motion at the bedload interface is balanced by the gradient of the horizontal mass sediment flux $q_b$. It well-known that the Exner equation assumes that the bottom characteristic velocity moves at the same velocity than the velocity fluid. This is not physically acceptable is constitutes an ad hoc assumption that produces the discrepancy observed in the test presented in Fig.(15). A modification of the bedload equation can be given to improve the results

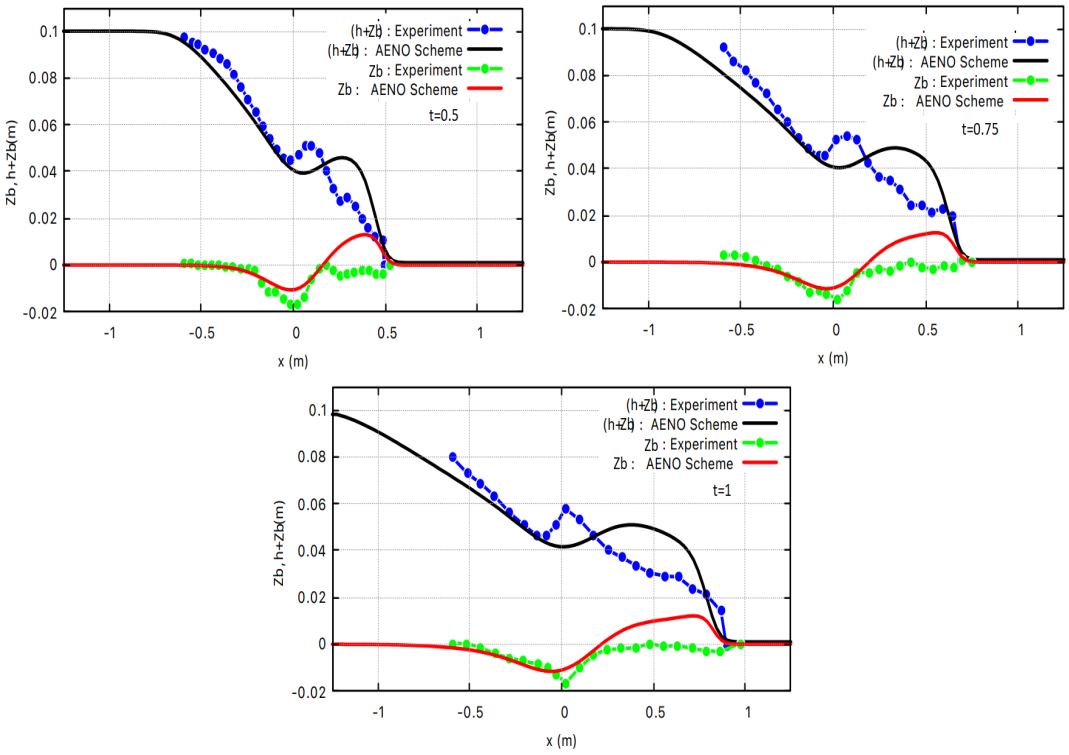


Figure 15: Free surfaces and bed levels profiles computed at second order using PCCU scheme. N=100 cells

observed. Alternative formulations have been recently proposed by Ngatcha et al.[34, 32, 33].

### *7.6 Comparison between CU and PCCU schemes*

In this test, we design a genuinely two-dimensional dam-break problem to validate our proposed scheme for the sediment transport model in nonhomogeneous SWE developed here. The initial water depth displayed in Fig. (16) is given by:

$$h(x,y,0) = 2 + 0.25(1 - tanh(c(\sqrt{ax^2 + by^2}) - 1)), \tag{159}$$

where $a = 2.5,\ \ b = 0.6,\ \ c = 10.$

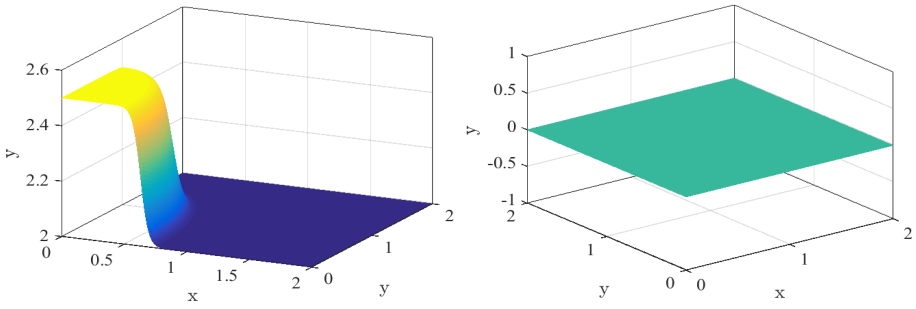


Figure 16: Initial water depth

The initial sediment concentration is $C(x, y, 0) = 0.001$. The initial velocities are $u(x, y, 0) = 0$ and $v(x, y, 0) = 0$, the initial bottom is $Z_b(x, y, 0) = 0$. The sediment porosity is $p = 0.25$. Manning's coefficient is $n = 0.02$, the erosion force $\phi = 0.015$, the diameter of sediment is $d_{50} = 0.001$. The Exner equation is used with $Ag = 0.001$. The boundary conditions read:

$$h.\mathbf{n} = 0, \quad \mathbf{u}.\mathbf{n} = 0, \quad C.\mathbf{n} = 0, Z_b.\mathbf{n} = 0 \tag{160}$$

The solution is computed using the 2D PCCU-AENO scheme presented here. All the unknowns are plotted and presented in Fig.(19). The results demonstrate that the 2D-PCCU scheme can predict stable morphodynamics.

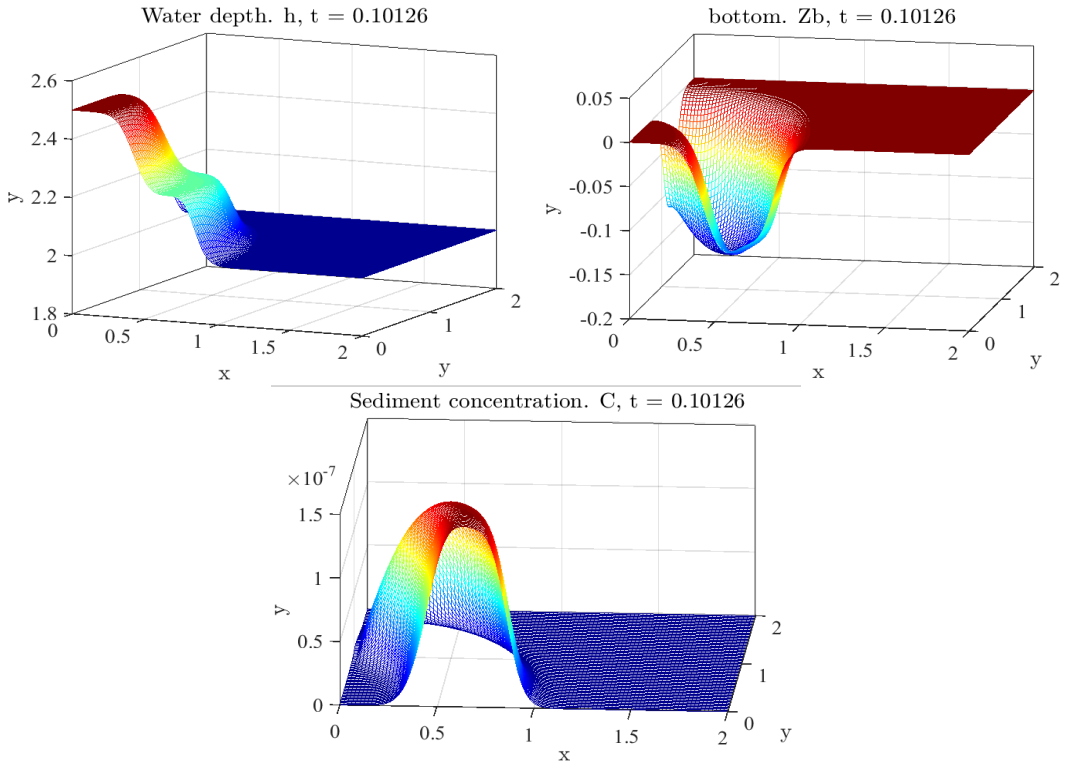


Figure 17: Free surface, bed level and sediment concentration profiles. N=100 cells

Now we compare the M-PCCU scheme and M-CU scheme by using the same computational parameters. The results are plotted in Figs. (18)-(20)

When the mesh is refined, the second-order convergence rate is observed for all the conserved variables, $h$, $hu$, $hv$, $C$, $Z_b$. The results of convergence for the two-dimensional problem on the structured mesh are shown in Table.(4)-(5).

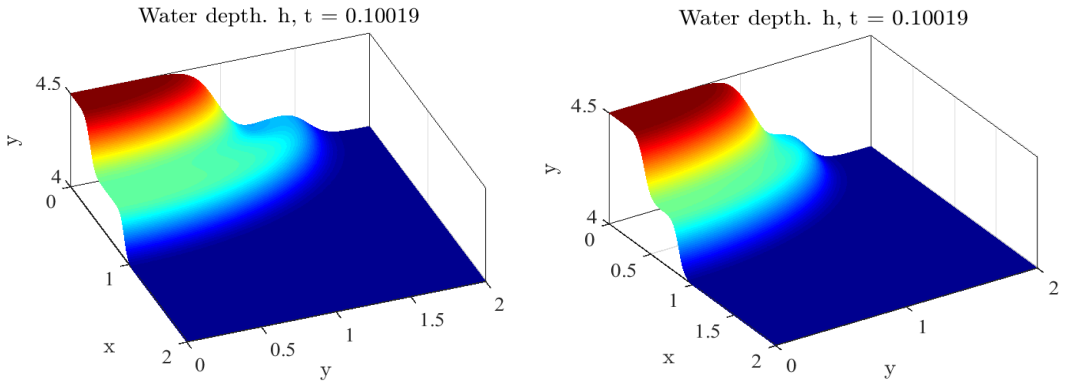


Figure 18: Free surface profiles. Comparison between PCCU and CU schemes. Left CU scheme, Right PCCU scheme. N=500 cells.

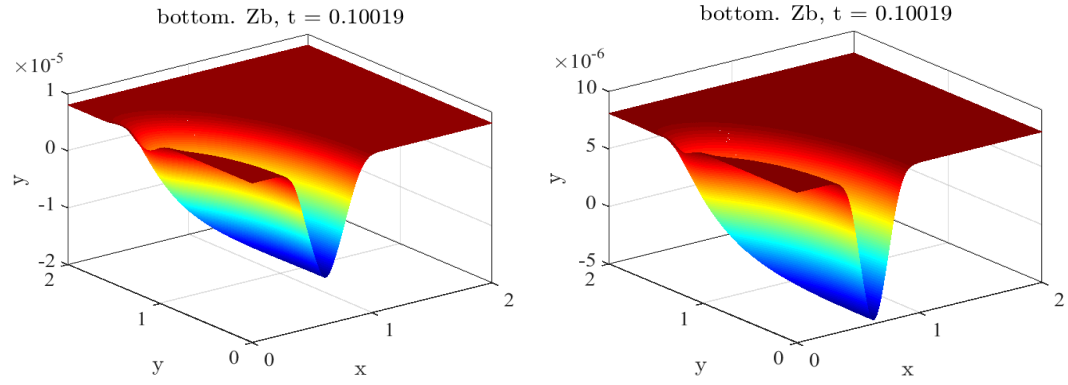


Figure 19: Bed evolution solutions. Comparison between CU scheme and PCCU scheme. Left CU scheme, Right PCCU scheme. N=500

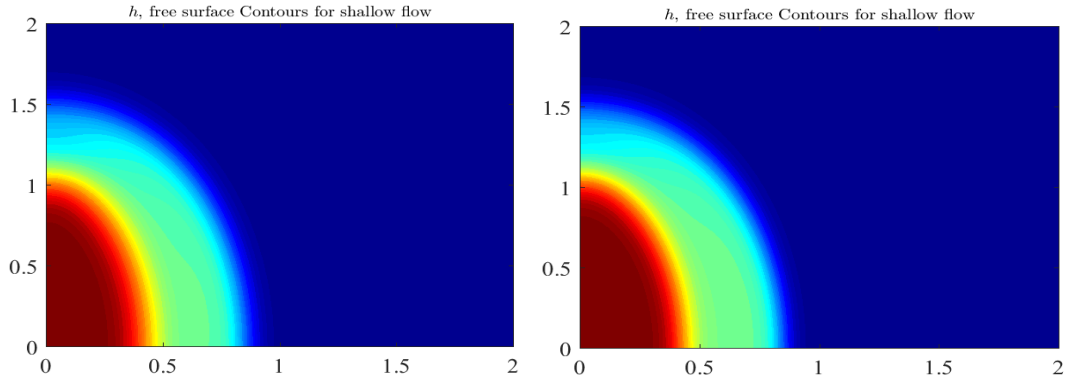


Figure 20: Free surface contours. Left CU scheme, Right PCCU scheme.

Table 4: The $L1-errors$ and convergence rates for $h$, $C$ and $Z_b$

| $N$ | $\|h^N - h^{N/2}\|_1$ | $\mathcal{O}(L^1)$ | $\|C^N - C^{N/2}\|_1$ | $\mathcal{O}(L^1)$ | $\|Z_b^N - Z_b^{N/2}\|_1$ | $\mathcal{O}(L^1)$ |
|---|---|---|---|---|---|---|
| **100** | 7.15E-3 | / | 9.83E-3 | / | 8.97E-3 | / |
| **200** | 1.969E-3 | 1.861 | 2.82E-3 | 1.801 | 2.14E-3 | 2.066 |
| **400** | 4.84E-4 | 2.021 | 7.21E-4 | 1.967 | 5.41E-4 | 1.986 |
| **800** | 1.189E-4 | 1.976 | 1.89E-4 | 1.925 | 1.38E-4 | 1.961 |
| **1600** | 2.97E-5 | 2.001 | 4.65E-5 | 2.025 | 3.65E-5 | 1.916 |

Table 5: The $L1-errors$ and convergence rates for $hu$ and $hv$

| $N$ | $\|(hu)^N - (hu)^{N/2}\|_1$ | $\mathcal{O}(L^1)$ | $\|(hv)^N - (hv)^{N/2}\|_1$ | $\mathcal{O}(L^1)$ |
|---|---|---|---|---|
| **100** | 3.45E-2 | / | 2.14E-2 | / |
| **200** | 8.97E-3 | 1.943 | 5.84E-3 | 1.872 |
| **400** | 2.45E-3 | 1.872 | 1.34E-3 | 2.002 |
| **800** | 7.84E-4 | 1.644 | 3.58E-4 | 1.904 |
| **1600** | 2.014E-5 | 1.959 | 8.91E-5 | 2.007 |

**Efficiency of the proposed well-balanced discretization**

Now we verify the efficiency of the proposed well-balanced discretization strategy. We use the simulation parameters of the previous test. The results are plotted in Fig. (21). We show that the PCCU scheme with the well-balanced strategy developed gives best results than PCCU without using this strategy.

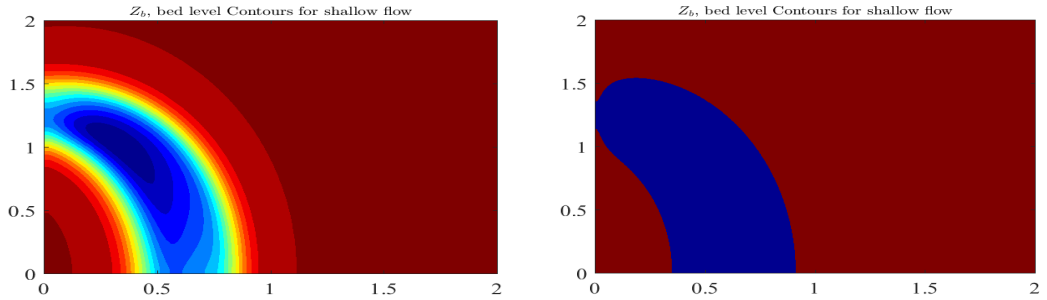


Figure 21: Bed evolution contours. Left non well-balanced PCCU scheme, Right well-balanced PCCU scheme.

*7.7 Processing of Dry/wet and dry cells on a 2D Riemann problem*

When utilizing WBPP shock-capturing PCCU-AENO scheme to predict sediment transport in coastal flows in real 2D geometry the processing of dry-wet and dry cells is an important step. We consider a 2D Riemann problem with dry/wet cells. The initial conditions given in Table. (6) are displayed in Fig.(22) and Fig.(24). Two tests are performed to show the positivity and robustness properties of our proposed 2D method. The Riemann problem performed here consists to a dam break over erodible bed with high sediment transport. The computational domain for both tests reads $\Omega = [-1;\ 1] \times [-1;\ 1]$ and as previously, the Neumann condition (160) is applied on all the boubdaries.

Table 6: Initial conditions of 2D Riemann problem with wet/dry zones

| **Test1: wet zones** | $h[m]$ | $Z_b[m]$ | $u[m/s]$ | $v[m/s]$ |
|---|---|---|---|---|
| $x \in [-0.5; 0.5], y \in [-0.5; 0.5]$ | 2 | 1.5 | 0 | 0 |
| $x \in [-1; 1], y \in [-1; 1]$ | 1 | 1 | 0 | 0 |
| **Test2: dry zones** | $h[m]$ | $Z_b[m]$ | $u[m/s]$ | $v[m/s]$ |
| $x \in [-0.5; 0.5], y \in [-0.5; 0.5]$ | 2 | 1.5 | 0 | 0 |
| $x \in [-1; 1], y \in [-1; 1]$ | 0 | 0 | 0 | 0 |

For the first test, we have removed the bedload sediment flux ($q_b = 0$) and for the second test, Grass formula is performed with $A_g = 0.003$ and bed porosity $p = 0.2$. The sediment concentration is plotted with $d_{50} = 8mm$, the friction term is considered with $n = 0.03$. The sediment concentration is $C = 0.001$, the erosion force is $\varphi = 0.25$

The rest of parameter used the test is available in Table (2). All the source terms are considered in the numerical simulations. We have used $N = 200$ structured cells for both tests. The solution obtained at different times $t = 0.2, t = 0.5$ are displayed in Figs (23) and (25)

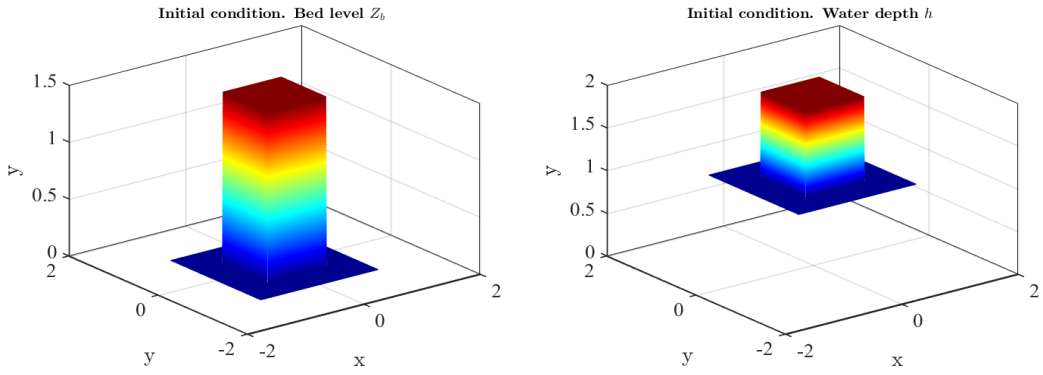


Figure 22: Initial condition of the Riemann problem: processing of wet cells

It is expected that all the profiles presented here describe well the dynamics of sediment and the free surface flow during the simulation time. It is observed in Fig. (23), that the positivity and robustness of the scheme are preserved during all the simulation. Therefore, we conclude that the proposed 2D AENO method has been successful in eliminating the numerical diffusion and does not give rise to nonphysical oscillations even near regions of large gradients while maintaining positive the water depth even in presence of dry cells. The two-dimensional AENO-hydrostatic reconstruction proposed in this work is clearly interesting and can be used for a wide range of two-dimensional conservative and nonconservative problems.

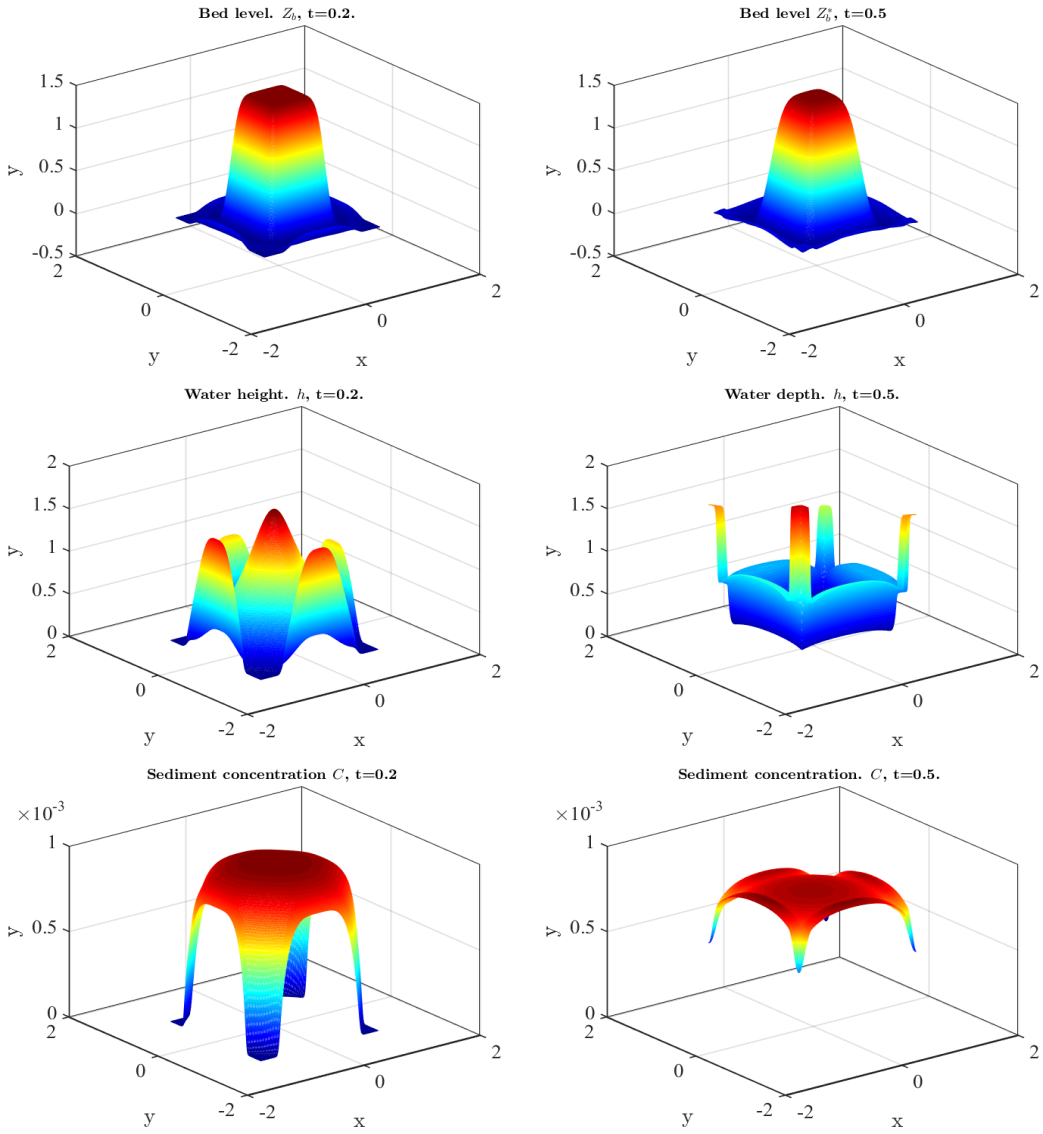


Figure 23: Dam break over dry bed. Bed evolution and water depth profiles for fully coupled model with PCCU-AENO scheme on structured meshes at different times

### *7.8 Low and high interaction between sediment and fluid. Comparison between Meyer&Peter-Muller formula and Grass formula*

In this test, we show that the proposed method can simulate the low and high interaction between sediment and fluid. In fact, this is one of the main problems in order to obtain precise numerical approximations. Due to the phase lag effect which does not integrate into the proposed sediment transport model, the numerical diffusion can appear. It's important to design a high-order PCCU scheme in order to avoid this phenomenon. The sediment transport flux can write by a unified formulation:

$$q_b = c_1 K_2(h,q)(c_2 + c_3 K_1(h,q))^m \tag{161}$$

where $m$, $c_1$, $c_2$ and $c_3$ are constant values and $K_1$, $K_2$ are scalar function of $h$ and $q$. For Grass formula $c_1 = Ag$, $K_2(h,q) = u$, $c_2 = 0$, $c_1 = 1$, $K_1 = |u|$, $m = m_g = 1$. To compare both Meyer&Peter-Muller

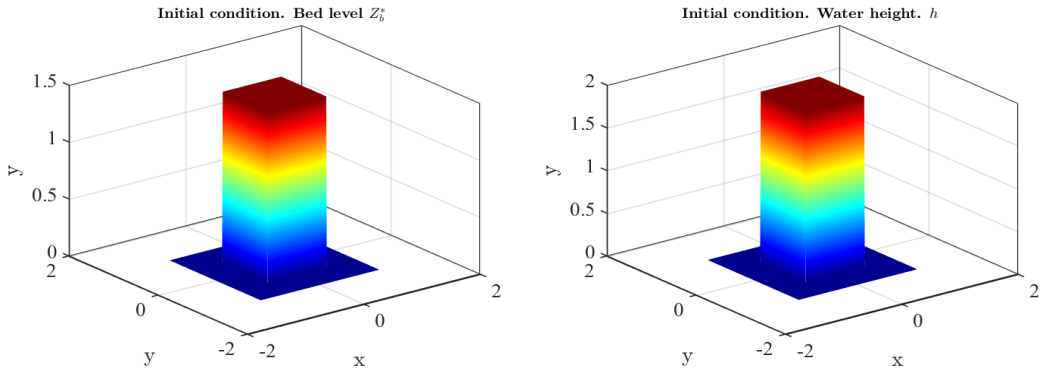


Figure 24: Initial condition of the Riemann problem: processing of dry cells

formula and the Grass formula we approximate with the Grass model. In fact, the MPM formula without critical shear stress can be interpreted as a particular case of the Grass model for values of $Ag$ and $m_g$. We recall that $Ag$ represents the type of interaction between fluid and sediment and for MPM model can read:

$$Ag = \frac{8\sqrt{g}\mathbf{d}^3}{(s-1)R_h^{1/2}}, \tag{162}$$

where $s$ is specific density ratio, $R_h$ is the hydraulic radius, we have $R_h \sim h$ and where $\mathbf{d}$ is constant. Considering $s = 2.65$, $g = 10$, $d = 0.0198$, we obtain for MPM model:

$$Ag = 1.19 \times 10^{-4} h^{-1/2}. \tag{163}$$

We observe that for a range of values of water depth, we have always had to do weak interactions.

The test is performed by a dam break. The fluid velocity $u(x, y, 0) = 0$. The domains of simulation are $\Omega = [0, 2000] \times [0, 10]$. For two-dimensional we consider triangular meshes with 1400 triangles. The dam is located in the middle of $\Omega$. The dam separates two initial water depth exhibits; wet zones are $h(x, y, 0) = 20m$ on the left side and $h(x, y, 0) = 1m$ on the right side of the domain. We perform the test by using both Grass and MPM formulas. The results of the simulation are presented in Fig. (26)-(27). Fig.(26) compares the solutions obtained by the our proposed second order TVD method. Fig.(27) shows the influence of the degree of interaction between sediment and fluid $Ag$. It is also seen that for the considered sediment flux formulae, the use of Gerschgorin disc theorem is particularly appropriate.

It is expected in Fig. (28) that the second order scheme becomes unstable when $Ag$ becomes greater. This unstability is due to the strong interaction between the sediment and fluid near the bottom. This scheme allows to obtain a stable evolution of the morphodynamics when the fluid/sediment interactions are strong. We conclude that it is important to develop a high order scheme to accurately capture these interactions. There are no particular difficulties in extending these tests with a high-order scheme. This last step does not pose any particular difficulty and will be useful for concrete applications. This would not be surprising since we have demonstrated theoretically that our method is able to achieve a high order accuracy. Tests will be done in a future article to confirm this. We have limited ourselves this paper only to the second-order test. Exner equation is not appropriate to describe the morphodynamics in presence of strong sediment/fluid interactions [32],[34]. A bed-load equation must be able to describe the movement of the bottom even when the sediment/fluid interaction becomes greater.

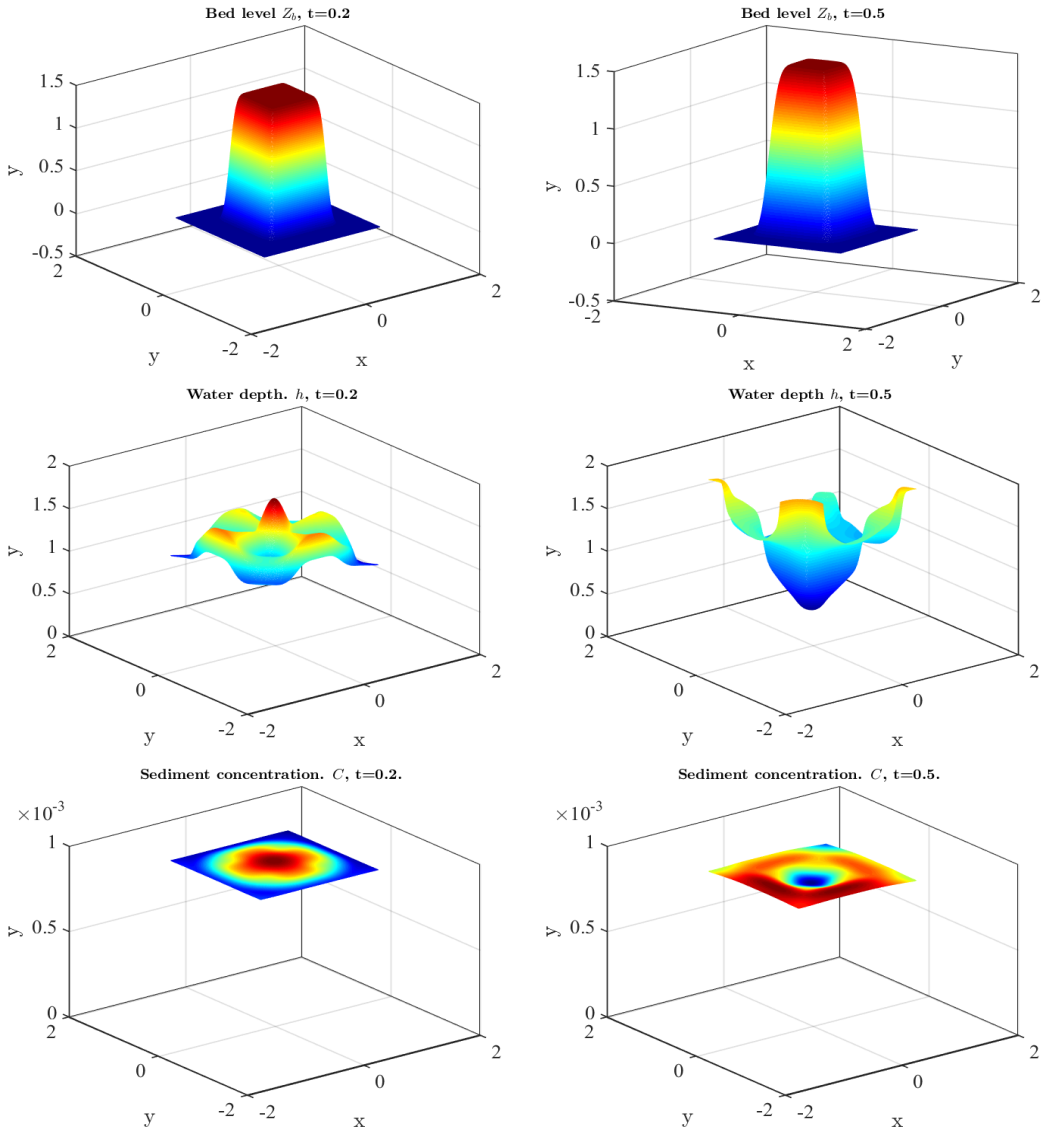


Figure 25: Dam break over wet bed. Bed evolution and water depth profiles for fully coupled model with PCCU-AENO scheme on structured meshes at different times

## 8 Concluding and perspectives

In this paper, an unstructured path-conservative central-upwind scheme has been introduced and applied to solve a new sediment transport model. The model is a coupling of nonhomogeneous shallow water equations with sediment transport phenomena. The model generalizes several recent sediment transport models based on Shallow Water equations. The proposed model is a nonconservative system of nonlinear equations admitting a complex Jacobian matrix. The existence of global weak solution of the model remains an open problem. The Gerschgorin disc theorem has been applied with success to reduce the cost of finding the eigenvalues of the complicated Jacobian matrix. We have used these computed eigenvalues to design an original simple, robust and highly accurate path-conservative method based on combination of 1D Riemann solvers without any intermediate states. Contrarily to some mutlidimensional schemes available in the literature, the total eigenstructure of the model is not necessary. A novel multidimensional well-balanced discretization

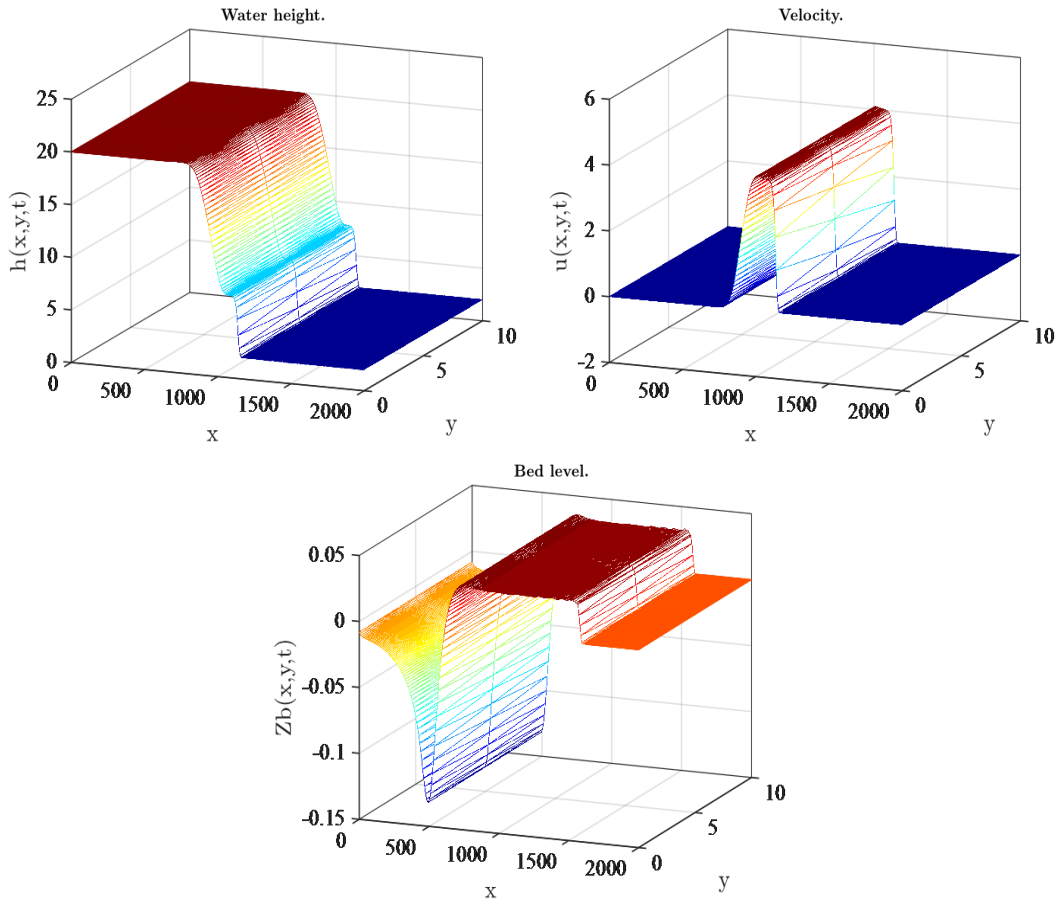


Figure 26: Numerical solution of a dam break problem obtained using our unstructured PCCU method TVD method. The time of simulation is $T = 40s$, MPM formula is used with Ag given by Eq.(163)

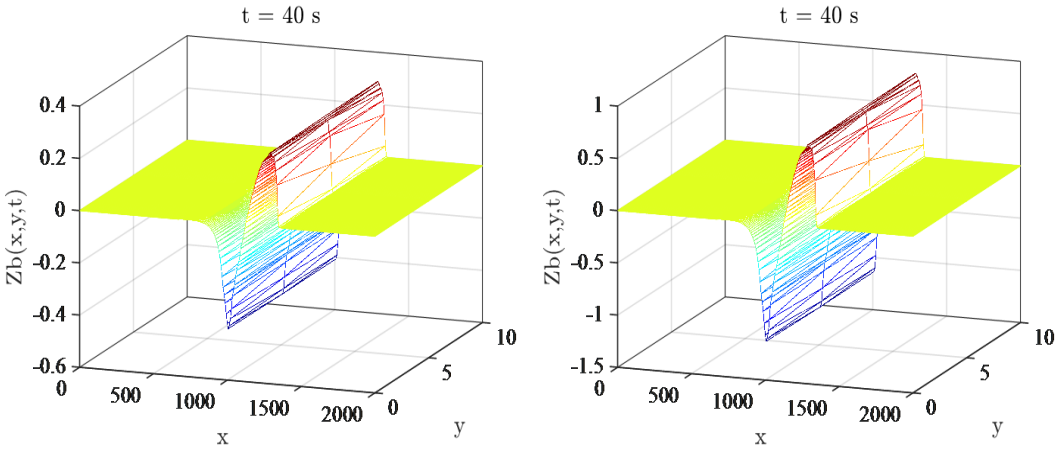


Figure 27: Dam break over mobile bed. Bed evolutions $Z_b$ with Grass formmulae. Left strong interaction $Ag = 0.009$ with Grass formula, right weak interaction $Ag = 0.09$ with MPM formula.

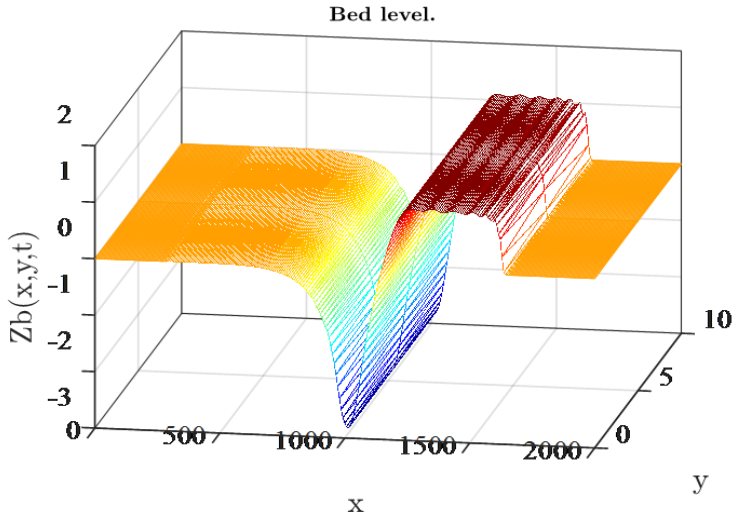


Figure 28: Dam break over high fluid-sediment interaction using the second order PCCU scheme, $Ag = 0.9$ The time of simulation is $T = 40s$

strategy has been developed and implemented here. With that, the scheme has been proven well-balanced and is able to capture steady-state solutions. The piecewise polynomial reconstruction procedure developed here allows us to develop a high-order M-PCCU scheme. Some results related to the method have been proved rigorously with acceptable mathematic formulations. Some tests have been made to show the performance and interesting properties of our method (positivity-preserving, shock-capturing, well-balanced, stability). The developed high-order unstructured PCCU method can be used to simulate sediment transport models in complex flow while remaining robust and accurate. The proposed method is computationally efficient and easy to apply in most computer programming languages.

### Advantages and limitations of the numerical modeling

The use of the M-PCCU scheme will be appropriate to capture the shocks even when the number of cells is small. It's proven experimentally that the Exner's equation is not applicable to accurately describe the morphodynamics. There is a need to reformulate this equation in order to extend it to a wide range of sediment transport problems in coastal environments. The bedload equation given by (11) can be a opportunity of modeling and this has been proved in a recent work of Ngatcha et al[32]. The bed-load equation proposed by these authors is susceptible to be improved. The well-balanced discretization strategy of the source terms for multidimensional scheme can also be improved.

### Perspectives

Future works are extended to: (i) The proposed model can be extended to a multi-class sediment transport model; (ii) study the case where the distortion effect in the fluid flow plays an important role; (iii) other types of meshes can be implemented.

### Data availability

The data that support the findings of this study are available on request from the corresponding author.

**Conflict of Interests**

The authors declare that there is no conflict of interests regarding the publication of this paper.

**Acknowledgements**

The authors would like to thank an anonymous referee for giving very helpful comments and suggestions that have greatly improved this paper.

[1] D. S. Balsara, M. Dumbser, and R. Abgrall, Multidimensional HLLC Riemann Solver for Unstructured Meshes - with Application to Euler and MHD Flow, J. Comput. Phys.(2014) 261, 172-208.

[2] Benkhaldoun, F., Sari, S., Seaid, M. A Flux-Limiter Method for Dam-Break Flows over Erodible Sediment Beds. Applied Mathematical Modelling (2012) 36, 4847-4861.

[3] C. Berthon, S. Cordier„ Delestre, O., HoangLe, M. An Analytical Solution of the Shallow Water System Coupled to the Exner Equation, In: Comptes Rendus Mathematique 350.3 (2012), pp. 183-186. doi: 10.1016/j.crma.2012.01.007.

[4] Berthon, C., Boutin, B., Turpault, R. (2015). Shock Profiles for the Shallow-Water Exner Models. Advances in Applied Mathematics and Mechanics, 7(3), 267-294. doi:10.4208/aamm.2013.m331.

[5] A. Bhole, B. Nkonga, S. Gavrilyuk, and K. Ivanova. Fluctuation Splitting Riemann Solver for a Nonconservative Modeling of Shear Shallow Water Flow. Journal of Computational Physics(2019) 392, 205-226.

[6] M.J. Castro, A. Kurganov and T. Morales de luna, Path Conservative Central-Upwind for Nonconservative Hyperbolic Systems", ESAIN M2AN(2019) 53, 959-985.

[7] M.J. Castro Diaz, E.D. Fernandez-Nieto, A.M. Ferreiro, Two-dimensional Sediment Transport Models in Shallow Water Equations. A Second Order Finite Volume Approach on Unstructured Meshes. Comput. Methods Appl. Mech. Engrg., 198:2520-2538, 2009.

[8] Carraro, F., Valiani, A., Caleffi, V. Efficient Analytical Implementation of the DOT Riemann Solver for the Saint Venant-Exner Morphodynamic Model. Advances in Water Resources (2018), 113, 189-201.

[9] C. Parés, Numerical Methods for Nonconservative Hyperbolic Systems: A Theoretical Framework., SIAM Journal on Numerical Analysis (2006), 44,300-321.

[10] Z. Cao, G. Pender, S. Wallis, and P. Carling, Computational Dam-Break Hydraulics over Erodible Sediment Bed. J. Hydraul. Eng.(2004) 130(7), 689-703.

[11] L. Fraccarollo, and H. Capart. Riemann Wave Description of Erosional Dam-Break Flows. J. Fluid Mech (2002). Vol. 461, pp. 183-228.

[12] A. Chertock, A. Kurganov, and W. Tong, Steady State and System Preserving Semi-Implicit Runge-Kutta Methods for ODEs with Stiff Damping Term. Inter. J. Num. Meth fluids (2015) 78,355-383.

[13] M. Charafi, M. Menai, A. Sadok, A. Kamal, Numerical Modeling of change bottom elevation in a cohesive bed channel. Comput. Phys. Commun, (1999) Vol 121-122.

[14] M. C. A. Clare, J. R. Percival, A. Angeloudis, C. J. Cotter and M. Piggot. Hydro-morphodynamics 2D modelling using a discontinuous Galerkin discretization. Computers&Geosciences 146, 104658, 2021.

[15] G. Dal Maso, P. G. Lefloch, and F. Murat, Defintion and weak stability of nonconservative products, J .Math.Pures Appl.(1995) 74. 483-548.

[16] M. Dumbser, E. F. Toro, A Simple Extension of the Osher Riemann Solver to Non-conservative Hyperbolic Systems. Journal of Scientific Computing 48 (1-3), 70-88.

[17] B. A. J. C. De Saint-Venant, Théorie du Mouvement Non-Permanent des Eaux, avec Application aux Crues des Rivière et à l'Introduction des Marées dans leur Lit. Comptes Rendus de L'Académie des Sciences (1871), 73:147-154.

[18] F. M. Exner, Über die Wechselwirkung zwischen Wasser und Geschiebe in Flüssen. Akademie der Wissenschaften (1925), Sitzungsberichte 134, Wien, Austria.

[19] A. J. Grass. Sediment transport by waves and currents department of civil engineering, University college, London, 1981.

[20] S. Godunov. A Finite Difference Method for the Computation of Discontinuous Solutions of the Equations of Fluid Dynamics. Sbornik: Mathematics (1959) 47 (8-9), 357-393.

[21] B. P. Greimann, J. C. Huang. Two-dimensional Total Sediment load Model Equations. J. Hydraul. Eng, 134, 1142-1146.

[22] S. Gottlieb, C.W. Shu. and E. Tadmor, Strong Stability Preserving High order Time Discretization Methods. SIAM REVIEW 2001, Vol.43, No 1, pp.89-112.

[23] A. Harten, P. Lax, and B. Van Leer, Upstream Differencing and Godunov-type Scheme for Hyperbolic Conservation laws, Upwind and High-Resolution Schemes, 1982, pp. 53-79, DOI: 10.1007/978-3-642-60543-74.

[24] H. P. Gunawan, X. Lhébrad, Hydrostatic Relaxation Scheme for the 1D Shallow Water-Exner Equations in Bedload Transport. Comput.& Fluids , Vol. 121, 2015.

[25] F. M. Holly, J. M. Rahuel, New Numerical/Physical framework for Mobile Bed Modelling, part1: Numerical and Physical Principles. Journal Hydraul. Res. 1990, 28,401-416.

[26] N. Huybrechts, C. Villaret, J.M. Hervouet, Comparison between 2D and 3D Modelling of Sediment Transport. Application to the Dune Evolution in Proceedings of the 5th International Conference on Fluvial Hydraulics, Braunschweig, Germany.

[27] S. Huabin, Y. Xiping, A. R. Dalrymple, Development of a two phase SPH model for sediment laden flow, Comput. Phys. Commun, (2017), vol 221, p. 259-272.

[28] A. Kurganov, E. Tadmor, New High-Resolution Central-Schemes for Nonlinear Conservation Laws and Convection-Diffusion Equations, J. Computer phys, 160(2000), pp. 241-282.

[29] A. Kurganov, G. Petrova, Central-upwind schemes on triangular grids for hyperbolic systems of conservation laws, Numer. Methods Partial Differ. Equ. 21 (2005) 536-552.

[30] Y. G. Lai, A Two-dimensional Depth Averaged Sediment Transport Mobile-Bed Model with Polygonal Meshes, Water 2020, 12, 1032, doi10.3390/w12041032.

[31] I. Moungnutu, A. R. N. Ngtacha, A. Njifenjou, Stabilization of a finite solution for 1D Shallow Water problems. Preprint ResearchGate, October 2022, DOI:10.13140/RG.2.2. 32013.82403

[32] N. A. R. Ngatcha, Y. Mimbeu, R. Onguene, S. Nguiya, A. Njifenjou, A Novel Sediment Transport Model Accounting Phase Lag Effect. A Resonance Condition, WSEAS Transactions on Fluid Mechanics, Vol 17, 2022, p.189-211. DOI: 10.37394/232013.2022.17.19.

[33] N. A. R Ngatcha A derivation of a 2D PCCU-AENO method for nonconservative problems. Methodology and theoretical arguments. In, 2022.

[34] N. A. R. Ngatcha, B. Nkonga, A. Njifenjou, R. Onguene, Sediment Transport Models in Generalized Shear Shallow Water Flow Equations. CARI 2022, Oct 2022, Dschang, Cameroon. https://hal.archives-ouvertes.fr/hal-03735893.

[35] N. A. R. Ngatcha, A. Njifenjou, A Well Balanced PCCU AENO Scheme for a Sediment Transport Model. Ocean Engineering Systems, 2022, vol 12, No 3. DOI:10.12989/ose.2022.12.3.359

[36] A. R. Ngatcha, B. Nkonga and A. Njifenjou. Finite Volume AENO methods with time-steps discretization for a averaged sediment transport model. Submited In 2022 available in https://hal.archives-ouvertes.fr/hal-03668098.

[37] P. L. Roe, Upwinding Difference Schemes for Hyperbolic Conservation Laws with Source terms. In Carasso, Raviart and Serre, editors, proceeding the conference on hyperbolic problems 41-51. Springer 1986.

[38] G. Rosatti, L. Fraccarolo, A Well-Balanced Approach for Flows over Mobile-Bed with High Sediment Transport. Journal of Computational Physics Volume 220, Issue 1, 20 December 2006, pp. 312-338.

[39] C. W. Shu, Essentially Non-Oscillatory and Weighted ENO for Hyperbolic Conservation Laws, Nasa CR 97-206-253, ICASE report No 97-65.

[40] Siviglia, A., Vanzo, D. and Toro, E. F. A Splitting Scheme for the Coupled Saint-Venant-Exner Model. Advances in Water Resources 2022, Vol 159, 104062.

[41] Schneider, K. A., Gallardo, J. M., Balsara, D., Nkonga, B. and Parés, C. Multidimensional Approximate Riemann Solvers for Hyperbolic Nonconservative Systems. Applications to Shallow Water Systems. Journal of Computational Physics,(2021) 444, 110547.

[42] R. L. Soulsby, R. J. S. Whitehouse, M.V. Marten, Prediction of Time-Evolving Sand Ripples in Shelf Seas. Continental Shelf Research(2012) (38):47-62.

[43] P. Tassi and C. Villaret, Sisyphe v6,3 user's Manual EDF, $R\&D$ Chatou, France 2014.

[44] E. F. Toro, A. Santaca, G. I. Montecinos, L. O. Muller, AENO: a Novel Reconstruction Method in Conjunction with ADER Schemes for Hyperbolic Equations. Communications on Applied Mathematics and Computation, 2021, https://doi.org/10.1007/s42967-021-00147-0.

[45] M. Vah, A. Jarno, F. Marin, S. Le Bot, Experimental Study on Sediment Supply-Limited Bedforms in a Coastal Context. Sixth International Conference on Estuaries and Coasts (ICEC-2018), August 20-23, 2018, Caen, France.

[46] L. C. Van Rijn Equivalent Roughness of Alluvial Bed. Journal of the Hydraulics Division (1982), 108(10): 1215-1218.

[47] Volpert, A. I. The spaces BV and quasilinear equations, Mathematics of the USSR-Sbornik,2 (1967), pp. 225-267.

[48] J. C. Warner, C. R. Sherwood, R. P. Signell, Harris, K. Courtney , H. G. Arango, Development of a Three-Dimensional, Regional, Coupled Wave, Current, and Sediment-Transport Model. Computers and Geosciences 34 (2008) 1284-1306.

[49] W. Wu and S. W. Sam, One-Dimensional Modeling of Dam-Break Flow Over Movable Beds. In Journal of Hydraulic Engineering 133.1(2007), pp. 48-58. DOI 10.1061/(ASCE)0733-9429 (2007)133:1(48).

[50] X. Liu, A. Mohammadian, A. Kurganov, J. A. I. Sedano, Well-Balanced Central-Upwind Scheme for a Fully Coupled Shallow Water System Modeling Flows Over Erodible Bed. Journal of Computational Physics 300 (2015) 202-218.

[51] X. Liu. A New Well-Balanced Finite Volume Scheme on Unstructured Triangular Grids for Two-Dimensional Two-Layer Shallow Water Flows with Wet-Dry Fronts. Journal of Computational Physics 438 (2021) 110380.